

July 2019

Variations of Global Ocean Salinity from Multiple Gridded Argo Products

Chao Liu

University of South Florida, charles1990lau@gmail.com

Follow this and additional works at: <https://digitalcommons.usf.edu/etd>



Part of the [Oceanography Commons](#)

Scholar Commons Citation

Liu, Chao, "Variations of Global Ocean Salinity from Multiple Gridded Argo Products" (2019). *USF Tampa Graduate Theses and Dissertations*.

<https://digitalcommons.usf.edu/etd/7848>

This Thesis is brought to you for free and open access by the USF Graduate Theses and Dissertations at Digital Commons @ University of South Florida. It has been accepted for inclusion in USF Tampa Graduate Theses and Dissertations by an authorized administrator of Digital Commons @ University of South Florida. For more information, please contact digitalcommons@usf.edu.

Variations of Global Ocean Salinity from Multiple Gridded Argo Products

by

Chao Liu

A thesis submitted in partial fulfillment
of the requirements for the degree of
Master of Science
College of Marine Science
University of South Florida

Major Professor: Xinfeng Liang, Ph.D.
Don P. Chambers, Ph.D.
Rui M. Ponte, Ph.D.

Date of Approval:
June 6, 2019

Keywords: global water cycle, ocean climate, freshwater flux, sea ice

Copyright © 2019, Chao Liu

DEDICATION

I would like to dedicate this thesis to my outstanding family members: my parents, Ling Li and Xiaoqing Liu from China, who have always encouraged me to pursue my academic degrees and being my personal role models; and my lovely wife, Yingqin Zhou, who has always been incredibly supportive throughout this fantastic new chapter of our lives.

ACKNOWLEDGMENTS

During my graduate studies, I was graciously supported by the College of Marine Science, University of South Florida. The NASA Earth and Space Science Fellowship (NESSF) Program provided partial funding for this Research. I thank my committee members Dr. Don Chambers and Dr. Rui Ponte for their precious comments and contributions for this work. Especially, I would like to thank my major professor, Dr. Xinfeng Liang, for his great patience, professional insights and editing expertise.

TABLE OF CONTENTS

List of Tables.....	iii
List of Figures.....	iv
Abstract.....	ix
Chapter One: Introduction.....	1
Chapter Two: Data and Methods	5
Global Gridded Salinity Products.....	5
Comparison Strategy.....	7
Chapter Three: Sea Surface Salinity.....	12
Mean State.....	12
Temporal Variability.....	14
Trend.....	17
Chapter Four: Layer One, 0-700 m.....	29
Mean State.....	29
Temporal Variability.....	30
Trend.....	33
Chapter Five: Layer Two, 700-2000 m.....	47
Mean State.....	47
Temporal Variability.....	48
Trend.....	51
Chapter Six: A Comparison with A Global Ocean State Estimate, ECCOv4r3.....	69
Introduction to ECCOv4r3.....	69
Mean State.....	70
Temporal Variability.....	71
Trend.....	74
Chapter Seven: Summary and Discussions.....	85
References.....	90
Appendix A: Zonal Analyses for Major Ocean Basins.....	99

Appendix B: Meridional Analyses for Subpolar Regions.....108

LIST OF TABLES

Table 2.1:	List of the global gridded Argo salinity products.....	10
Table 3.1:	Area-weighted Ensemble Spread of time mean on sea surface salinity.....	19
Table 3.2:	Variance explained by the first 5 principal components of the zonal mean sea surface salinity anomaly from 2005 through 2015.....	19
Table 3.3:	Decadal trends of global sea surface salinity from each individual dataset and Ensemble Mean.....	20
Table 4.1:	Area-weighted Ensemble Spread of time mean of the 0-700 m layer.....	35
Table 4.2:	Variance explained by the first 5 principal components of the zonal mean salinity anomaly of the 0-700 m layer from 2005 through 2015.....	35
Table 4.3:	Decadal trends of global mean salinity of the 0-700 m layer from each individual dataset and Ensemble Mean.....	36
Table 5.1:	Area-weighted Ensemble Spread of time mean of the 700-2000 m layer.....	54
Table 5.2:	Variance explained by the first 5 principal components of the zonal mean salinity anomaly of the 700-2000 m layer from 2005 through 2015.....	54
Table 5.3:	Decadal trends of global mean salinity of the 700-2000 m layer from each individual dataset and Ensemble Mean.....	55
Table 5.4:	Decadal trends of global mean salinity of the 0-2000 m layer from each individual dataset and Ensemble Mean.....	55
Table 6.1:	Variance explained by the first 5 principal components of the zonal mean salinity anomaly from ECCOv4r3 during 2005-2015.....	76
Table 6.2:	Correlations of the EOF modes and principle components between ECCOv4r3 and Argo ESM.....	76
Table 6.3:	Decadal trends of global mean salinity from ECCOv4r3.....	76

LIST OF FIGURES

Figure 2.1:	Illustration of the concepts of ESM, SPD, difference to ESM and largest deviation.....	11
Figure 3.1:	The spatial distributions of the salinity time mean on sea surface salinity, from 2005 through 2015.....	21
Figure 3.2:	The spatial distributions of the difference on salinity time mean on sea surface salinity.....	22
Figure 3.3:	Timeseries of global sea surface salinity anomaly.....	23
Figure 3.4:	Taylor diagram of the timeseries of sea surface salinity anomaly.....	23
Figure 3.5:	The spatial distributions of zonal mean of sea surface salinity anomaly from 2005 through 2015.....	24
Figure 3.6:	Taylor diagram of the zonal mean of sea surface salinity anomaly from 2005 through 2015.....	25
Figure 3.7:	First three EOF modes and principle components of the zonal mean of global sea surface salinity anomaly from 2005 through 2015.....	26
Figure 3.8:	The spatial distributions of linear trends on sea surface salinity from 2006 through 2014.....	27
Figure 3.9:	Taylor diagram of the spatial distributions of linear trends for the global ocean at sea surface from 2006 through 2014.....	28
Figure 4.1:	The spatial distributions of the salinity time mean of the 0-700 m layer, from 2005 through 2015.....	36
Figure 4.2:	The spatial distributions of the difference on salinity time mean of the 0-700 m layer.....	37
Figure 4.3:	Timeseries of global mean salinity anomaly of the 0-700 m layer.....	38
Figure 4.4:	Taylor diagram of the timeseries of global mean salinity anomaly of the 0-700 m layer.....	38

Figure 4.5:	The depth distributions of global salinity anomaly of the 0-700 m layer, from 2005 through 2015.....	39
Figure 4.6:	Taylor diagram of the depth distribution of global mean salinity anomaly of the 0-700 m layer.....	40
Figure 4.7:	The depth distributions of the difference on salinity anomaly of the 0-700 m layer.....	41
Figure 4.8:	The spatial distributions of zonal mean of salinity anomaly of the 0-700 m layer from 2005 through 2015.....	42
Figure 4.9:	Taylor diagram of zonal mean of salinity anomaly of the 0-700 m layer from 2005 through 2015.....	43
Figure 4.10:	First three EOF modes and principle components of zonal mean of global salinity anomaly of the 0-700 m layer from 2005 through 2015.....	44
Figure 4.11:	The spatial distributions of linear trends of the 0-700 m layer from 2006 through 2014.....	45
Figure 4.12:	Taylor diagram of the spatial distributions of linear trends of the 0-700 m layer from 2006 through 2014.....	46
Figure 5.1:	The spatial distributions of the salinity time mean of the 700-2000 m layer, from 2005 through 2015.....	56
Figure 5.2:	The spatial distributions of the difference on salinity time mean of the 700-2000 m layer.....	57
Figure 5.3:	Timeseries of global mean salinity anomaly of the 700-2000 m layer.....	58
Figure 5.4:	Taylor diagram of the timeseries of global mean salinity anomaly of the 700-2000m layer.....	58
Figure 5.5:	The depth distributions of global salinity anomaly of the 700-2000 m layer, from 2005 through 2015.....	59
Figure 5.6:	Taylor diagram of the depth distribution of global mean salinity anomaly of the 700-2000 m layer.....	60
Figure 5.7:	The depth distributions of the difference on salinity anomaly of the 700-2000 m layer.....	61
Figure 5.8:	The spatial distributions of zonal mean of salinity anomaly of the 700-2000 m layer from 2005 through 2015.....	62

Figure 5.9:	Taylor diagram of zonal mean of salinity anomaly of the 700-2000 m layer from 2005 through 2015.....	63
Figure 5.10:	First three EOF modes and principle components of zonal mean of global salinity anomaly of the 700-2000 m layer from 2005 through 2015.....	64
Figure 5.11:	The spatial distributions of linear trends of the 700-2000 m layer from 2006 through 2014.....	65
Figure 5.12:	Taylor diagram of the spatial distributions of linear trends of the 700-2000 m layer from 2006 through 2014.....	66
Figure 5.13:	The spatial distributions of linear trends of the 700-2000 m layer in the tropical Pacific from 2006 through 2014.....	67
Figure 5.14:	Taylor diagram of the spatial distributions of linear trends of the 700-2000 m layer in the tropical Pacific from 2006 through 2014.....	68
Figure 6.1:	The spatial distributions of the time mean and difference from ECCOv4r3 during 2005-2015.....	77
Figure 6.2:	Timeseries of global mean salinity anomaly from Ensemble Mean and ECCOv4r3.....	78
Figure 6.3:	The depth distributions of global salinity anomaly from 2005 through 2015.....	79
Figure 6.4:	The spatial distributions of zonal mean of salinity anomaly from ESM and ECCOv4r3 during 2005-2015.....	80
Figure 6.5:	First three EOF modes and principle components of the zonal mean of global sea surface salinity anomaly from Ensemble Mean and ECCOv4r3 during 2005-2015.....	81
Figure 6.6:	First three EOF modes and principle components of the zonal mean of global salinity anomaly of the 0-700 m layer from Ensemble Mean and ECCOv4r3 during 2005-2015.....	82
Figure 6.7:	First three EOF modes and principle components of the zonal mean of global salinity anomaly of the 700-2000 m layer from Ensemble Mean and ECCOv4r3 during 2005-2015.....	83
Figure 6.8:	The spatial distributions of linear trends from ESM and ECCOv4r3 during 2006-2014.....	84

Figure A1:	At the sea surface of the Atlantic Ocean, the spatial distributions of the difference on zonal mean salinity anomaly from 2005 through 2015 between each individual and the Ensemble Mean.....	99
Figure A2:	For the 0-700 m layer of the Atlantic Ocean, the spatial distributions of the difference on zonal mean salinity anomaly from 2005 through 2015 between each individual and the Ensemble Mean.....	100
Figure A3:	For the 700-2000 m layer of the Atlantic Ocean, the spatial distributions of the difference on zonal mean salinity anomaly from 2005 through 2015 between each individual and the Ensemble Mean.....	101
Figure A4:	At the sea surface of the Indian Ocean, the spatial distributions of the difference on zonal mean salinity anomaly from 2005 through 2015 between each individual and the Ensemble Mean.....	102
Figure A5:	For the 0-700 m layer of the Indian Ocean, the spatial distributions of the difference on zonal mean salinity anomaly from 2005 through 2015 between each individual and the Ensemble Mean.....	103
Figure A6:	For the 700-2000 m layer of the Indian Ocean, the spatial distributions of the difference on zonal mean salinity anomaly from 2005 through 2015 between each individual and the Ensemble Mean.....	104
Figure A7:	At the sea surface of the Pacific Ocean, the spatial distributions of the difference on zonal mean salinity anomaly from 2005 through 2015 between each individual and the Ensemble Mean.....	105
Figure A8:	For the 0-700 m layer of the Pacific Ocean, the spatial distributions of the difference on zonal mean salinity anomaly from 2005 through 2015 between each individual and the Ensemble Mean.....	106
Figure A9:	For the 700-2000 m layer of the Pacific Ocean, the spatial distributions of the difference on zonal mean salinity anomaly from 2005 through 2015 between each individual and the Ensemble Mean.....	107
Figure B1:	At the sea surface of 30-60°N, the spatial distributions of the difference meridional mean salinity anomaly from 2005 through 2015 between each individual and the Ensemble Mean.....	108
Figure B2:	For the 0-700 m layer of 30-60°N, the spatial distributions of the difference meridional mean salinity anomaly from 2005 through 2015 between each individual and the Ensemble Mean.....	109
Figure B3:	For the 700-2000 m layer of 30-60°N, the spatial distributions of the difference meridional mean salinity anomaly from 2005 through 2015 between each individual and the Ensemble Mean.....	110

Figure B4:	At the sea surface of 30-60°S, the spatial distributions of the difference meridional mean salinity anomaly from 2005 through 2015 between each individual and the Ensemble Mean.....	111
Figure B5:	For the 0-700 m layer of 30-60°S, the spatial distributions of the difference meridional mean salinity anomaly from 2005 through 2015 between each individual and the Ensemble Mean.....	112
Figure B6:	For the 700-2000 m layer of 30-60°S, the spatial distributions of the difference meridional mean salinity anomaly from 2005 through 2015 between each individual and the Ensemble Mean.....	113
Figure B7:	At the sea surface of 30°S-30°N, the spatial distributions of the difference meridional mean salinity anomaly from 2005 through 2015 between each individual and the Ensemble Mean.....	114
Figure B8:	For the 0-700 m layer of 30-60°S, the spatial distributions of the difference meridional mean salinity anomaly from 2005 through 2015 between each individual and the Ensemble Mean.....	115
Figure B9:	For the 700-2000 m layer of 30-60°S, the spatial distributions of the difference meridional mean salinity anomaly from 2005 through 2015 between each individual and the Ensemble Mean.....	116

ABSTRACT

Salinity is one of the fundamental ocean state variables. Variations of ocean salinity can be used to infer changes in the global water cycle and air-sea freshwater exchange. Many institutions have developed gridded Argo products of global coverage. However, the existing gridded salinity products have not yet been dedicatedly intercompare and assessed. In this study, the mean state, annual and interannual variabilities, and decadal changes of ocean salinity from five Argo-based gridded salinity products, available from UK Met Office, JAMSTEC, Scripps Institution of Oceanography, China Second Institute of Oceanography, and International Pacific Research Center, are examined and compared for their overlapping period of 2005-2015 within two depth intervals (0-700 m and 700-2000 m), as well as the sea surface. Though some global and regional features are relatively reproducible, obvious discrepancies are found particularly for the deeper layer. These discrepancies are not apparent on the 11-year climatological mean or the trend patterns, but are readily evident on temporal variations. For instance, the potentially undersampled current systems in the North Atlantic and Southern Ocean are one of the main reasons for the observed discrepancies. The gridded products from Scripps, JAMSTEC and Met Office show large deviation from the ensemble mean, particularly in regions like the Atlantic Ocean and the tropical Pacific. Large disagreements are found in the first and final years, which can lead to different estimates on decadal trends. This study can serve as a useful reference on how to utilize and improve the existing gridded salinity products.

CHAPTER ONE:

INTRODUCTION

Ocean salinity is strongly impacted by air-sea freshwater exchange, land freshwater discharges, and ocean dynamics (Rao and Sivakumar, 2003; Foltz et al., 2004; Dong et al., 2014). It is a useful proxy to describe and understand changes in the global water cycle. As one of the primary forcings for the mixed layer, freshwater input at the ocean surface heavily impacts the distribution of surface and subsurface salinity. Since ocean salinity is more measurable than the air-sea freshwater exchange, the surface and/or near-surface salinity is often used as a “rain gauge” for the global water cycle under certain circumstances. Over decadal and shorter time scales, however, the exact relationship between surface freshwater fluxes and sea surface salinity can be more complicated (Yu 2011; Vinogradova and Ponte, 2013, 2017).

Extending from the “rain gauge” concept, one of the most interesting findings in recent years is the hydrological cycle intensification. Many studies have found that the spatial pattern of the mean salinity field strongly resembles that of the salinity change on multi-decadal or shorter time scales (Hosoda et al., 2009; Helm et al., 2010; Skliris et al., 2014), with lower values in subpolar and equatorial regions and higher values in the subtropical regions. Hence the contrast between low and high sea surface salinity zones has intensified. On the large scale, these salinity changes demonstrate that the ocean is getting saltier in evaporation-dominated regions and fresher in precipitation-dominated regions, in response to a strengthened water cycle driven by the warming of the surface and near-surface atmosphere (Durack et al., 2012).

Changes in ocean salinity and salinity-driven halosteric changes also provide an alternative perspective on long-term sea-level change (Durack et al., 2014). Sea-level changes can be associated with two primary processes: increase of water mass from continental freshwater discharge into the global ocean, and volume/density changes either driven by temperature/heat changes (thermosteric) or salinity changes (halosteric). The global-scale halosteric changes are often ignored on multi-decadal time scales, for the halosteric fluctuations and salinity variations are small and have been poorly measured until recently. On basin-scale, however, a number of studies have highlighted the relative importance of salinity to regional halosteric changes for different time scales (Llovel et al., 2011; von Schuckmann and Traon, 2011; Purkey et al., 2014). For instance, the Atlantic Ocean features density compensating long-term trends on thermosteric and halosteric changes from the 1950s to 1990s (Levitus et al., 2005). On the interannual scale, the halosteric component contributes negatively to the global steric change with a modest correlation with the El Niño–Southern Oscillation (ENSO) since 2005 (Wang et al., 2017).

The description of global ocean salinity variations largely relies on available observational datasets (e.g., the World Ocean Database 2013). While ocean salinity, particularly sea surface salinity can be measured from automated Argo floats after 2000 and recent satellites (post 2011), the paucity of historical measurements of ocean salinity before 2000 has been an issue for oceanography research and climate studies. For instance, World Ocean Database 2018 shows that while the in-situ observations have been growing in number since the 1970s, there is still a significant bias toward the Northern Hemisphere, particularly in the coastal waters and marginal seas (Boyer et al., 2018). In contrast, the Southern Hemisphere and in particular the Southern Ocean are poorly sampled.

Since 2001, the Argo Program has become one of the most important components of the present global ocean observing system, utilizing a large number of autonomous floats. The Argo floats typically have a 10-day observational cycle. During each cycle, the float rises to the surface from its parking depth (~2000 m) while collecting temperature and salinity data, then transmits the data to satellites when they are at surface. This has allowed for the first time a nearly global sampling of the upper 2000 m ice-free ocean with relatively small bias since about 2005 (Abraham et al., 2013; Roemmich et al., 2009). A number of institutions and research groups hence have developed gridded products and analyses based on Argo profiles, using different statistical methods. These gridded Argo products have been widely used and have been considered as the “truth” within some measurement uncertainties (e.g., Chang et al., 2014; Wang et al., 2017).

As many studies have revealed, however, large discrepancies are readily evident among these gridded Argo products (von Schuckmann and Traon, 2011; Lee, 2016; Trenberth et al., 2016; Wang et al., 2017). A large portion of these differences relate to the mapping techniques for filling the gaps in time and space (Araham et al., 2013; Boyer et al., 2016), and systematic errors also exist in the Argo autonomous measurements (Jayne et al., 2017). For instance, around 25% of real time profiles might be subject to salinity errors larger than the 0.01 accuracy target since 2016 (http://www.argo.ucsd.edu/Salinity_errors_Sept_2018.pdf). The existence of the large discrepancies suggests that estimates of temporal variability and decadal trends in ocean salinity are likely product-dependent. It is therefore vital to assess the products and quantify robust as well as inconsistent features. While there have been a number of assessments of the salinity products from various ocean reanalyses and some selected gridded Argo products (Xue et al.,

2012; Chang et al., 2014; Shi et al., 2017), a thorough examination of all the existing gridded Argo-based salinity products has not yet been performed.

In this study, our primary goal is to conduct an assessment to identify the robust as well as inconsistent features from various Argo salinity products. By recognizing existing discrepancies, the results presented here will serve as a reference for the use of gridded Argo products and their future development. The data and methods are described in Chapter 2. In Chapter 3 to Chapter 5, we show the agreements and disagreements in the mean state, temporal variability and decadal trends at the sea surface and within two depth intervals: 0-700 m and 700-2000 m. Chapter 6 presents an intercomparison with an state-of-the-art ocean state estimate, and Chapter 7 presents conclusions and implications for future work.

CHAPTER TWO: DATA AND METHODS

Global Gridded Salinity Products

Many institutions have developed gridded Argo products, but only five are updated frequently, at least on an annual basis (<http://www.argo.ucsd.edu/>). Therefore, those five Argo-based salinity gridded products are used in this study for the common time period 2005-2015: **BOA**-Argo from the China Second Institute of Oceanography (CSIO), **EN4** from UK Met Office, **IPRC**-Argo from the International Pacific Research Center (IPRC), **MOAA** from the Japanese Agency for Marine-Earth Science and Technology (JAMSTEC), and the Roemmich-Gilson Argo (**RG**) from the Scripps Institution of Oceanography (SCRIPPS). All these products provide monthly gridded fields of temperature and salinity, with horizontal resolution of $1^{\circ} \times 1^{\circ}$. Note that EN4, MOAA and IPRC used other raw data besides Argo profiles, but the amount of Argo data after 2005 dominates as the major data source. Key information (e.g., references, mapping methods, vertical resolutions, spatial and temporal coverage) of these products is summarized in Table 2.1.

Though all five gridded Argo products are considered as objective analyses data, the mapping methods vary. BOA used Cressman analysis, which applies a linear combination of corrections between prediction and observation, to iteratively correct the background values (first guesses). Then a modified Gaussian function (Barnes successive correction method) was used to iteratively generate gridded data (Li et al., 2017, Eq. 4). The main source of data for EN4 is

World Ocean Database (WOD) 2009 (three other data compilations are also added), but used an older climatology based on World Ocean Atlas 1998. The covariance is specified using two second-order autoregressive (SOAR) functions. Analysis Correction process was used in EN4 to iteratively generate gridded data with a recursive filter, hence there is no need to subselect the observations for each grid point (Good et al., 2013, Section 2.3). IPRC used a variational analysis technique, which includes calculated absolute dynamic height (ADH) from satellite data. While a harmonic/biharmonic operator is applied to suppress the noise on the grid scale, the tilt of the isopycnal of the mixed-layer depth and the gradient of the gridded ADH were also considered in the cost function which gets iteratively minimized (<http://apdrc.soest.hawaii.edu/projects/Argo/data/Documentation/gridded-var.pdf>). The “first guess” of MOAA was obtained from World Ocean Atlas (WOA) 2001 which also provided annual mean standard deviation for its exponential weighting function (Hosoda et al., 2008, Eq. 15). For RG, a 5-year mean field for each month was used to arrive at a stable “first guess” with a weighted least-squares procedure. The covariance function used for the objective analysis was represented as the sum of a small-scale Gaussian function and large-scale exponential decay (Roemmich and Gillson, 2009, Section 2).

While the original aim of the Argo Program was focused on the global ice-free open ocean between 60°S and 60°N (Roemmich and Gilson, 2009; Roemmich et al., 2009), increasing numbers of Argo floats have been deployed in the seasonally ice-covered polar regions (Jayne et al., 2017). Here the gridded fields from all the salinity products are limited to the latitudes from 60°S to 60°N (referred as the “common domain”, in comparison to each specific data domain, called the “native domain”), excluding marginal seas like Gulf of Mexico.

Comparison Strategy

Apart from the sea surface salinity (SSS), which is defined here as the vertical average of the upper 20 m/dbar surface and subsurface ocean, the focus of this study is also on the different features of the salinity variations within different vertical layers. A number of studies (Curry et al., 2003; Boyer et al., 2005; Durack and Wijffels 2010; Shi et al., 2017) have found substantial variability and change in ocean salinity in the upper 700 m of the global ocean. In the meantime, the deeper ocean (below 700 m) also presents apparent basin-scale changes associated with density compensation, circulation changes and water mass changes (e.g., Durack et al., 2014; Purkey et al., 2014; Storto et al., 2017). In this study, we focused on two layers: the upper 0-700 m and the deeper 700-2000 m. In addition, the common time period 2005-2015 is divided into two subsets to examine potential drift in the first and last years: the full coverage of 2005-2015, and the partial coverage 2006-2014. If not specified, the “full coverage” is the default time period for the time mean, and “partial covered” is the default for most of the linear trend calculation through least squares estimation.

For our intercomparison, the following three terms are used to assess the global averaged salinity: depth-averaged, area-weighted and volume-weighted. Depth-averaged salinity is calculated as:

$$\overline{S}_d(x, y, t) = \frac{\sum_{z=l}^L (S(x, y, z, t) \times \Delta d(z))}{\sum_{z=l}^L \Delta d(z)} \quad (1)$$

where S represents the temporally dependent (t) 3-D gridded salinity field in the xyz -coordinate system (i.e., longitude, latitude and depth). Δd is the time-independent grid spacing in the vertical direction, and L and l are the mid-depth of the bottom and top predefined layers.

Area-weighted salinity is defined as:

$$\overline{S}_A(z, t) = \frac{\sum_{n=1}^N (S(x, y, z, t) \times A(x, y))}{\sum_{n=1}^N A(x, y)} \quad (2)$$

where N is the total number of grid points of the 2- D salinity field at any given depth or layer, and A denotes the time-independent 2- D area field (common domain) corresponding to the grid points.

Combining Eq. (1) and Eq. (2), volume-weighted salinity is therefore given by:

$$\overline{S}_v(t) = \frac{\sum_{n=l}^L (S(x, y, z, t) \times \Delta V(x, y, z))}{\sum_{n=l}^L \Delta V(x, y, z)} \quad (3)$$

where ΔV is the time-independent 3- D grid volume field corresponding to the grid points. In this study, area-weighted and volume-weighted techniques are applied to global domain, as well as in zonal and meridional mean analyses.

A common method for assessing uncertainty in data from two or more processing centers is computing statistics of their differences (i.e., mean, standard deviation, correlation, etc.). Here we used the Taylor diagram, which is designed to facilitate the comparative assessment of different models, to graphically depict three statistics: the correlation coefficient, the root-mean-square error (RMSE) error, and the standard deviation. However, this will only account for uncertainties arising from different mapping methods, quality controls and randomness in the observations. It will not account for common, systematic error (such as a bias or bias change).

Here, we use the concept of the Ensemble Spread (SPD, modified from Balmaseda et al., 2015; Shi et al., 2017) of the five gridded Argo products relative to their corresponding Ensemble Mean (ESM). Lower Ensemble Spread means the products are more consistent. The salinity fields of the Ensemble Mean (S_{ESM}) from the gridded Argo products is given by:

$$S_{ESM}(x, y, z, t) = \frac{1}{N} \sum_{n=1}^N S_n(x, y, z, t) \quad (4)$$

where N is the total number of the Argo products ($N=5$), and S_n represents the salinity field or other diagnosed variables.

The Ensemble Spread of the gridded Argo products about the corresponding ESM (S_{SPD}) is calculated as:

$$S_{SPD}(x, y, z, t) = \sqrt{\frac{1}{N} \sum_{n=1}^N (S_n(x, y, z, t) - S_{ESM}(x, y, z, t))^2} \quad (5)$$

Note that both ESM and SPD should have the same dimensions as the variable S , which can also represent spatial mean (i.e., global mean, zonal mean, meridional mean, etc.) or time mean salinity with reduced dimension. Therefore, not all four dimensions are required for calculation.

Estimates of ESM and SPD will be used to assess the agreement and disagreement of the datasets. For example, SPD can be used as a proxy of the uncertainty induced by different mapping methods and sampling conditions, although it will not detect common errors. The difference of each product to the calculated ESM is also measured, and the largest difference (absolute value) is labeled as “largest deviation” (illustrated in Figure 2.1).

It is worth noting that the gridded Argo products or ESM should not be simply considered as an equivalent to the “truth” due to the spatially and temporally inhomogeneous distribution of Argo floats. For example, significant sampling and mapping error can arise at regions where eddy kinetic energy is high (Kosempa and Chambers, 2016). Also, since not all the datasets provide a corresponding error matrix (e.g., BOA, IPRC), here we have assumed that these Argo-based gridded salinity products have similar quality for the calculation of ESM and SPD (Balmaseda et al., 2015).

Table 2.1. List of the global gridded Argo salinity products. Details about reference, mapping method, vertical resolution, temporal and spatial coverage in high latitude regions and marginal seas are also listed.

Product	Institute	References	Mapping Method	Data Source	Vertical Resolution	Tem. Cov.^a	Nat. Dom.^b	Arctic	60° S+^c
BOA	CSIO	Li et al., 2017	Barnes Method	Argo Only	58 levels to 1975 dbar	2004-2017	80°S-80°N	×	<i>p</i> ^d
EN4	Met Office	Good et al., 2013	Objective Analyses	Argo Included	42 levels to 5350 m	1999-present	83°S-90°N	√	√
IPRC	IPRC	http://apdrc.soest.hawaii.edu/projects/argo/	Variational Interpolation	Argo with Altimetry	27 levels to 2000 m	2005-present	90°S-90°N	×	×
MOAA	JAMSTEC	Hosoda et al., 2008	Optimal Interpolation	Argo Included	25 levels to 2000 dbar	2001-present	60°S-70°N	×	×
RG	SIO	Roemmich and Gillson, 2009	Optimal Interpolation	Argo Only	58 levels to 2000 dbar	2004-present	65°S-80°N	×	×

^a *Tem. Cov.*, Temporal Coverage; ^b *Nat. Dom.*, Native Domain, ^c 60°S+, south of 60°S; ^d *p*, partial coverage.

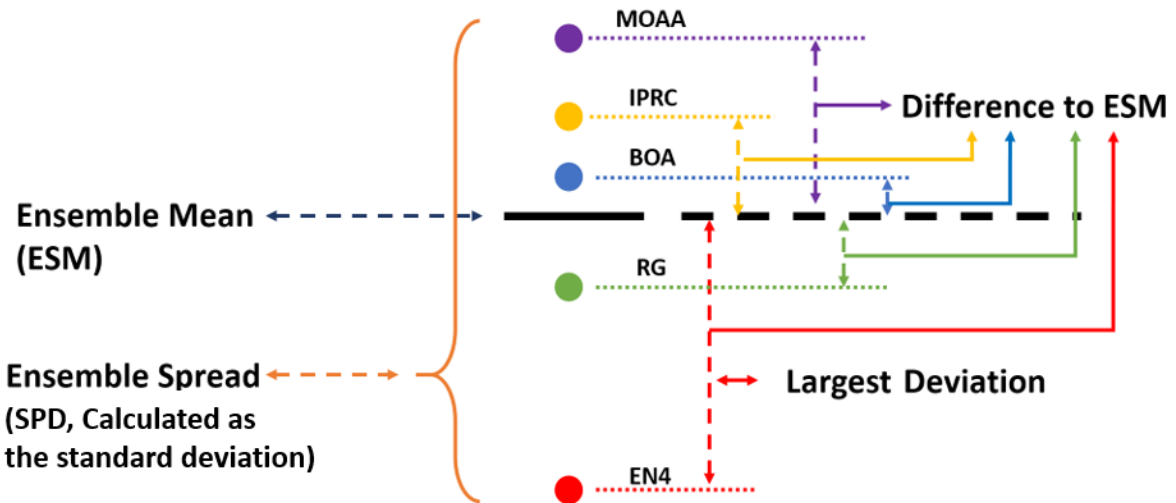


Figure 2.1. Illustration of the concepts of ESM, SPD, difference to ESM and largest deviation. For most variables used in this study, we can calculate a set of ESM and SPD following Eq.1 and Eq.2 based on the five results from different gridded products. The difference of each product to the calculated ESM is also measured, and the largest difference (absolute value) is labeled as “largest deviation”.

CHAPTER THREE: SEA SURFACE SALINITY

Mean State

The decadal mean state of sea surface salinity, which is described as the 11-year (2005-2015) climatological mean in this study, shows some well-known and robust regional features (e.g., Figure 3.1a). Higher salinities (above 35 psu) are found in the evaporation dominated mid-latitudes, and lower salinities (below 35 psu) in the precipitation dominated regions such as the Inter Tropical Convergence Zone (ITCZ) and polar regions. The temporal standard deviation of ESM (dots in Figure 3.1a) shows zonal banding in the tropics, where there is strong variability in tropical rainfall. Higher variances occur in the eastern and western equatorial Pacific, likely related to regional air-sea exchanges through the Walker Circulation over the 11-year period. This will be discussed in the following section.

The SPD of the SSS time mean (Figure 3.1b) is relatively small and negligible. The spatial distribution of SPD roughly resembles the temporal standard deviation pattern. High SPD tends to appear in the major surface current systems (e.g., the Gulf Stream, east equatorial Pacific, tropical Atlantic and the south Indian Ocean), where sharp frontal salinity gradients caused by oceanic jets and mesoscale eddies are challenging to resolve with Argo floats. These regions are generally poorly sampled (except the Gulf Stream). The paucity of salinity observations in these areas can lead to high sampling errors when mapping the data to $1^{\circ} \times 1^{\circ}$

grids (e.g., Kosempa and Chambers, 2016). Error analyses with a regional focus on these particular regions might provide further information.

While the global mean of SPD is small (0.032 psu, Table 3.1), higher area-averaged SPD is detected in the Northern Hemisphere and the tropical regions, particularly in the Atlantic Ocean. Since these regions have been better sampled both historically and during the Argo Era, such large-scale difference might not be the result of sampling error but likely due to the different background climatology fields and mapping methods.

By looking at the differences between each individual dataset and ESM (Figure 3.2), an obvious conclusion is that BOA and EN4 are closer to the Ensemble Mean. The most noticeable differences on these two products are found in the Gulf Stream, where the mean salinity is higher in the south and fresher in the north, and the equatorial Atlantic, where the mean salinity is higher near the coast and lower to the north. These distinct dipoles offset the large (and opposite) deviations found in the IPRC product to an extent.

Comparing the largest deviation (Figure 3.2f) to SPD pattern (Figure 3.1b), the broad-scale zonal deviations in IPRC can account for much of the spatial structure of SPD. The pattern in the IPRC is likely due to the use of harmonic/biharmonic operator and the isopycnals calculated from the ADH, as the ADH represents the mean fields since 1993, while the salinity climatology represents the mean from 2005 to 2015. Thus, the isopycnals from the ADH may be shifted from those implied in the climatology due to changes in the path and strength of currents, which could manifest in the patterns observed. Moreover, the ADH will have spatial errors from both the sea surface height and geoid data used in the computation.

In comparison, MOAA shows broad-scale deviation but very little small-scale structure, which is likely because of MOAA's special data sources (Japan-based in situ measurements) and

pre-Argo background field (WOA01). RG shows some resemblance to EN4 but is more dispersed in the Pacific, which highlights the difference between the mapping techniques in suppressing the noises.

Overall, the climatological mean of sea surface salinity is robust, with BOA and EN4 showing the smallest deviation to ESM. The largest deviation comes from IPRC on large-scales, in which the mapping method (i.e., variational interpolation) generates strong zonal dipoles. These subtle but measurable differences highlight the fact that the mapping methods and the background climatological fields used in practice could cause non-negligible disagreements on the salinity climatology during the Argo era (Abraham et al., 2013; Chang et al. 2014).

Temporal Variability

Variations in sea surface salinity provide useful information for understanding the changes of the water cycle and climate. For area-weighted, globally averaged SSS, temporal anomalies vary from -0.04 to 0.04 psu with small seasonal and interannual-decadal fluctuations (Figure 3.3, right axis). In this study, the common time period 2005-2015 covers the La Niña events in 2007-2008 and 2010-2012, as well as the El Niño event in 2014-2016. The strong 2010/11 La Niña affected global precipitation patterns and caused broad-scale drought (e.g., Boening et al., 2012). As a result, the unfiltered global mean SSS shows a bell shape (high in the center, low on both sides) and have a modest correlation with the Multivariate ENSO Index (MEI) index at 0.67 after 2010 while the correlation is only 0.31 before 2010.

Although the number of deployed Argo floats has grown over time, the SPD of the global mean timeseries does not show any visible trend (shade in Figure 3.3, left axis). A Taylor diagram of the global mean SSS timeseries shows that most Argo products are highly correlated

(around 0.95) with ESM (Figure 3.4), although RG has a slightly lower correlation near 0.9 because of large deviations in 2008 and after 2014. All five products and ESM also have similar temporal standard deviations and root mean square difference (RMS) values, whether for 2005-2015 or the subset of 2006-2014.

As the mean sea surface salinity and the freshwater flux pattern have a rich zonal structure, zonal averages and associated analysis would provide further information about the temporal variability of the SSS. For instance, the zonal mean of SSS anomaly reveals strong interannual variation in the tropical regions and visible trends in the mid-latitudes after removing the annual signal with sinusoid model (Figure 3.5a). Also, all gridded products show good agreements on the zonal mean pattern with correlations over 0.9 (Figure 3.6). Interestingly, the large SPD values (dots in Figure 3.5a) are found when the salinity anomaly is above average (> 0), implying a disagreement on the dry events. In Figure 3.5a, a strong freshening is found at 40-60°N, which is primarily due to freshening of the North Atlantic (see next section and Appendix A & B), and a salinification appears between 20-40°S, which corresponds to a broad salinification in the mid-latitude Southern Hemisphere. In addition, another prominent major features on the zonal mean of SSS is the linkage to ENSO in the tropical region (30°S-30°N). There is also another weak but visible freshening in the Southern Ocean (50-60°S).

To better diagnose the temporal variations revealed above, an empirical orthogonal function (EOF) analysis is conducted on the zonal mean SSS (Figure 3.7). The first three EOF modes account for 55.5% of the total variance, and the first five EOF modes account for almost 70%. Since the pattern and magnitude of the zonal mean SSS are highly robust, the differences between the five gridded products and ESM (Figure 3.5b-f) are not large for most regions (< 0.025 psu) after a 7-month running mean, especially for the Southern Ocean (50-60°S). One of

the major deviations is the equatorial region for RG, which suggests a weaker ENSO signal with an opposite spatial pattern (Figure 3.5f).

The EOF mode 1 (Figure. 3.7a) shows a strong minimum (-0.8 psu) located at the tropical region (10°S-20°N) and two peaks (15°S and 30°N) with maximum value around 0.4 psu. The first principal component (PC, Figure 3.7b) fluctuates between -0.2 to 0.3, which makes the maximum magnitude of the first EOF mode pattern around -0.08-0.12 psu. It has an evident upward trend after 2014, and a modest correlation with MEI (0.69) for 2005-2015 which increases for the zonal mean of Pacific (0.74) especially between 20°S-20°N (0.85). Therefore, the first EOF mode of zonal mean SSS anomaly likely represents the impacts of ENSO, which has an averaged explained variance of 30.9% (Table 3.2).

The second EOF mode shows a different spatial structure: a large portion of the ocean around 20°N is positive with a maximum near 0.5 psu, and the subpolar region north to 40°N is negative with a minimum -0.4 psu (Figure 3.7c). Despite its semiannual fluctuations, the second principal component (Figure 3.7d) steadily increases from -0.2 to 0.2 with small semiannual variations, making the magnitude of EOF mode 2 around ± 0.1 psu. EOF mode 2 explains almost 15% of the total variance of the zonal mean SSS, and likely represents a positive decadal trend at 20°N and 40°S, and a negative trend between 40-60°N. The third EOF mode very likely represents a semiannual variability with maxima in the equatorial region, but it is relatively noisy and explains less than 10% of the variance (Figure 3.7e-f).

In general, the sea surface salinity changes over time are robust and reproducible with correlation over 0.95 on globally averaged timeseries, and over 0.9 on zonal mean anomalies. The SPD of the timeseries does not increase in time, indicating the sampling error is not a major contributor for SPD. The first EOF mode of the zonal mean SSS represents the ENSO variability

and accounts for 30% of the total variance. The second EOF mode, a linear trend with semiannual variability, explains 15% while each of the remaining modes explains less than 10%. One noticeable discrepancy is that the RG product suggests weaker ENSO variation in the equatorial Pacific than the other gridded products.

Trend

The linear trend of each salinity time series has been computed using a least square method, fitting a model of the form:

$$S = a_0 + a_1 t + a_3 \cos(\omega t) + a_4 \sin(\omega t) \quad (6)$$

where S is the salinity time-series, and the parameters (a_0 to a_4) represent bias, trend, and annual signal, respectively. Uncertainty reflects the 95% confidence interval but has been adjusted to reflect reduced effective Degrees of Freedom (eDOF) due to serial correlation in the residuals. Here eDOF is computed from the lag-1 autocorrelation of the residuals.

For the time period of 2005-2015, the trend value of the global mean SSS ranges from 0.31 (BOA) to $1.61 \text{ (RG)} \times 10^{-3}$ psu/year (Table 3.3). However, none of the trends is different from zero at 95% confidence, so statistically, they are in agreement. The bell shape of global mean SSS anomaly (Figure 3.3) lead to considerable uncertainties of the trend estimates, with a minimum at 2.12 (RG) and a maximum at $2.88 \text{ (IPRC)} \times 10^{-3}$ psu/year.

The trends for the subset of 2006-2014 are between $1.28\text{-}3.01 \times 10^{-3}$ psu/year, with uncertainties reduced by an average of 8%. It is also noteworthy that RG for 2006-2014 exhibits the only statistically significant trend ($3.01 \pm 1.99 \times 10^{-3}$ psu/year) but is still not significantly different from the other estimated trends accounting for their overlaps within the estimated

uncertainties. Therefore, we conclude that no significant decadal change in the global mean SSS since the mid-2000s can be detected with the existing gridded Argo products.

On regional or basin-scale, changes in ocean salinity will affect the local buoyancy balance and density stratification, hence a number of studies have examined the regional salinity changes as well as the derived halosteric heights (Durack et al., 2014; Llovel and Lee, 2015; Wang et al., 2017, Tesdal et al., 2018). Compared to the trend of the global mean SSS, regional salinity trends at the sea surface can be over 10 to 15 times larger than that of the global mean SSS (Figure 3.8). All the products show a similar pattern with high spatial correlations (over 0.9), although the magnitudes are slightly different (Figure 3.9). The standard deviations of the trend patterns are smaller in MOAA and RG, while EN4 has the largest regional trends.

However, the general patterns are similar in all products: broad increasing SSS in the subtropical Pacific, and two decreasing SSS in the central North Atlantic and Eastern Indian Ocean. The freshening (negative SSS trend) in the subpolar North Atlantic is possibly associated with the North Atlantic Oscillation (Dickson et al., 2002) and the increase of Arctic freshwater input (Proshutinsky et al., 2009). The freshening in the East Indian Ocean likely represents the Indian Ocean Dipole (IOD, Saji et al., 1999), and could be related to the strengthening of the Indonesian throughflow and enhanced regional precipitation (Llovel and Lee, 2015). The positive trend in EN4 north of the Ross Sea (south of 60°S, 150°E-120°W) may be related to the increase of sea-ice formation (e.g., Haumann et al., 2016). However, since EN4 observes this regional feature while BOA, the only other to extend so far south, does not, the observed trend could also be due to limited sampling and/or the mapping strategy.

Table 3.1. Area-weighted Ensemble Spread of time mean for sea surface salinity (unit: psu). Bold number denotes results higher than global mean.

Region	Northern	Southern	Tropical	Total
Global	0.037	0.026	0.033	0.032
Pacific	0.031	0.019	0.030	0.026
Atlantic	0.049	0.034	0.045	0.043
Indian	N/A	0.031	0.029	0.030
Southern Ocean	N/A	N/A	N/A	0.018

Northern: 30-60°N; Tropical: 30°S-30°N; Southern: 30-50°S; Southern Ocean: 50-60°S.

Table 3.2. Variance explained by the first 5 principal components of the zonal mean sea surface salinity anomaly from 2005 through 2015. Averaged explained variance of the six products (five gridded Argo data and ESM), total number of the first three modes and first five modes and are also given.

Products	Mode 1	Mode 2	Mode 3	Subtotal	Mode 4	Mode 5	Total
BOA	31.4%	12.2%	9.4%	53.0%	7.9%	6.7%	67.6%
EN4	28.9%	13.4%	10.4%	52.7%	8.5%	7.1%	68.3%
IPRC	33.3%	15.8%	8.4%	57.5%	7.3%	6.6%	71.4%
MOAA	31.6%	13.9%	10.3%	55.8%	7.2%	6.3%	69.3%
RG	27.2%	19.0%	10.0%	56.2%	7.6%	6.5%	70.3%
ESM	33.0%	14.8%	9.9%	57.7%	7.8%	7.2%	72.7%
AVERAGE	30.9%	14.9%	9.7%	55.5%	7.7%	6.7%	69.9%

Table 3.3. Decadal trends of sea surface salinity from each individual dataset and Ensemble Mean (unit: 10^{-3} psu/year). Bold number indicates result significantly different from zero at the 95% confidence level.

Products	Subset 1: 2005-2015	Subset 2: 2006-2014
BOA	0.31±2.47	1.46±2.40
EN4	0.57±2.65	1.75±2.43
IPRC	0.39±2.88	1.28±2.52
MOAA	0.81±2.53	1.90±2.33
RG	1.61±2.12	3.01±1.99
ESM	0.74±2.76	1.88±2.42

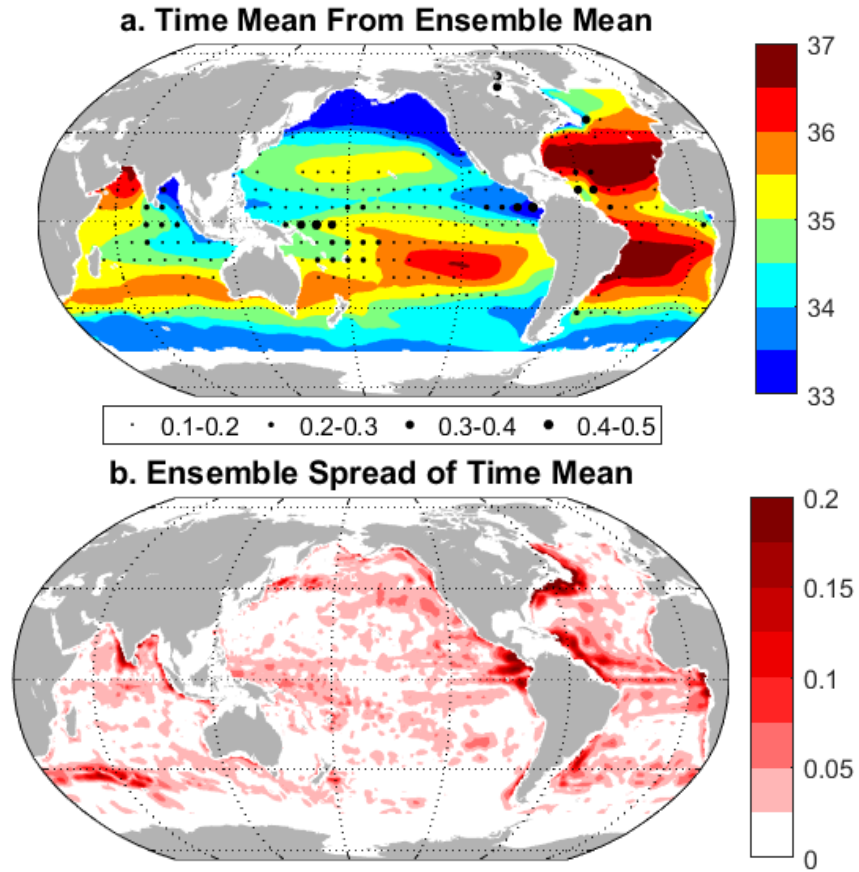


Figure 3.1. The spatial distributions of the salinity time mean on sea surface salinity, from 2005 through 2015. (a) the Ensemble Mean, stippling marks the temporal standard deviation, (b) its Ensemble Spread. (unit: psu)

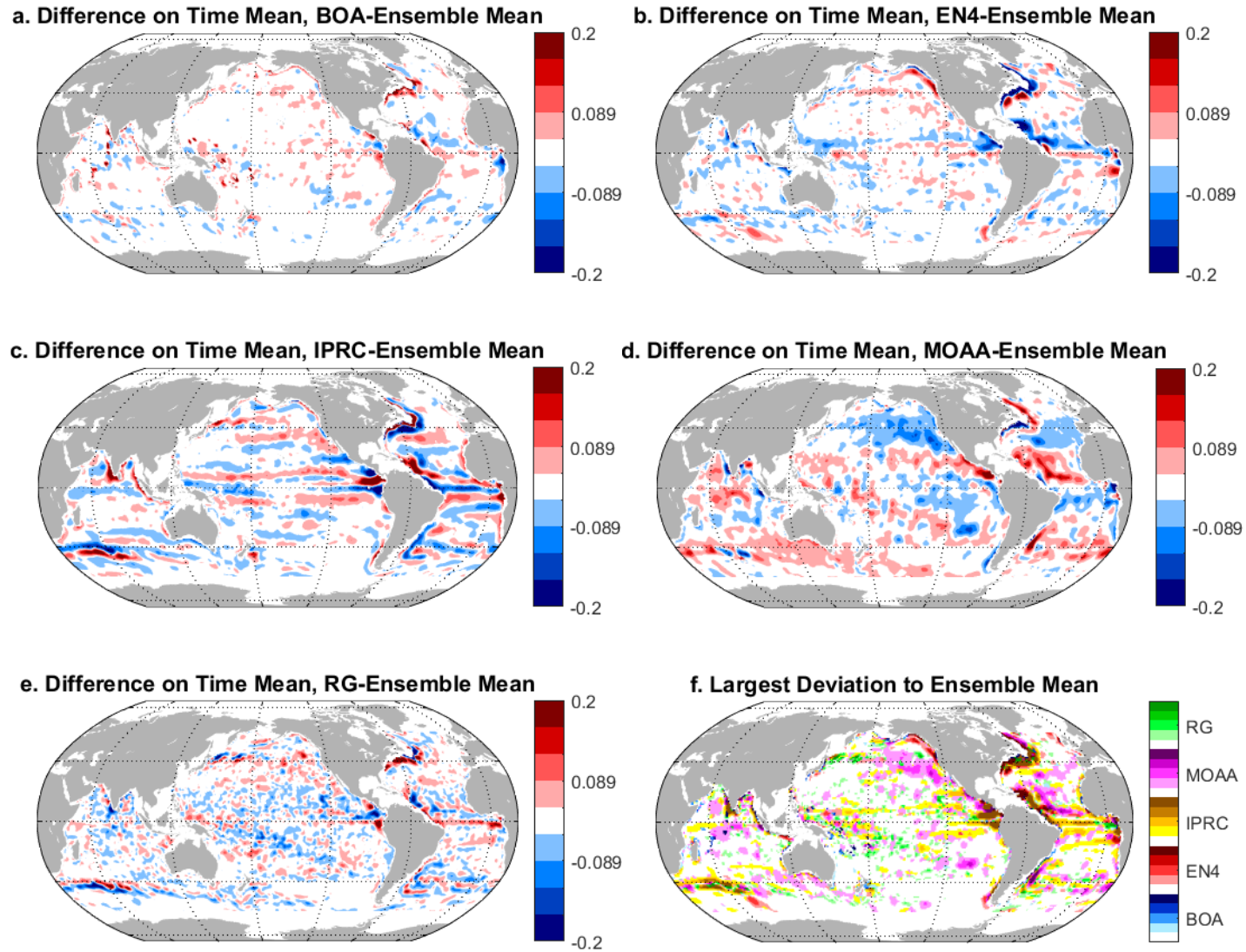


Figure 3.2. The spatial distributions of the difference on salinity time mean on sea surface salinity. (a-e) The difference on time mean, (f) the largest deviation to the Ensemble Mean The range for each color is the same as the difference. (unit: psu)

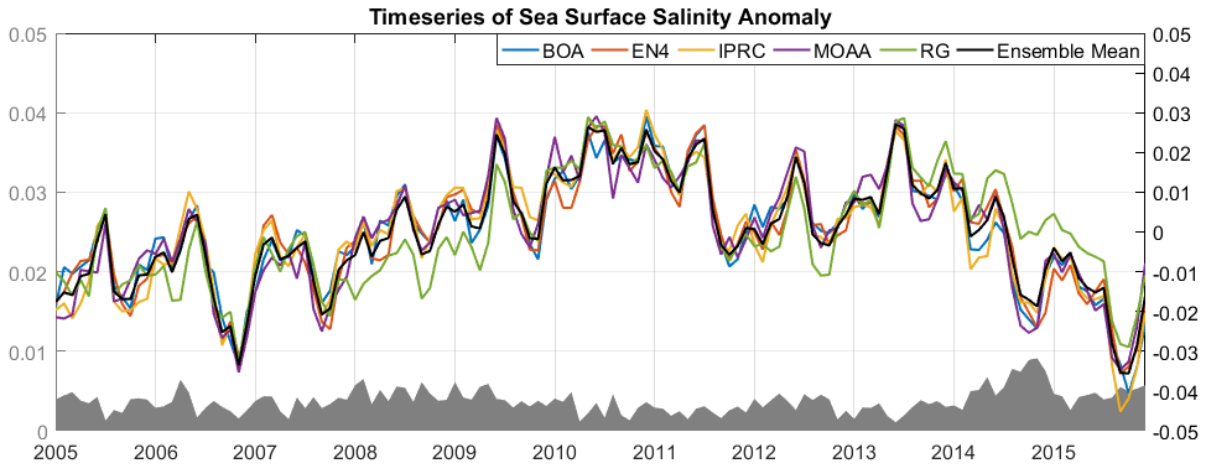


Figure 3.3. Timeseries of sea surface salinity anomaly (right axis). Shade (left axis) indicates the Ensemble Spread of the datasets. (unit: psu)

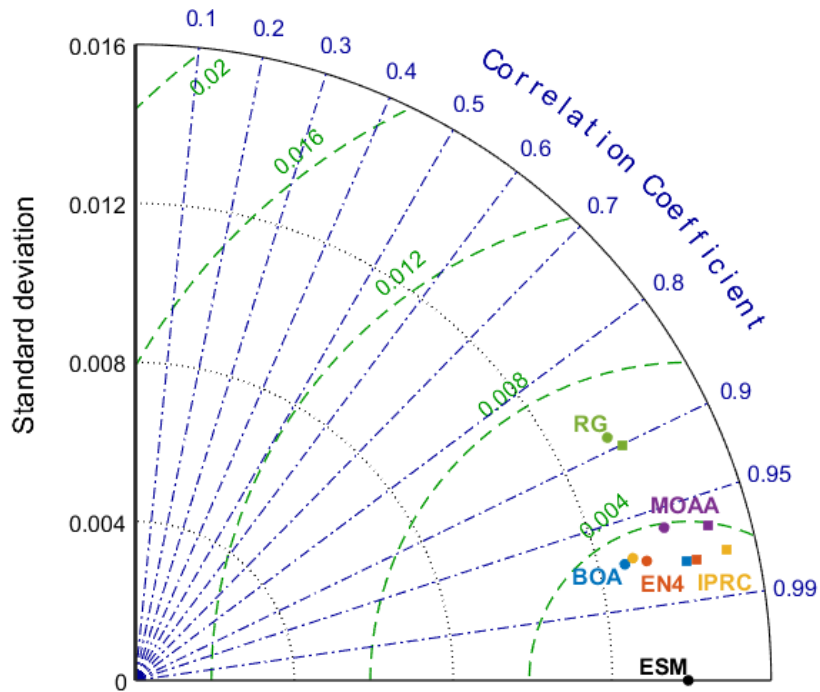


Figure 3.4. Taylor diagram of the timeseries of sea surface salinity anomaly. Squares mark the subset from 2005 through 2015 and circles mark from 2006 through 2014. The plot summarizes the correlation, root mean square difference, and temporal standard deviation of each of the Argo products with respect to ESM.

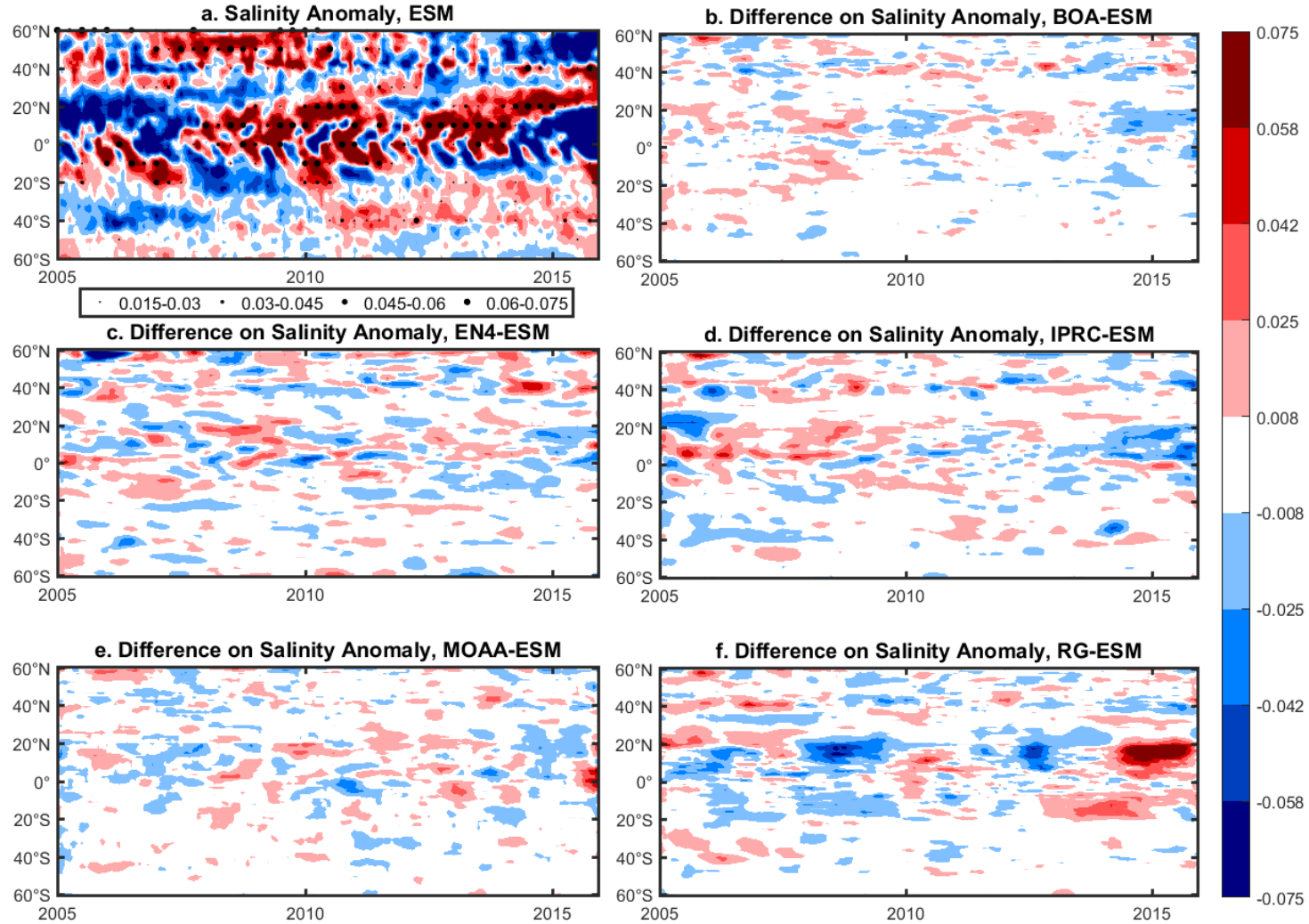


Figure 3.5. The spatial distributions of zonal mean of sea surface salinity anomaly from 2005 through 2015. (a) The Ensemble Mean, (b-f) the difference between each individual dataset and the Ensemble Mean. The annual signal is removed using an annual sinusoid model. Stippling in (a) indicates the range of the Ensemble Spread. A 7-month running mean is applied to (b-f). (unit: psu)

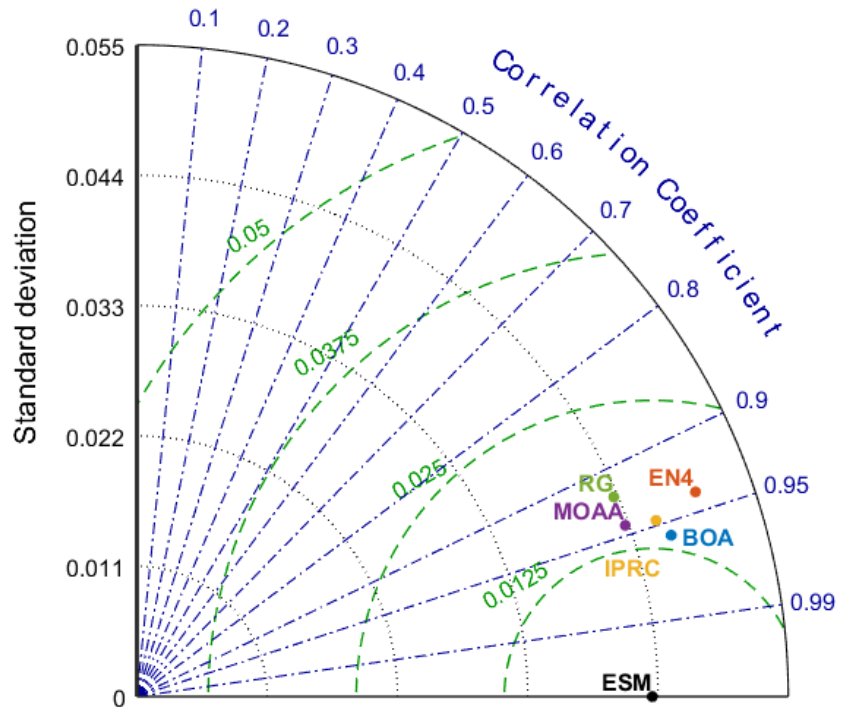


Figure 3.6. Taylor diagram of the zonal mean of sea surface salinity anomaly from 2005 through 2015. The plot summarizes the correlation, root mean square difference, and standard deviation of the observed pattern of each Argo products with respect to ESM.

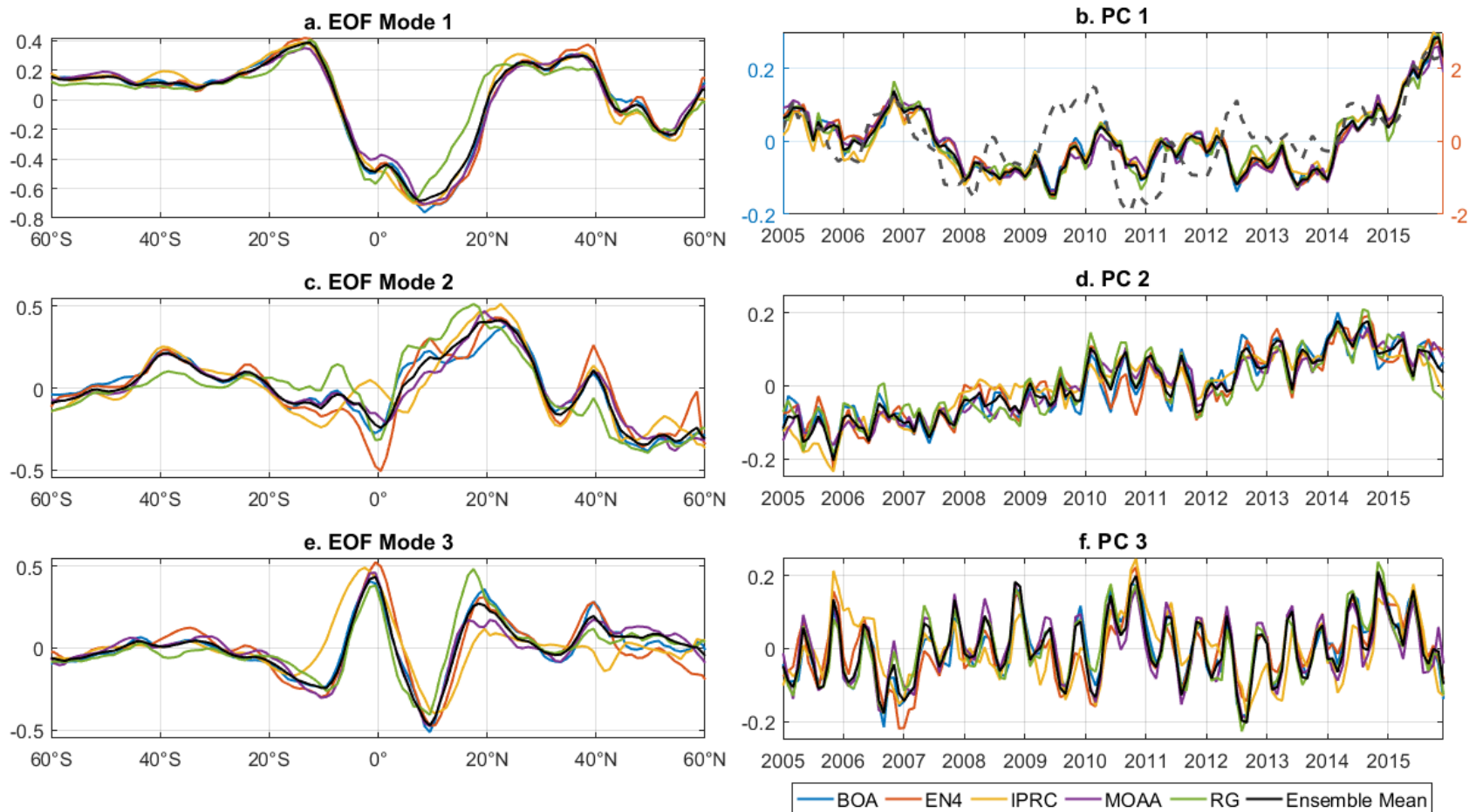


Figure 3.7. First three (a, c, e) EOF modes and (b, d, f) principle components of the zonal mean of sea surface salinity anomaly from 2005 through 2015. Dash line in the PC 1 denotes the MEI (right axis).

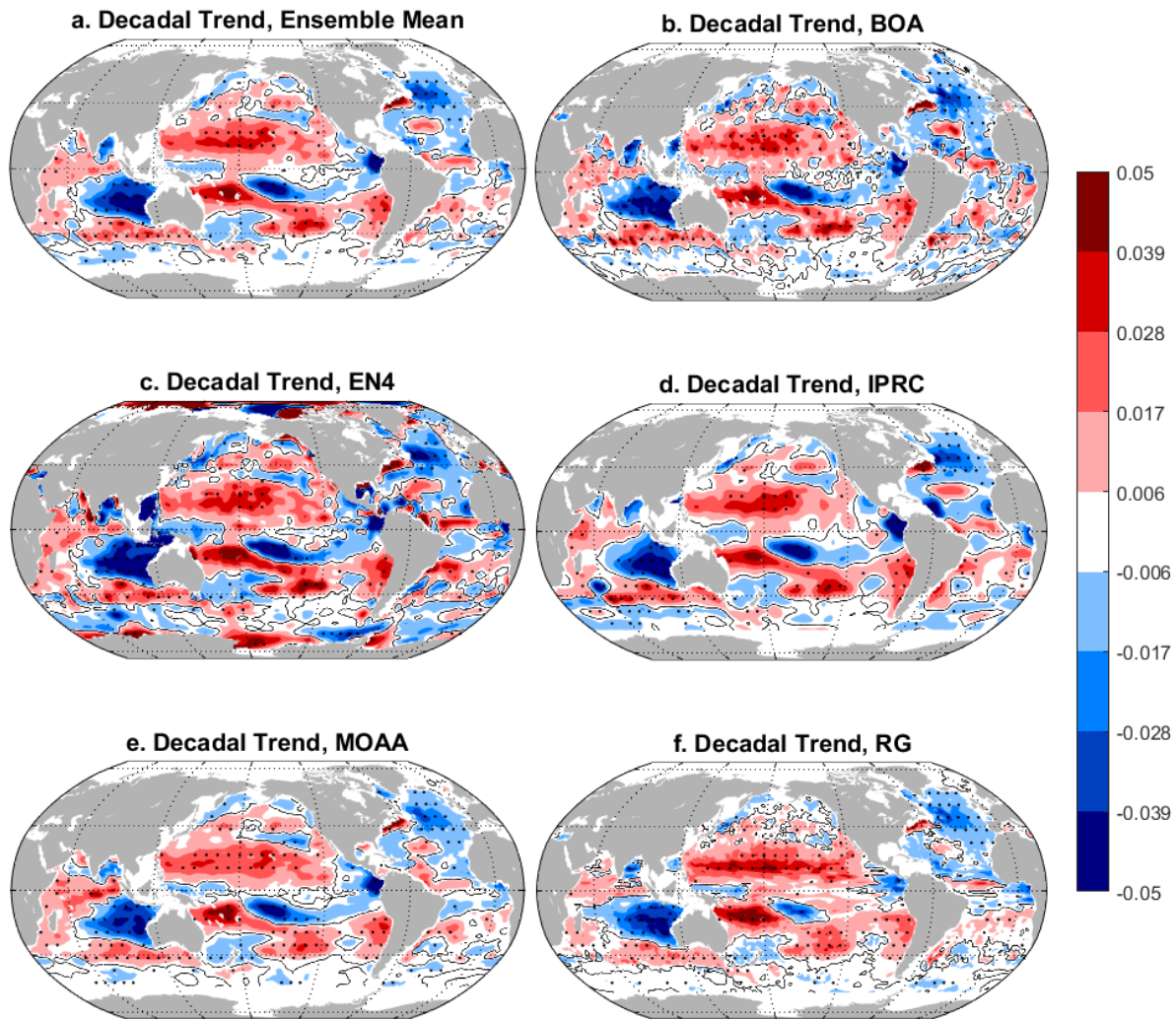


Figure 3.8. The spatial distributions of linear trends on sea surface salinity from 2006 through 2014. (a) The Ensemble Mean and (b-f) each individual dataset. Black contours mark zero. Stippling indicates areas of statistically significant non-zero values at the 95% confidence level. (unit: psu/year)

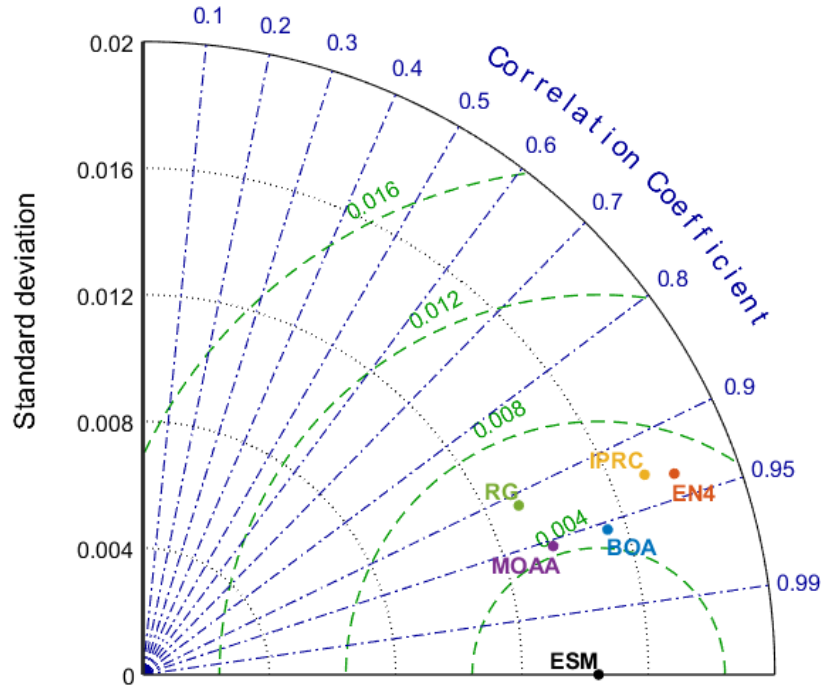


Figure 3.9. Taylor diagram of the spatial distributions of linear trends for the global ocean at sea surface from 2006 through 2014. The plot summarizes the spatial correlation, root mean square difference, and standard deviation of the observed pattern of each Argo products with respect to ESM.

CHAPTER FOUR:

LAYER ONE, 0-700 M

Mean State

The spatial pattern of the climatological mean of the 0-700 m depth-averaged salinity is broadly similar to that of the SSS, confirming that the air-sea freshwater flux is one of the major forcings for upper ocean salinity (Figure 4.1a). Here, we will emphasize features that are different from the sea surface. For example, high surface salinity in the subtropical North Pacific and South Atlantic is diluted in the depth-averaging process by fresher intermediate water, such as the North Pacific Intermediate Water (NPIW) and the Antarctic Intermediate Water (AAIW). Large temporal standard deviations appear along the ACC and the North Atlantic, suggesting the horizontal salinity gradients across major currents and eddy activities are probably major contributors to the temporal variability.

Like the SSS, the distribution of temporal standard deviation of the 0-700 m layer averaged salinity can also be translated into the spatial pattern of SPD with large consistency (Figure 4.1b). Again, the mean SPD of the Atlantic Ocean (0.023 psu) is higher than the global mean of 0.014 psu (Table 4.1). The regions with above average SPD usually have frontal structures and strong flows both in the lateral and vertical direction, many caused by eddies, suggesting that sampling error of the complex, small-scale structure is interfered by vertical averaging.

Further investigation reveals more details on the deviations (Figure 4.2). For the 0-700 m layer, BOA, IPRC and RG are closer to Ensemble Mean (albeit with some small-scale departures near western boundary currents and regions of mesoscale turbulence), while EN4 and MOAA have significant large-scale deviations. This may be due to the background climatological field (primarily the time of the field). While the salinity data and first guess fields of BOA, IPRC and RG solely come from the Argo floats, EN4 and MOAA include other observations and historical data. For instance, the background climatology of EN4 and MOAA approximately represents the average over 1971-2000 with a mean time in 1985, which is approximately 25-years older than that of RG and BOA. Therefore, a paucity of historical salinity measurements in the South Pacific and South Atlantic could lead to high bias in the climatological field, while the disagreements in the better-sampled North Atlantic might indicate the change of the Atlantic Meridional overturning circulation (AMOC) in the Argo Era, or a different mode of the Atlantic Multidecadal Oscillation.

Overall, the climatology pattern of the 0-700 m layer ocean salinity is robust with most of the deviation arising from EN4 and MOAA grids. The zonal patterns in IPRC are still visible, but are offset by similar, yet anti-correlated patterns in RG for the Gulf Stream and ACC regions, in generating the ensemble means

Temporal Variability

For the 0-700 m layer, the disagreements on timeseries of globally averaged salinity anomaly are more visible, although most of the temporal variation is within the 0.01 psu Argo target (Figure 4.3, right axis). The area-weighted, globally averaged salinity anomaly varies from

-0.006 to 0.005 psu with small annual and interannual-decadal fluctuations. The SPD of the horizontally and layered averaged salinity does not exhibit a significant trend, but shows relatively large deviation both in the first and last years (shade in Figure 4.3, left axis), which supports the use of a subset from 2006-2014 to determine the estimated errors.

A Taylor diagram also suggests that higher correlations (0.05 increase for most products) can be achieved using the 2006-2014 rather than 2005-2015 (Figure 4.4). MOAA is the only product that has a correlation less than 0.8, whether using the shorter time period or not. In addition, EN4 and IPRC have the highest temporal standard deviation (over 0.002 psu) as well as the largest increase in correlation when considering the shorter 2006-2014 period (0.07 and 0.06 respectively).

A full-depth salinity anomaly diagram is also used to obtain further details on the robustness and discrepancies at different depths (Figure 4.5a). Much like the SSS, the global ocean salinity in the upper 700 m does not have a strong annual signal. Large interannual variations are particularly strong in the upper 100 m, however, and there appears to be a 2-year lag for the subsurface, as signals travel downwards to the 100-200 m layer. Although the maximum SPD of the global ocean salinity anomaly (0.025 psu) is smaller than that of the climatological mean (0.1 psu, Figure 4.5b). The large values of SPD concentrate in the top 50 m. Based on the corresponding Taylor diagram (Figure 4.6), four out of five products (i.e., MOAA, BOA, RG and IPRC) have similar correlation (above 0.85) and standard deviation, which slightly decreases for period 2006-2014. The only exception is EN4, which has moderate correlation with ESM (0.65) and higher standard deviation (close to 0.01 psu). Further diagnosis (Figure 4.7) supports that EN4 is the leading cause for the relatively high SPD in the upper 50 m.

Horizontally, the spatial pattern of the 0-700 m layer zonal mean (as well as the corresponding SPD) (Figure 4.8a) has a very similar structure to that of SSS (Figure 3.5a) but with a clearer freshening trend between 40-60°N, which is possibly because the vertical averaging dilutes the impact of freshwater input from sea surface of the North Atlantic. Like the sea surface, all gridded Argo products show good agreement on the zonal mean pattern with correlation over 0.85 (Figure 4.9). It is worth note that RG and MOAA have smaller standard deviation (around 0.009 psu) while those of the other products are higher than the 0.01 psu Argo target and close to 0.012 psu. Lower standard deviations suggest the reconstructed variability is weaker in RG and MOAA.

An EOF analysis further reveals that the temporal variations are different between SSS and the averaged 0-700 m salinity (Figure 4.10). While the first three EOF modes account for 56% of the total variance, and the first five EOF modes account for an average of 67%.

The spatial structure of EOF mode 1 (Figure. 4.10a) is similar to that of the EOF mode 2 of SSS, in which two maximum centers (0.13 psu) are found at 40°S and 20°N. The first principal component (Figure 4.10b) resembles a trend with high frequency noises and increases from -0.15 to 0.2, which makes the maximum magnitude of the first EOF mode pattern around -0.02-0.026 psu. EOF mode 1 explains almost 34.7% of the total variance (Table 4.2), and represents a positive decadal trend at 20°N and 40°S, and negative trend between 40-60°N.

For the second EOF mode, an ENSO-like pattern emerges (Figure 4.10c). Two peaks at 0.1 psu are found at 10°S as well as 40°N where the IPRC and BOA salinities are visibly higher at 0.2 psu. The second principal component (Figure 4.10d) is correlated with MEI at 0.74 for 2005-2015. Though the ENSO signals from 2007-2009 are seemingly not well captured, the

second EOF mode of zonal mean salinity anomaly likely represents the ENSO variations and explains an averaged 12.5% variance.

The third EOF mode shows a complicated principal component, which implies some interannual variations but with high frequency noises, and mainly affects 40°N (Figure 4.10e-f). Though most of the products agree in the principal component, EN4 visibly deviates in 2005 that between 40-60°S and near 30°N. The EOF mode 3 alone explains less than 9% of the variance.

Much like for the SSS, the differences between the five gridded products and ESM (Figure 4.8b-f) are negligible for their small values (<0.003 psu) after a 7-month running mean, especially for the tropical region (20°S-20°N). For IPRC and EN4, the large deviations in 2005, examined as part of the third EOF principal component can be further located, as EN4 shows a salty “core” between 40-60°S (Figure 4.8c), and IPRC a fresh “core” near 30°N (Figure 4.8d).

In general, the temporal variability of the 0-700 m layered averaged salinity are robust with correlation over 0.8 for most Argo products. It also should be noted that MOAA has the lowest correlation for the global average timeseries at 0.7, and EN4 has the lowest correlation for the full-depth salinity anomalies at 0.6. The first EOF mode of the zonal mean is a trend that explains 35% of the total variance. The second EOF mode resembles ENSO and explains 12% of the variance, while each of the remaining modes explains less than 10% each. The shift of the dominant mode from ENSO to trend for surface and the layer 0-700 m is possibly due to the vertical averaging, in which the underlying long-term change is highlighted.

Trend

The estimated trends of depth-averaged salinity in the 0-700 m layer are summarized in Table 4.3. While the trend values and uncertainties are smaller than that of SSS, the linear trend

value ranges from 0.45 (RG) to $1.78 \text{ (IPRC)} \times 10^{-4}$ psu/year for 2005-2015, and from 0.95 (MOAA) to $2.84 \text{ (BOA)} \times 10^{-4}$ psu/year for 2006-2014. Most of the trends for period 2006-2014 are larger than those for 2005-2015 except for MOAA, where the estimated trend drops from 1.52 to 0.95×10^{-4} psu/year. However, all uncertainties increase by 30%-45%, when data from 2005-2015 are used. Though a few results are significantly different from zero at 95% confidence interval (i.e., BOA for both subsets, and MOAA for 2005-2015), they are not significantly different from each other due to the large uncertainties. Therefore, it is safe to conclude that for the 0-700 m layer no significant decadal change in the global mean salinity can be detected with the examined gridded Argo products.

Regionally, the estimated trends in the 0-700 m layer largely resemble those of the SSS in the spatial structure with similar major patches of freshening and salinification (Figure 4.11). Values of the regional salinity trends in the 0-700 m layer are around 30-40% of the SSS trends. Many interesting regional patterns appears, such as the salinification patch in the subtropical Atlantic, which is likely due to the denser and saltier Mediterranean outflow since the climate shift in 2005 (e.g., Schroeder et al., 2016). All products show a similar pattern with high spatial correlations to the ESM (over 0.9, Figure 4.12), and MOAA and RG have smaller standard deviation of the observed trend pattern.

In summary, the linear trends in the 0-700 m layer have a similar spatial structure as the SSS and are generally robust. For instance, the correlations of the trend pattern are all over 0.9. However, the estimated trends in RG and MOAA are notably smaller than the other products (although they agree within uncertainty). While the zonal uncertainties are relatively small, large uncertainties are found in the middle southern latitudes on EN4.

Table 4.1. Area-weighted Ensemble Spread of time mean for the 0-700 m layer (unit: psu). Bold number denotes results higher than global mean.

Region	Northern	Southern	Tropical	Total
Global	0.018	0.016	0.013	0.014
Pacific	0.012	0.010	0.010	0.010
Atlantic	0.029	0.023	0.020	0.023
Indian	N/A	0.019	0.011	0.015
Southern Ocean	N/A	N/A	N/A	0.013

Northern: 30-60°N; Tropical: 30°S-30°N; Southern: 30-50°S; Southern Ocean: 50-60°S.

Table 4.2. Variance explained by the first 5 principal components of the zonal mean salinity anomaly of the 0-700 m layer from 2005 through 2015. Averaged explained variance of the six products (five gridded Argo data and ESM), total number of the first three modes and first five modes and are also given.

Products	Mode 1	Mode 2	Mode 3	Subtotal	Mode 4	Mode 5	Total
BOA	29.8%	13.0%	8.7%	53.0%	5.7%	4.6%	61.8%
EN4	31.4%	13.3%	10.3%	52.7%	6.5%	6.1%	67.6%
IPRC	34.4%	12.5%	10.0%	57.5%	7.4%	6.5%	70.8%
MOAA	37.3%	10.5%	7.9%	55.8%	5.2%	4.2%	65.1%
RG	35.8%	12.5%	6.7%	56.2%	5.1%	4.2%	64.3%
ESM	39.3%	13.2%	8.2%	57.7%	5.8%	4.5%	71.0%
AVERAGE	34.7%	12.5%	8.6%	55.8%	6.0%	5.0%	66.8%

Table 4.3. Decadal trends of global mean salinity of the 0-700 m layer from each individual dataset and Ensemble Mean (unit: 10^{-4} psu/year). Bold number indicates result significantly different from zero at the 95% confidence level.

Products	Subset 1: 2005-2015	Subset 2: 2006-2014
BOA	1.96±1.36	2.84±1.81
EN4	0.49±2.51	1.89±3.30
IPRC	1.78±2.21	2.68±3.23
MOAA	1.52±1.12	0.95±1.65
RG	0.45±1.72	1.69±2.21
ESM	1.24±1.54	2.01±2.15

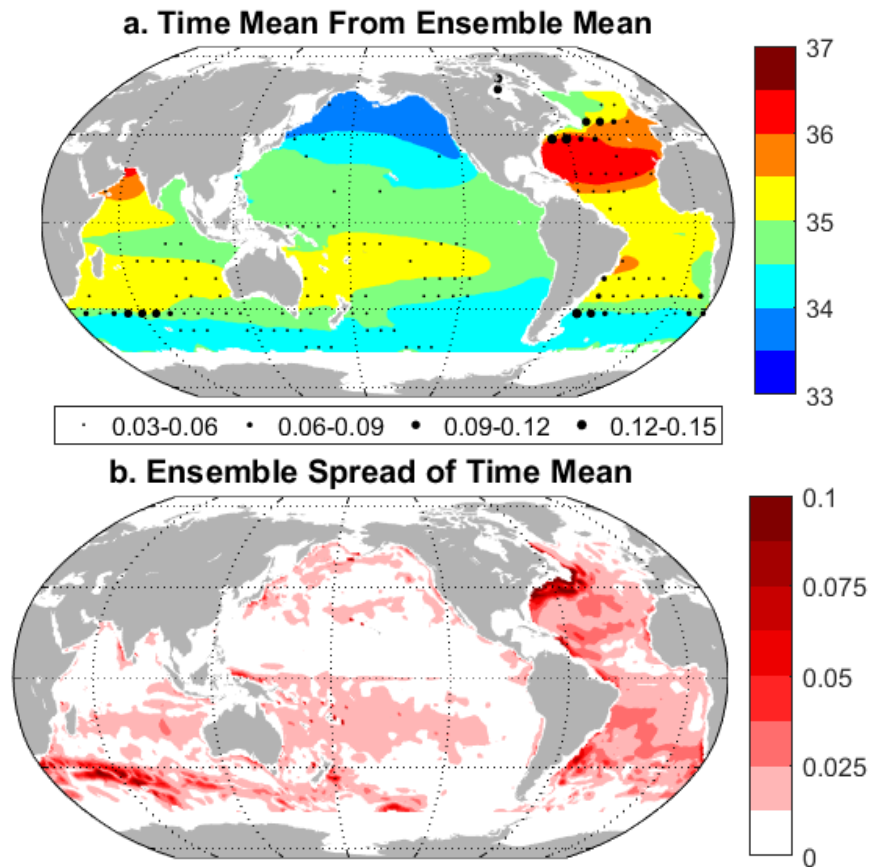


Figure 4.1. The spatial distributions of the salinity time mean of the 0-700 m layer, from 2005 through 2015. (a) The Ensemble Mean, stippling marks the temporal standard deviation, (b) its Ensemble Spread. (unit: psu)

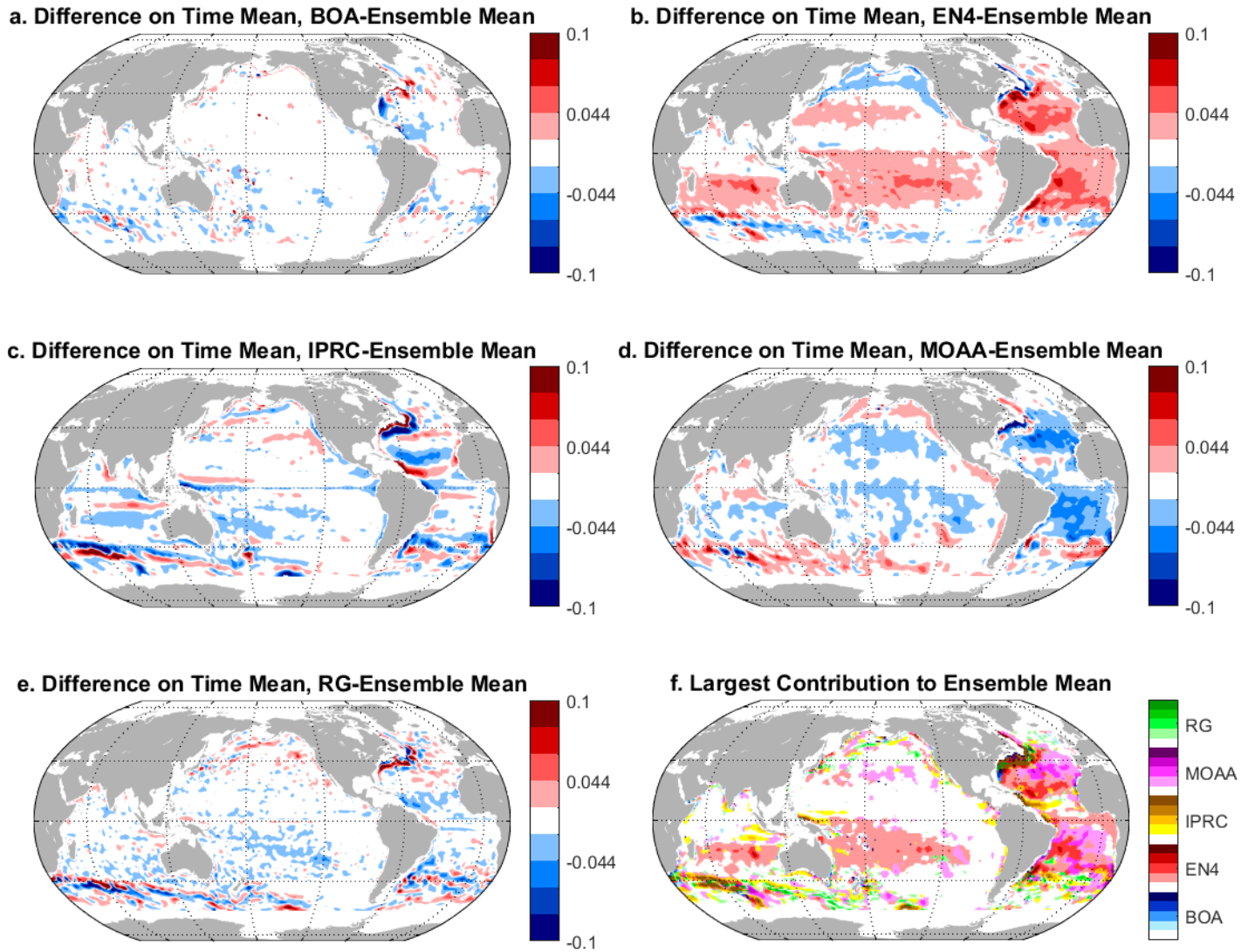


Figure 4.2. The spatial distributions of the difference on salinity time mean of the 0-700 m layer. (a-e) The difference on time mean, (f) the largest deviation to the Ensemble Mean. The range for each color is the same as the difference. (unit: psu)

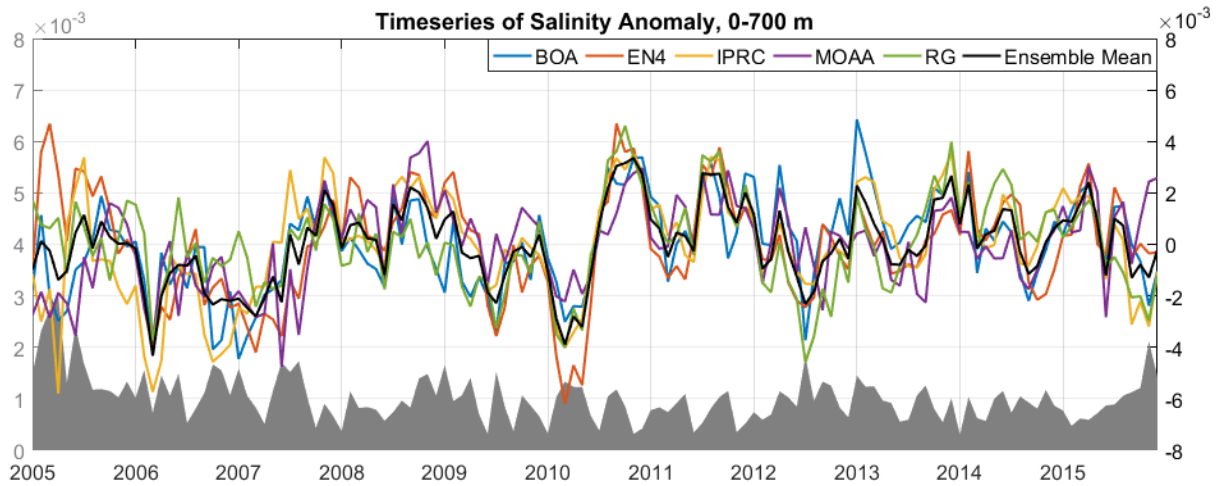


Figure 4.3. Timeseries of global mean salinity anomaly of the 0-700 m layer (right axis). Shade (left axis) indicates the Ensemble Spread of the datasets. (unit: psu)

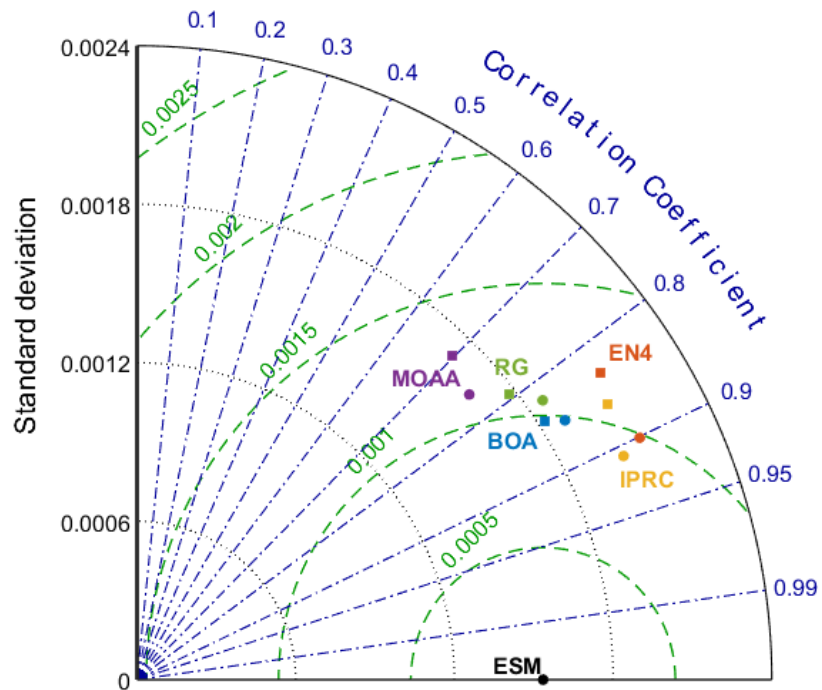


Figure 4.4. Taylor diagram of the timeseries of global mean salinity anomaly of the 0-700 m layer. Squares mark the subset from 2005 through 2015 and circles mark from 2006 through 2014. The plot summarizes the correlation, root mean square difference, and temporal standard deviation of each of the Argo products with respect to ESM.

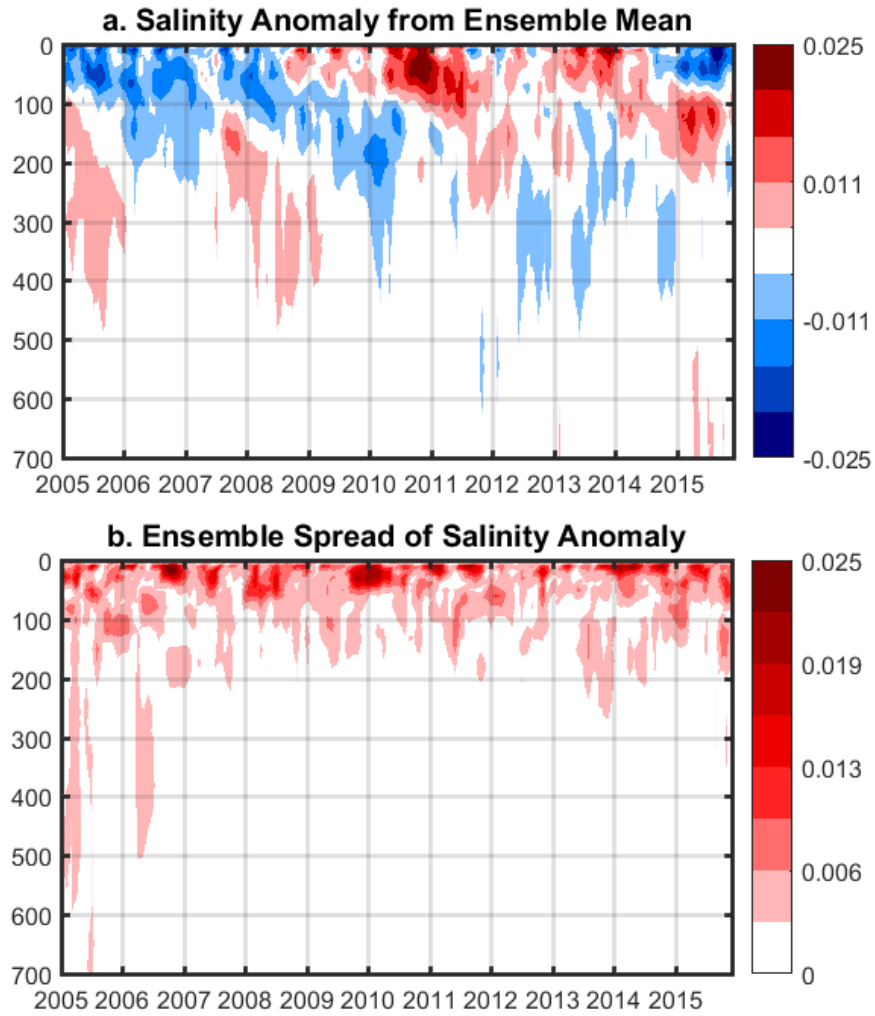


Figure 4.5. The depth distributions of global mean salinity anomaly over the 0-700 m layer, from 2005 through 2015. (a) The Ensemble Mean and (b) its Ensemble Spread. (unit: psu)

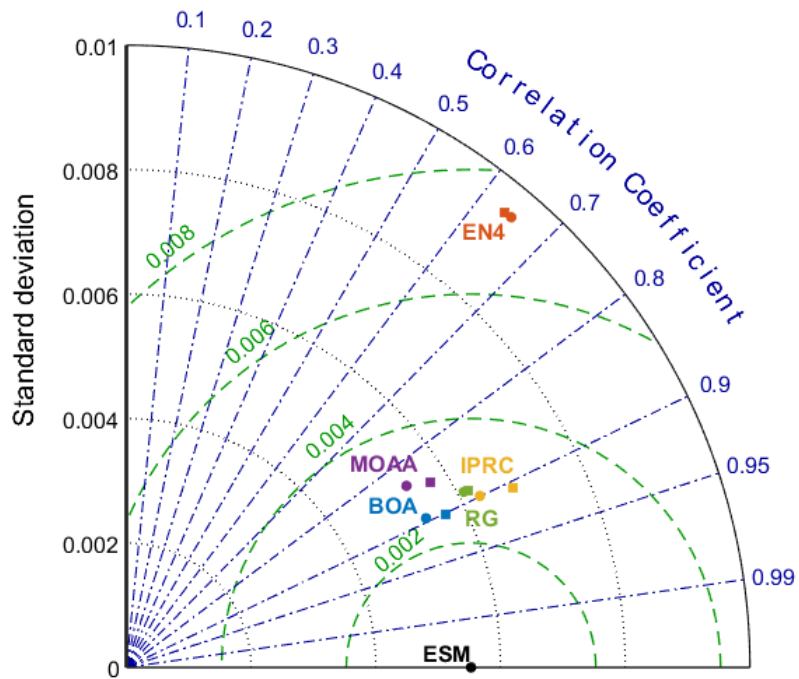


Figure 4.6. Taylor diagram of the depth distribution of global mean salinity anomaly over the 0-700 m layer. Squares mark the subset from 2005 through 2015 and circles mark from 2006 through 2014. The plot summarizes the correlation, root mean square difference, and standard deviation of the observed pattern of each Argo products with respect to ESM.

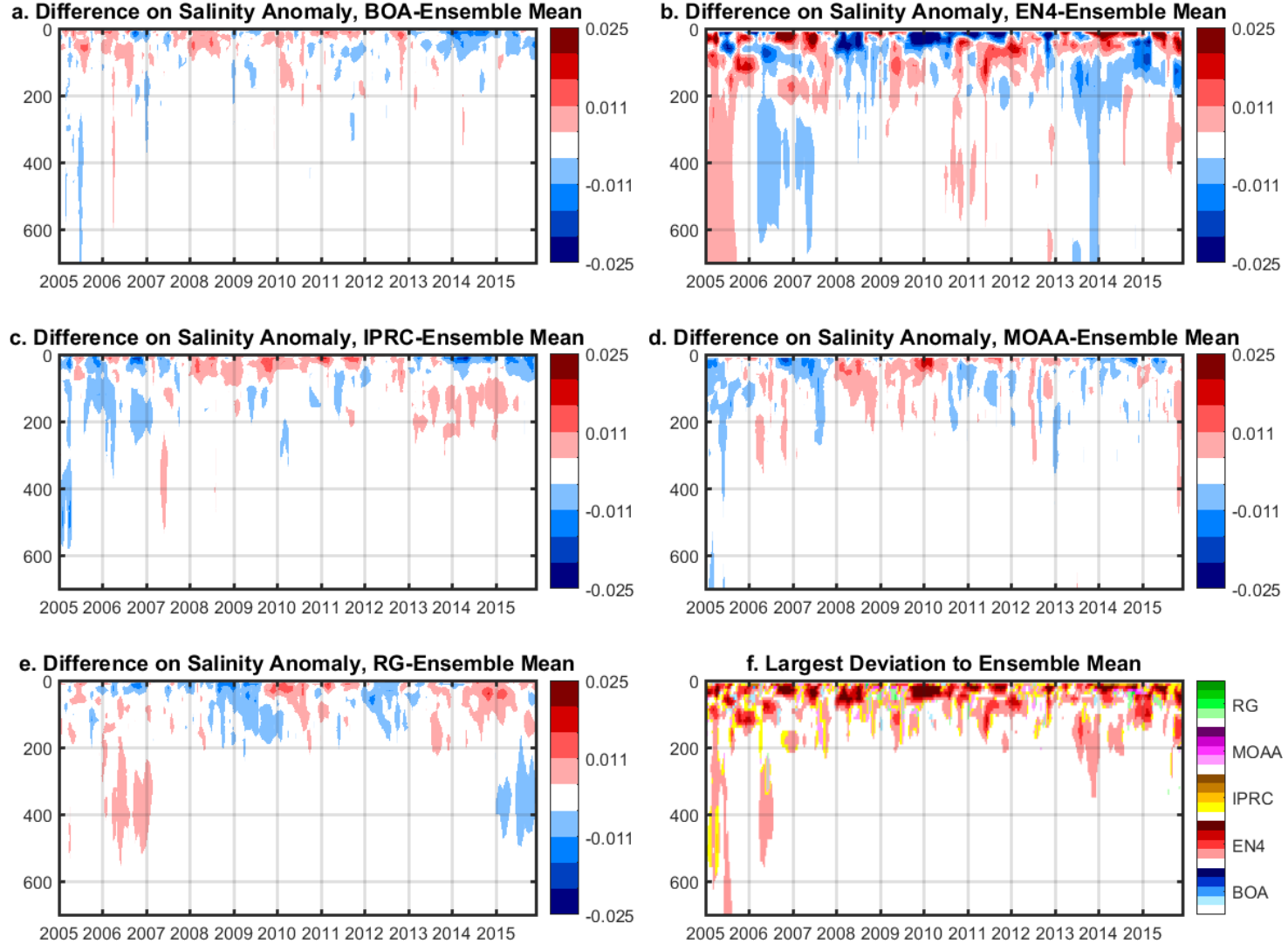


Figure 4.7. The depth distributions of the difference on salinity anomaly over the 0-700 m layer. (a-e) The difference on salinity anomaly and (f) the largest deviation to the Ensemble Mean. The range for each color is the same as the difference. (unit: psu)

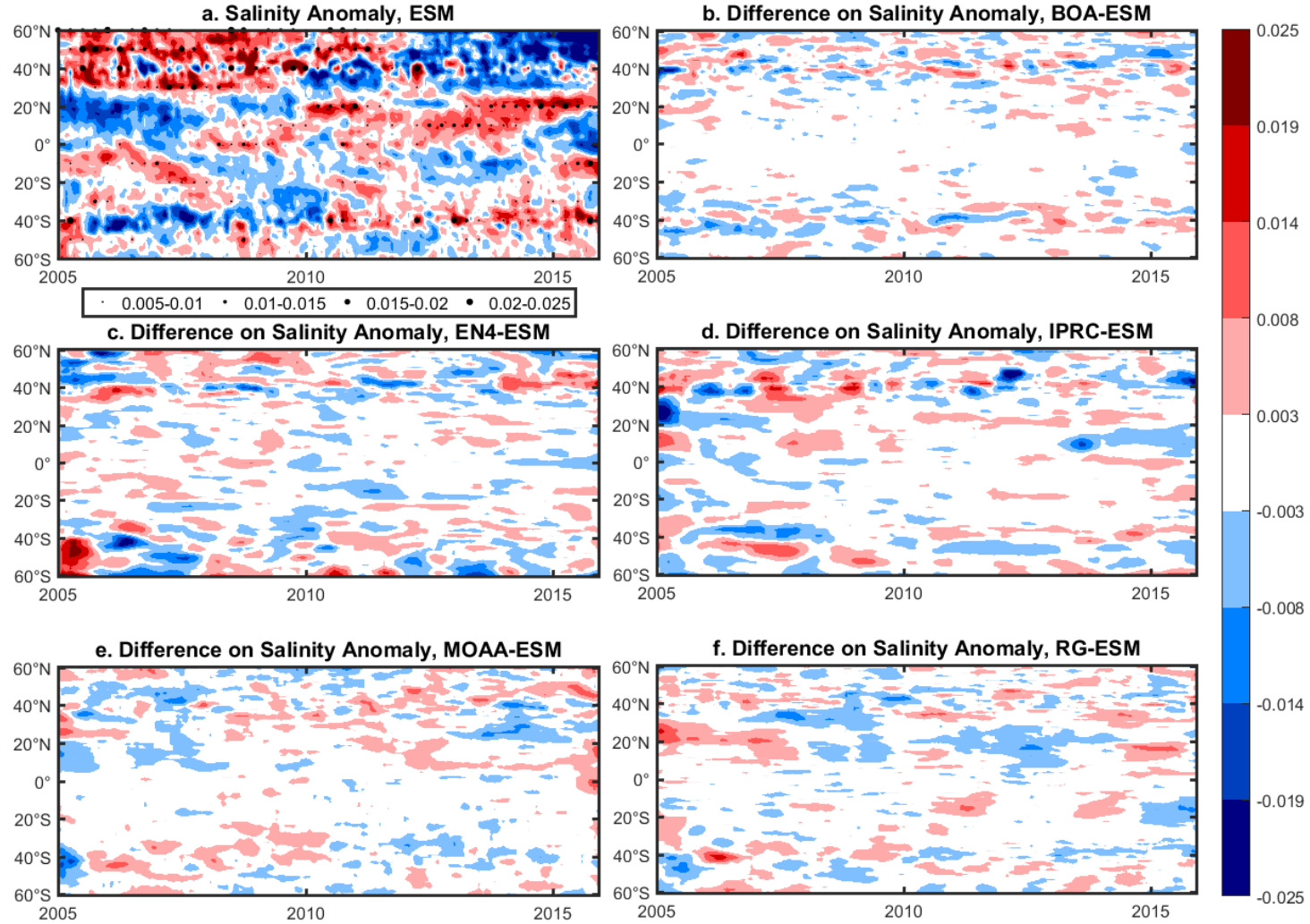


Figure 4.8. The spatial distributions of zonal mean of salinity anomaly of the 0-700 m layer from 2005 through 2015. (a) the Ensemble Mean, (b-f) the difference between each individual dataset and the Ensemble Mean. The annual signal is removed using an annual sinusoid model. Stippling in (a) indicates the range of the Ensemble Spread. A 7-month running mean is applied to (b-f). (unit: psu)

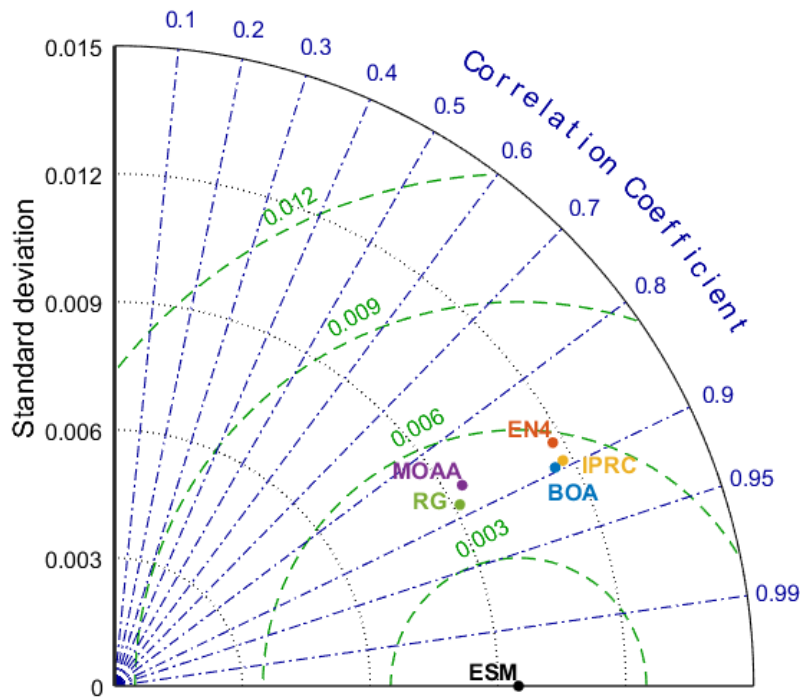


Figure 4.9. Taylor diagram of zonal mean of salinity anomaly of the 0-700 m layer from 2005 through 2015. The plot summarizes the correlation, root mean square difference, and standard deviation of the observed pattern of each Argo products with respect to ESM.

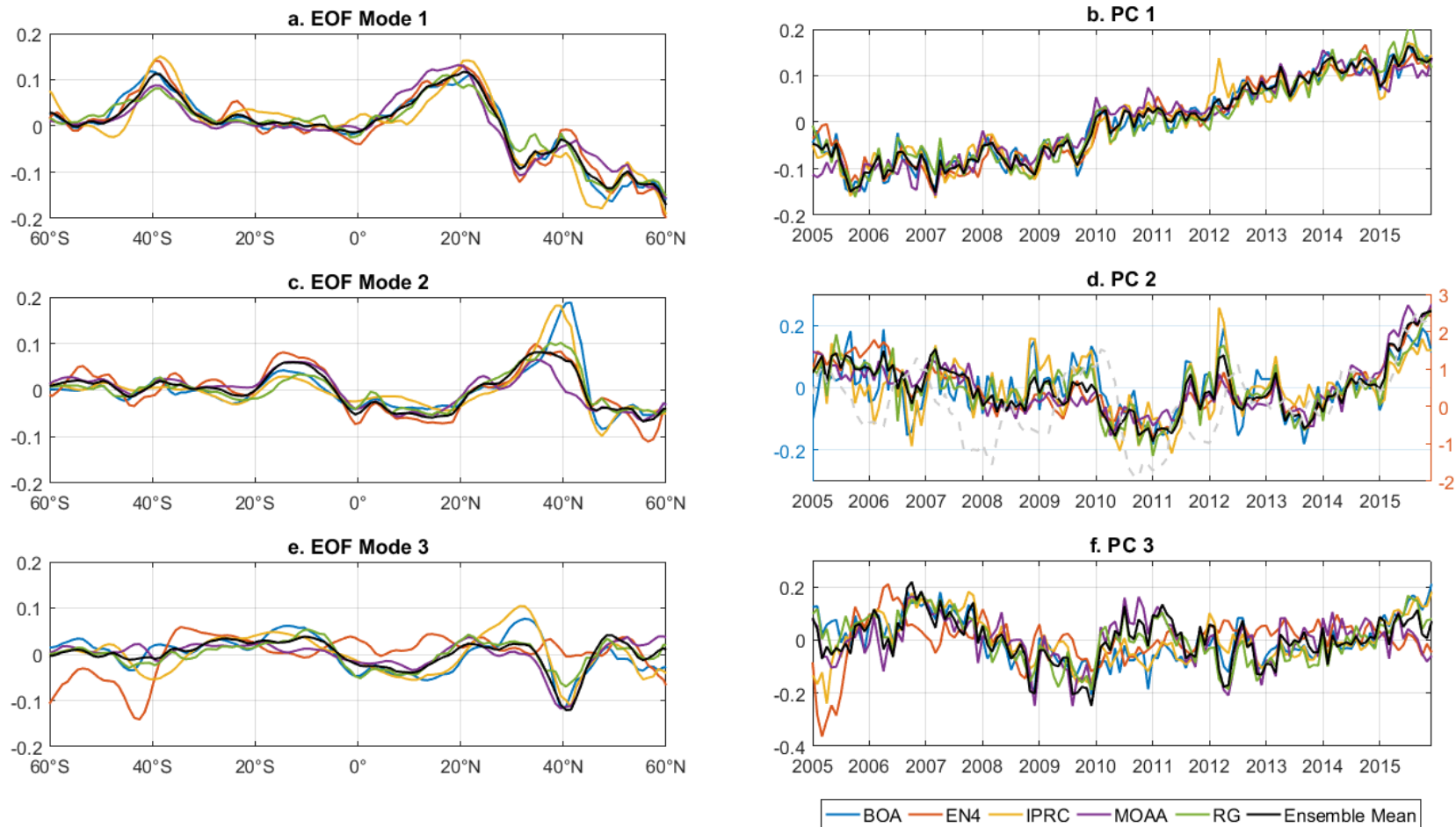


Figure 4.10. First three (a, c, e) EOF modes and (b, d, f) principle components of zonal mean of salinity anomaly of the 0-700 m layer from 2005 through 2015. Dash line in the PC 2 denotes the MEI (right axis).

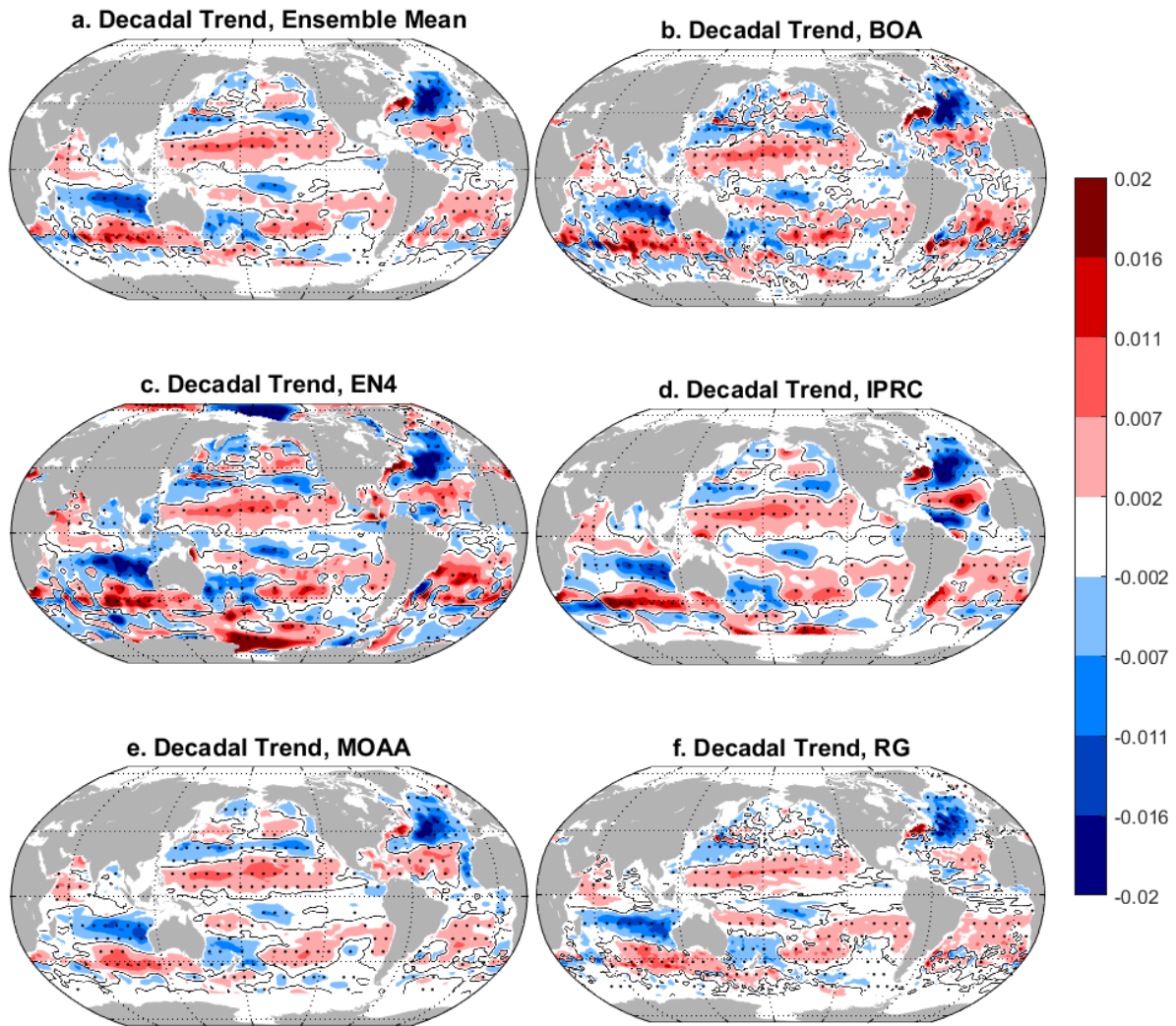


Figure 4.11. The spatial distributions of linear trends of the 0-700 m layer from 2006 through 2014. (a) The Ensemble Mean and (b-f) each individual dataset. Black contours mark zero. Stippling indicates areas of statistically significant non-zero values at the 95% confidence level. (unit: psu/year)

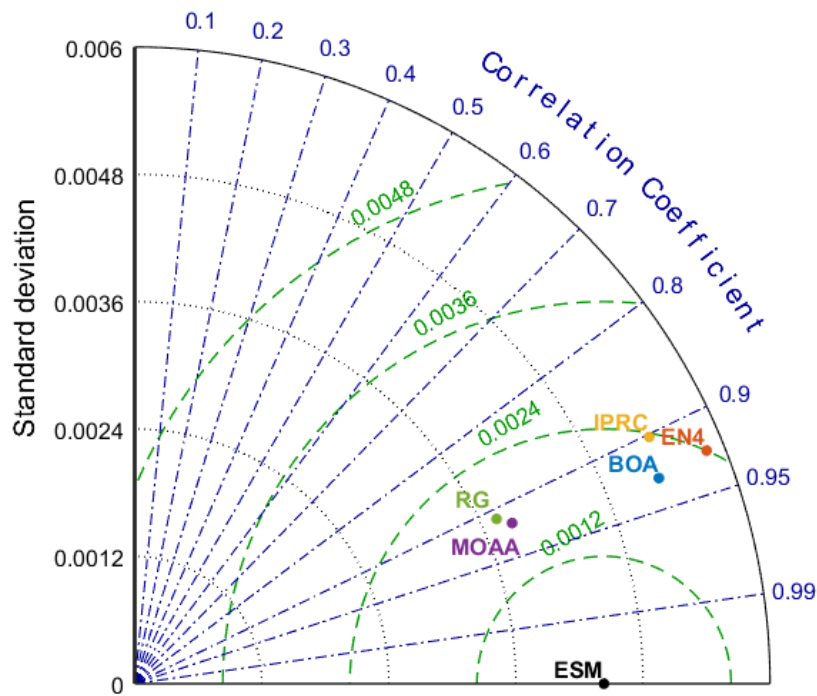


Figure 4.12. Taylor diagram of the spatial distributions of linear trends of the 0-700 m layer from 2006 through 2014. The plot summarizes the spatial correlation, root mean square difference, and standard deviation of the observed pattern of each Argo products with respect to ESM.

CHAPTER FIVE:

LAYER TWO, 700-2000 M

Mean State

The climatological mean of 700-2000 m depth-averaged salinity is markedly different from the upper 700 m and sea surface (Figure 5.1a). Only the northern tip of the Indian Ocean and the northern sub-tropical North Atlantic have salinity higher than 35 psu. This distribution is attributed to the density-driven flows from saltier and denser semi-enclosed marginal seas (the Red Sea and the Mediterranean Sea), which is supported by the matching pattern of temporal standard deviation. For the layer of 700-2000 m, relatively strong temporal variation can only be seen in the aforementioned two regions and the ACC. Meanwhile low salinity regions appear in the Southern Ocean and North Pacific, being associated with the fresher AAIW and NPIW, respectively.

The largest values of SPD occur in regions of both low and high salinity (Figure 5.1b). While the global mean SPD (0.007 psu) is significantly smaller than the upper ocean, the mean SPD in the Southern Ocean is 2-3 times larger (Table 5.1). The Atlantic and Indian Oceans also show similar high SPD except in the tropics. Since the intermediate water in the Southern Hemisphere is less sampled, paucity of salinity observations and sampling errors is a likely contributor to the high SPD.

The majority of the high SPD can be attributed to large deviations in EN4 (Figure 5.2b, f), where the Mediterranean Outflow and North Indian Ocean are substantially below ESM, and

the Southern Ocean is above. The historical background climatological field used in EN4 (WOA98) might cause these broad-scale deviations, but further investigation is required to confirm this. The bias in the Southern Ocean in EN4 are offset by BOA and RG in which the background fields are solely based on the better sampled Argo profiles after mid-2000s. This supports the hypotheses that the climatology from pre-Argo dataset (e.g., WOA98, WOA01) is biasing the results.

In general, the mean state of the 700-2000 m layer ocean salinity is still robust, with most of the deviation coming from EN4.

Temporal Variability

The timeseries of globally averaged salinity anomaly with in the layer 700-2000 m generally varies between -0.0015 and 0.002 psu (Figure 5.3, right axis). The variation is well below the 0.01 psu Argo target and thus should not be overinterpreted. The largest disagreements in this layer occur in 2005, when EN4 is above average in the summer and IPRC is far below average in the first few months. MOAA is above ESM from 2011 to mid-2014, and nearly all products become more dispersed after 2014. Based on the corresponding SPD (Figure 5.3, left axis), differences are only small during 2009-2011. Therefore, the necessity to use a subset from 2006-2014 to reduce error is again highlighted.

The Taylor diagram (Figure 5.4) shows that MOAA has the lowest correlation with ESM (0.5-0.6), and BOA has the highest (0.85-0.9). Only data from 2006-2014 slightly increases the correlations and reduces the temporal standard deviations, particularly for BOA, EN4 and IPRC.

The most striking features of the non-vertically averaged salinity anomalies (Figure 5.5a), are the bands of positive and negative anomalies in some years (e.g., 2006, 2008, 2011 and

2015), suggesting similar magnitude of salinity anomalies at all depths. It should be noted that the SPD for many of these is small, indicating all products show the same feature. It is physically implausible for the global ocean to behave in this manner, so this either indicates a level of uncertainty in the deep salinity data from the grids or could be the result of deep convection in one or two small regions that aliases into the global average.

The ratio of SPD to ESM is high (50%), especially in 2005 and 2013, even though the maximum value is still much smaller than 0.01 psu (Figure 5.5b). The corresponding Taylor diagram (Figure 5.6) again suggests most of the deviations come from the first and last years on EN4 and IPRC, while the other three products (i.e., MOAA, BOA and RG) have similar correlation (0.65-0.8) and standard deviation. EN4 has the lowest correlation with ESM around 0.55-0.6. Further diagnosis (Figure 5.7) reveals that EN4 is the leading cause for most of the high SPD due to weaker variations. MOAA shows an increasing trend which can also be seen in Figure 5.3, while BOA and RG vary oppositely. Interestingly, a reoccurring annual signal is visible between 800-1000 m on IPRC, in which a fresh center appears in 2005 and impacts the depth-averaged salinity, and a salty signal reappears annually afterwards. In summary, most of the largest deviation comes from EN4, followed by IPRC.

Horizontally, all Argo products show good agreement on the pattern of the zonal mean with small SPD (Figure 5.8, a) and have correlations around 0.8 (Figure 5.9). The spatial structure of the zonal pattern consists of a series of trends, which are positive mostly in the tropical and negative in 30-50°S, and an interannual-decadal variation at 40-60°N. In addition, after a 7-month running mean, the differences between the five gridded products and ESM (Figure 5.8, b-f) are much smaller than the 0.01 psu Argo target in most circumstances. Nevertheless, a few interesting features emerge on the pattern. The reoccurring annual anomaly

on IPRC resurfaces again at 30°N, and can be further located at 25°W in the North Atlantic. RG shows broad and weaker salinity variations by presenting an opposite pattern of difference to the ESM salinity anomaly, which are mostly offset by MOAA and IPRC. These below average variabilities on RG are particularly evident in the tropical region and 40-60°N, and come mostly from the tropical Pacific and North Atlantic (see next section).

An EOF analysis reveals that strongest signals are located in the subpolar regions of the Northern Hemisphere (Figure 5.10a). The spatial structure of EOF mode 1 has a peak of 0.05 psu around 35°N (except IPRC, in which the peak shifts to 27°N). This striking peak corresponds to the Mediterranean Outflow region, where the temporal variability is obviously stronger than the rest of the ocean (Figure 5.1a). The first principal component (Figure 5.10b) represents interannual-decadal variability (ranging from -0.2 to 0.2) for most of the products (i.e., BOA, EN4, MOAA, RG) that is high in 2006-2007 and low in 2010-2011. It explains an average of 26.3% of the total variance (Table 5.2).

Larger discrepancies arise in the second EOF modes (Figure 5.10c-d), indicating less agreement in the products. This mode explains 15-21% of the observed variance in the products. The second principle component resembles a trend varying from -0.2 to 0.2 with high frequency noise for most of the gridded products, but BOA and IPRC are visibly smaller. For the spatial pattern, BOA is slightly positive around 40-60°N while the other products are negative with two valleys, and IPRC is high near the equator and low at 20-40°N.

The third EOF mode for the 700-2000 m layer resembles that of 0-700 m layer to an extent (Figure 5.10e-f). The third principal component is dominated by high frequency noise, and its mainly expression is around 40°N. The EOF mode 3 explains 10% of the variance, while the

first three EOF modes account for 53.9% of the total variance on average, and the first five EOF modes account for an average of 64.2%.

In general, the temporal variability of the 700-2000 m layer is less robust than that of the 0-700 m. For most gridded Argo products, the correlations are at 0.6-0.8 for both the depth-averaged timeseries and full-depth salinity anomalies. The ratio of SPD to ESM is still high (50%), implying large noise. The first EOF mode of the zonal mean represents an interannual-decadal fluctuation that explains 26% of the total variance. The second EOF mode roughly resembles a trend and explains 17% while each of the rest modes explains less than 10% on average. A suspicious annual anomaly on IPRC is revealed around 900 m in the North Atlantic, approximately at 30°N, 25°W (Figure A3, Figure B3), which again locates in the Mediterranean Outflow region. Meanwhile, RG shows below average salinity variations in the tropical Pacific.

Trend

The estimated trends of depth-averaged salinity in the 700-2000 m layer are summarized in Table 5.3. The depth-averaged salinity trends for the deeper layer are comparable to the upper 700 m layer with similar trend values and smaller uncertainties. For the period 2005-2015, the estimated trend value ranges from -0.69 (EN4) to $1.54 \text{ (MOAA)} \times 10^{-4}$ psu/year, and the uncertainties varies from 0.47 (MOAA) to $1.23 \text{ (EN4)} \times 10^{-4}$ psu/year. Although the trends in IPRC and MOAA are significantly different from zero at 95% confidence interval, the decadal change of depth-averaged salinity is still insignificant due to the overlaps with other products. Similarly, the linear trends for period 2006-2014 also show a wide range from -1.16 (EN4) to $1.68 \text{ (MOAA)} \times 10^{-4}$ psu/year. MOAA and EN4 still show smallest and largest uncertainties at 0.68 and 1.02×10^{-4} psu/year, respectively. While most of the uncertainty (i.e., BOA, EN4 and

IPRC) is reduced by 15-20%, the positive and negative trends estimated for EN4, MOAA and RG are enhanced and significantly different from zero. Therefore, extra attention should be paid on the trend evaluation of depth-averaged salinity during 2006-2014.

In addition, the decadal trends of the depth-averaged salinity in the entire 0-2000 m layer are also calculated (Table 5.4). Though the estimated trend values and uncertainties are at the same level to those of the 700-2000 m layer for all products, it is noteworthy that only MOAA and RG are significantly different from zero (although still not significant different from the other results), however MOAA and RG trends have opposite signs. Thus, based on the high uncertainty in some products and the opposite trends between MOAA and RG, we must conclude there has been no significant trend in the globally averaged salinity for 0-2000 m.

Regionally, some large-scale features (e.g., salinification in the Pacific, freshening in the Atlantic) are still relatively robust between 700-2000 m, but trends in BOA and EN4 are substantially noisy (Figure 5.11). For example, IPRC and MOAA show a noticeable positive trend in the East Indian Ocean, RG and BOA show lesser trends, but EN4 shows large positive and negative trends. In the North Atlantic, most datasets suggest large scale freshening in the Sargasso Sea, but RG indicates a smaller value. Unlike the sea surface, the robust positive trend in the Pacific sector of the Polar Front (south of 50°S, 150°E-120°W) is observed by all gridded products.

The corresponding Taylor diagram (Figure 5.12) shows the spatial correlations for the 700-2000 m layer are around 0.9, but the trends of MOAA and RG are generally smaller, consistent with their lower standard deviations.

The most obvious discrepancy in the spatial patterns for the 700-2000 m layer occurs in the tropical Pacific Ocean (Figure 5.13). As shown before (Figure. 5.8 and 5.9), the positive

trend in the tropical Pacific is readily evident in all products except RG, where the salinity change is visibly smaller. Between 25°S-25°N, though the regional trends in EN4 are less statistically significant than others, nearly all the products suggest a more saline tropical Pacific since 2006. The estimated trend for the regional area-averaged salinity ranges from 2.45 (EN4) to $9.38 \text{ (MOAA)} \times 10^{-4}$ psu/year with relatively small uncertainty ($1.0\text{-}2.0 \times 10^{-4}$ psu/year). While trend values in MOAA are much larger than the other results, most trends overlap around 4.0×10^{-4} psu/year. However, the salinity trend on RG gives the only insignificant trend ($1.75 \pm 2.89 \times 10^{-4}$ psu/year) among all the results. Although the trend number on RG still overlaps with other datasets except MOAA, it is worth Note that most of the regional trend in RG, whether positive or negative, are statistically significant. RG also has the lowest regional spatial correlation around 0.6 (Figure 5.14), while that of the other products is 0.7-0.9.

Much like the conclusions on temporal variability, the regional salinity trends in the 700-2000 m layer are robust on the broad-scale (i.e., global and basin-scale), but can be very different on smaller scales (i.e., mesoscale). RG and MOAA show below and above average trends in the tropical Pacific, respectively. EN4 shows considerable uncertainty in the South Atlantic and South Indian Ocean. It is also noteworthy that the uncertainties of the linear trends are generally larger in the subpolar region rather the tropical ocean, which is the opposite of the sea surface. It should also be noticed that strong deep vertical transport is found in the North Atlantic (Buckley and Marshall, 2016) and North Indian Ocean (Thompson et al., 2016), which might contribute to these discrepancies and uncertainties as well.

Table 5.1. Area-weighted Ensemble Spread of time mean for the 700-2000 m layer (unit: psu). Bold number denotes results higher than global mean.

Region	Northern	Southern	Tropical	Total
Global	0.007	0.010	0.004	0.007
Pacific	0.005	0.008	0.004	0.005
Atlantic	0.011	0.013	0.006	0.009
Indian	N/A	0.010	0.006	0.008
Southern Ocean	N/A	N/A	N/A	0.007

Table 5.2. Variance explained by the first 5 principal components of the zonal mean salinity anomaly of the 700-2000 m layer from 2005 through 2015. Averaged explained variance of the six products (five gridded Argo data and ESM), total number of the first three modes and first five modes and are also given.

Products	Mode 1	Mode 2	Mode 3	Subtotal	Mode 4	Mode 5	Total
BOA	22.4%	15.8%	8.1%	46.3%	5.2%	5.1%	56.6%
EN4	24.8%	15.9%	13.0%	53.7%	6.0%	4.9%	64.6%
IPRC	34.5%	18.8%	11.0%	64.3%	6.0%	4.0%	74.3%
MOAA	25.5%	16.9%	8.0%	50.4%	4.9%	4.5%	59.8%
RG	23.8%	17.3%	11.5%	52.6%	6.2%	4.2%	63.0%
ESM	26.6%	21.2%	8.5%	56.3%	5.5%	5.0%	66.8%
AVERAGE	26.3%	17.7%	10.0%	53.9%	5.6%	4.6%	64.2%

Table 5.3. Decadal trends of global mean salinity of the 700-2000 m layer from each individual dataset and Ensemble Mean (unit: 10^{-4} psu/year). Bold number indicates result significantly different from zero at the 95% confidence level.

Products	Subset 1: 2005-2015	Subset 2: 2006-2014
BOA	0.39±1.19	-0.27±1.01
EN4	-0.69±1.23	-1.15±1.02
IPRC	1.50±1.10	0.08±0.73
MOAA	1.54±0.47	1.68±0.68
RG	-0.56±0.58	-0.81±0.76
ESM	0.43±0.89	-0.09±0.87

Table 5.4. Decadal trends of global mean salinity of the 0-2000 m layer from each individual dataset and Ensemble Mean (unit: 10^{-4} psu/year). Bold number indicates result significantly different from zero at the 95% confidence level.

Products	Subset 1: 2005-2015	Subset 2: 2006-2014
BOA	0.65±1.20	-0.11±0.94
EN4	-0.69±1.98	-0.92±1.30
IPRC	1.17±1.18	0.13±1.13
MOAA	1.15±0.61	0.80±0.69
RG	-1.08±0.97	-1.31±1.17
ESM	0.24±1.25	-0.24±1.07

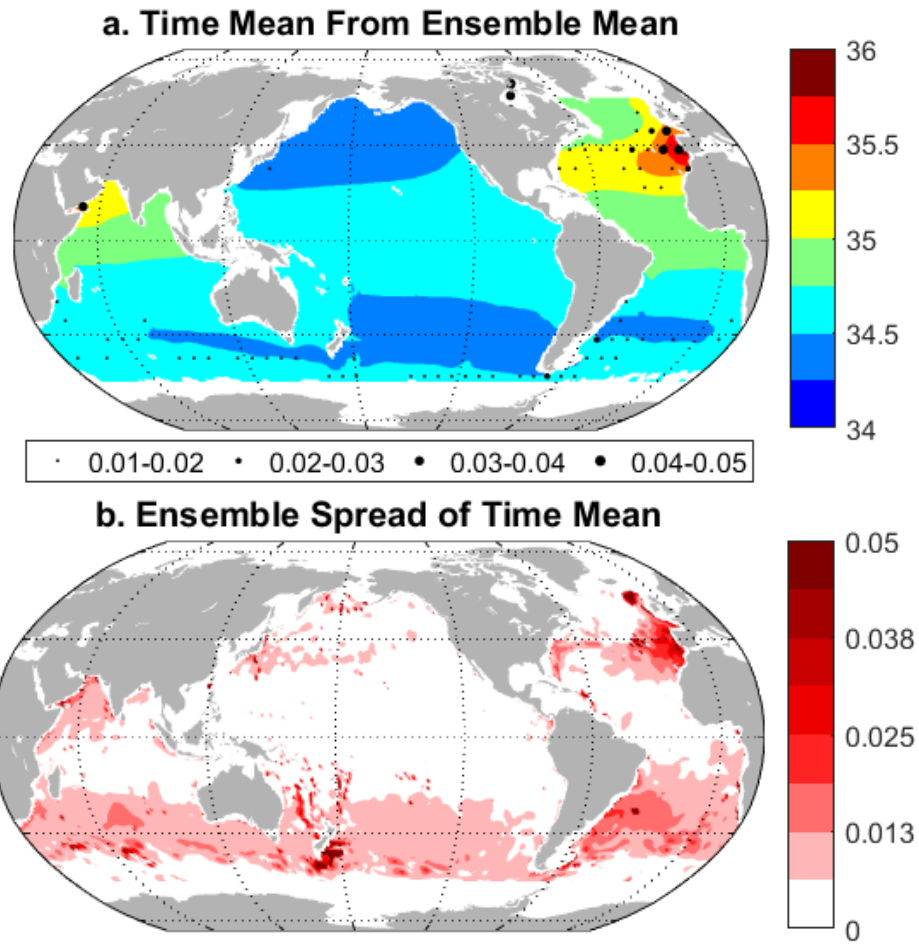


Figure 5.1. The spatial distributions of the time mean of the 700-2000 m layer, from 2005 through 2015. (a) The Ensemble Mean, stippling marks the temporal standard deviation, (b) its Ensemble Spread (unit: psu)

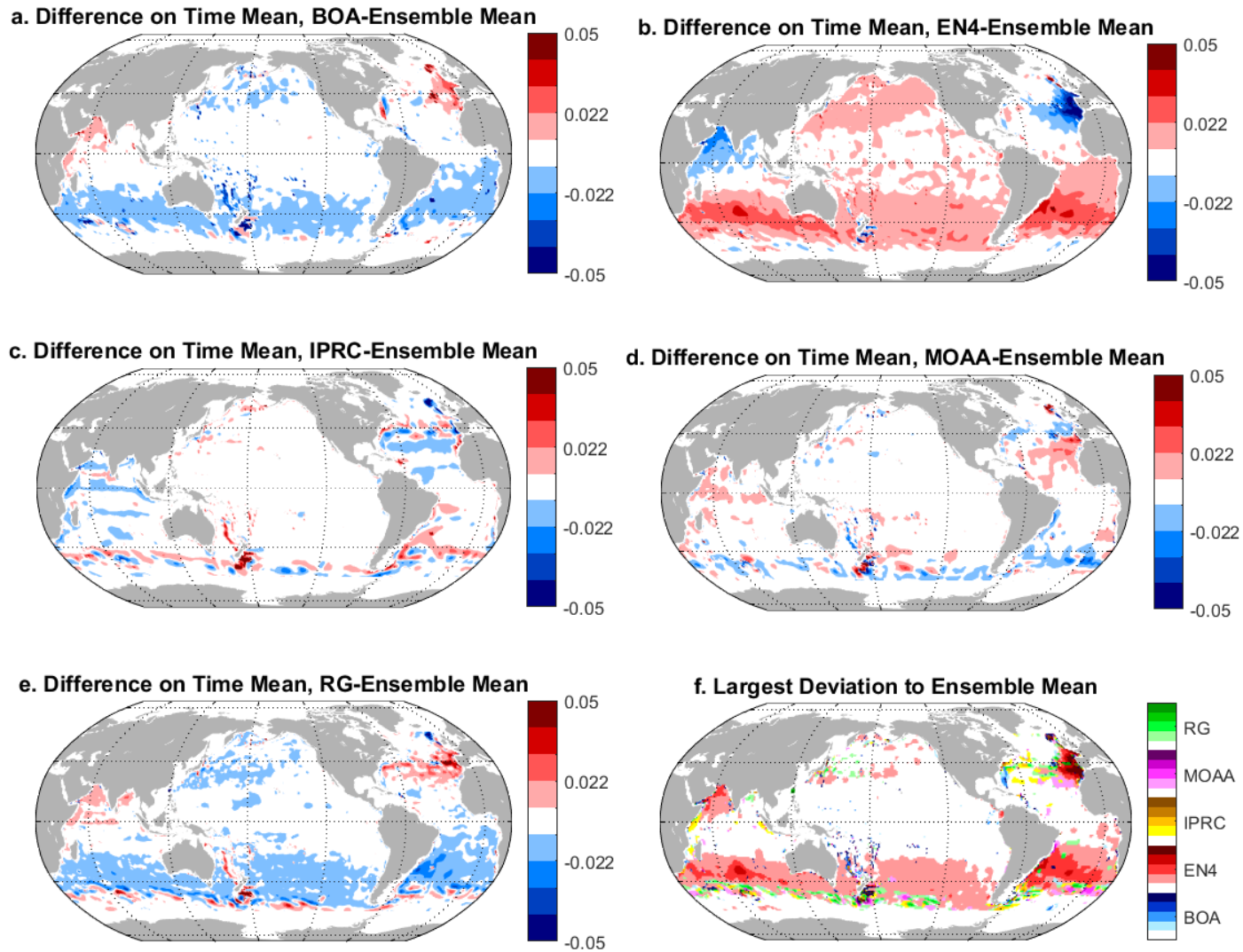


Figure 5.2. The spatial distributions of the difference on salinity time mean of the 700-2000 m layer. (a-e) the difference on time mean, (f) the largest deviation to the Ensemble Mean. The range for each color is the same as the difference. (unit: psu)

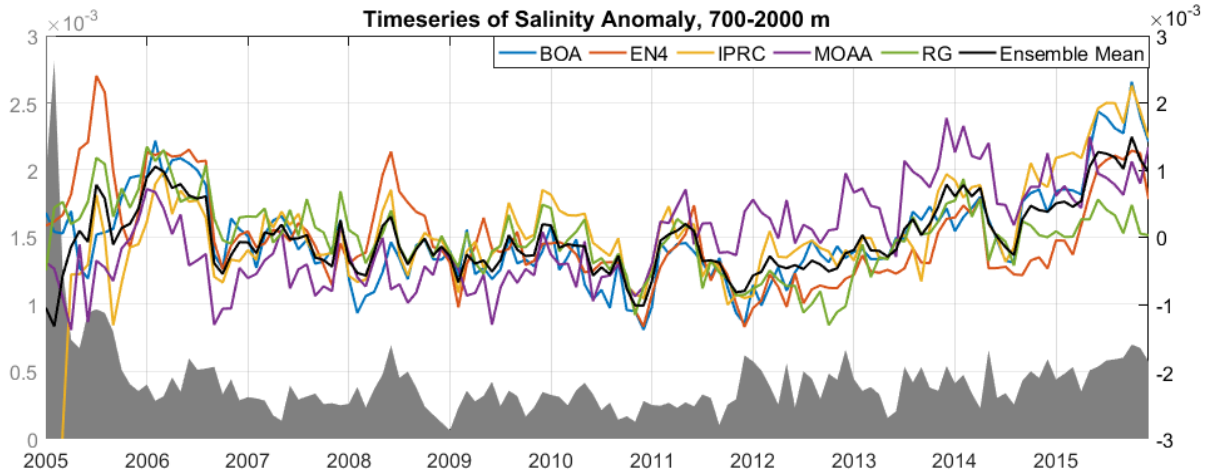


Figure 5.3. Timeseries of global mean salinity anomaly of the 700-2000 m layer (right axis). Shade (left axis) indicates the Ensemble Spread of the datasets. (unit: psu)

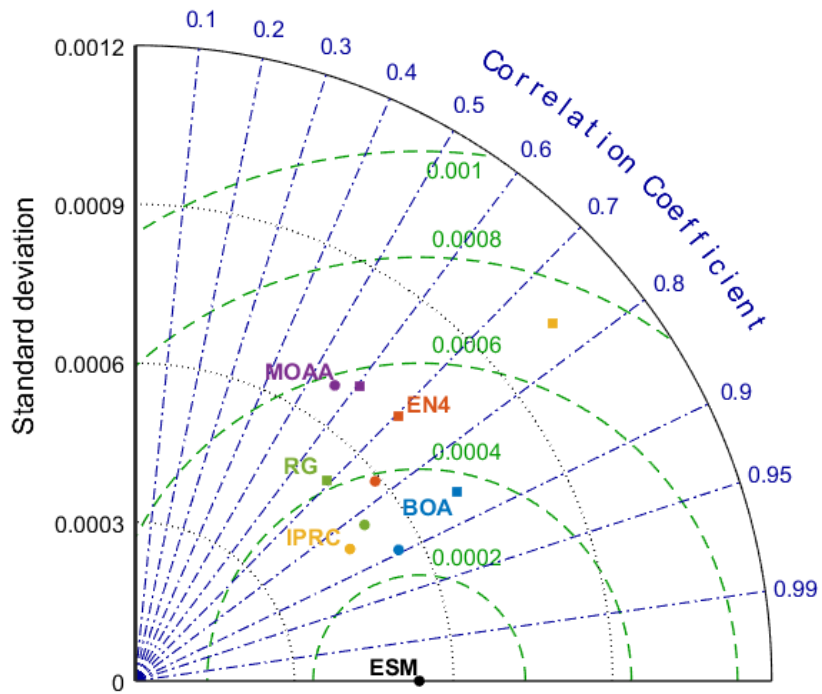


Figure 5.4. Taylor diagram of the timeseries of global mean salinity anomaly of the 700-2000 m layer. Squares mark the subset from 2005 through 2015 and circles mark from 2006 through 2014. The plot summarizes the correlation, root mean square difference, and temporal standard deviation of each of the Argo products with respect to ESM.

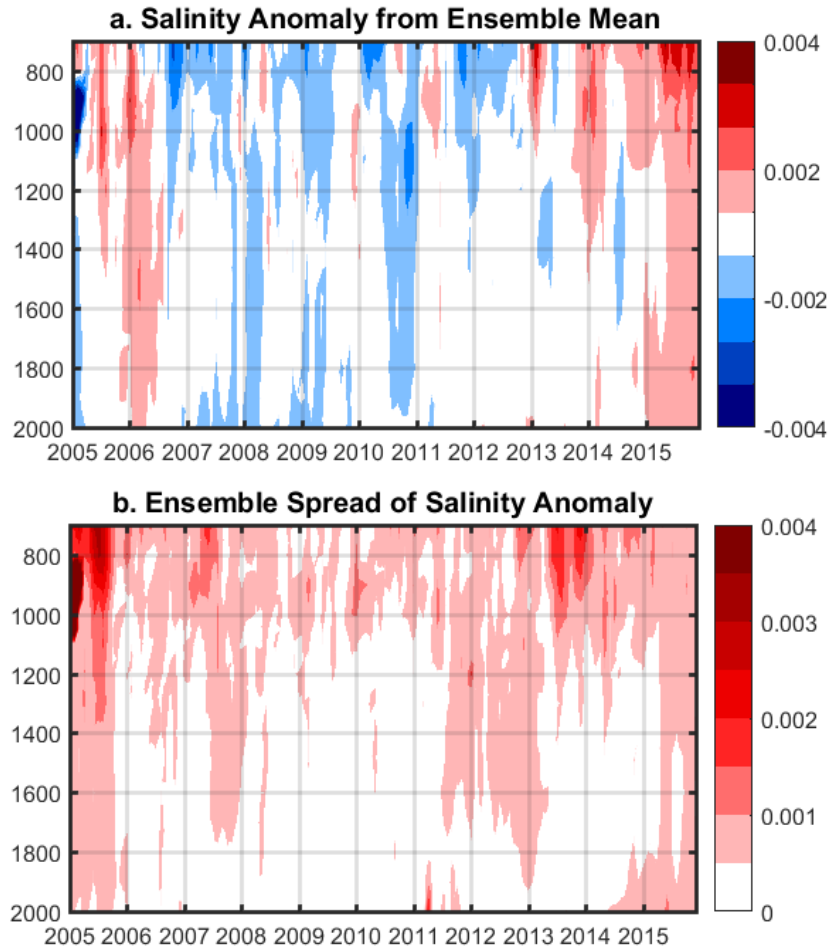


Figure 5.5. The depth distributions of global mean salinity anomaly over the 700-2000 m layer, from 2005 through 2015. (a) The Ensemble Mean, (b) its Ensemble Spread (unit: psu)

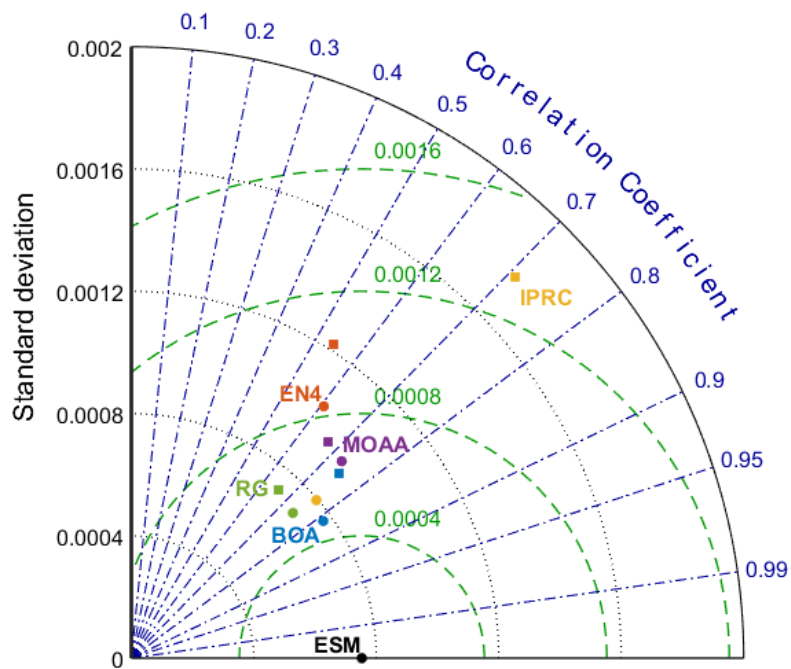


Figure 5.6. Taylor diagram of the depth distribution of global mean salinity anomaly over the 700-2000 m layer. Squares mark the subset from 2005 through 2015 and circles mark from 2006 through 2014. The plot summarizes the correlation, root mean square difference, and standard deviation of the observed pattern of each Argo products with respect to ESM.

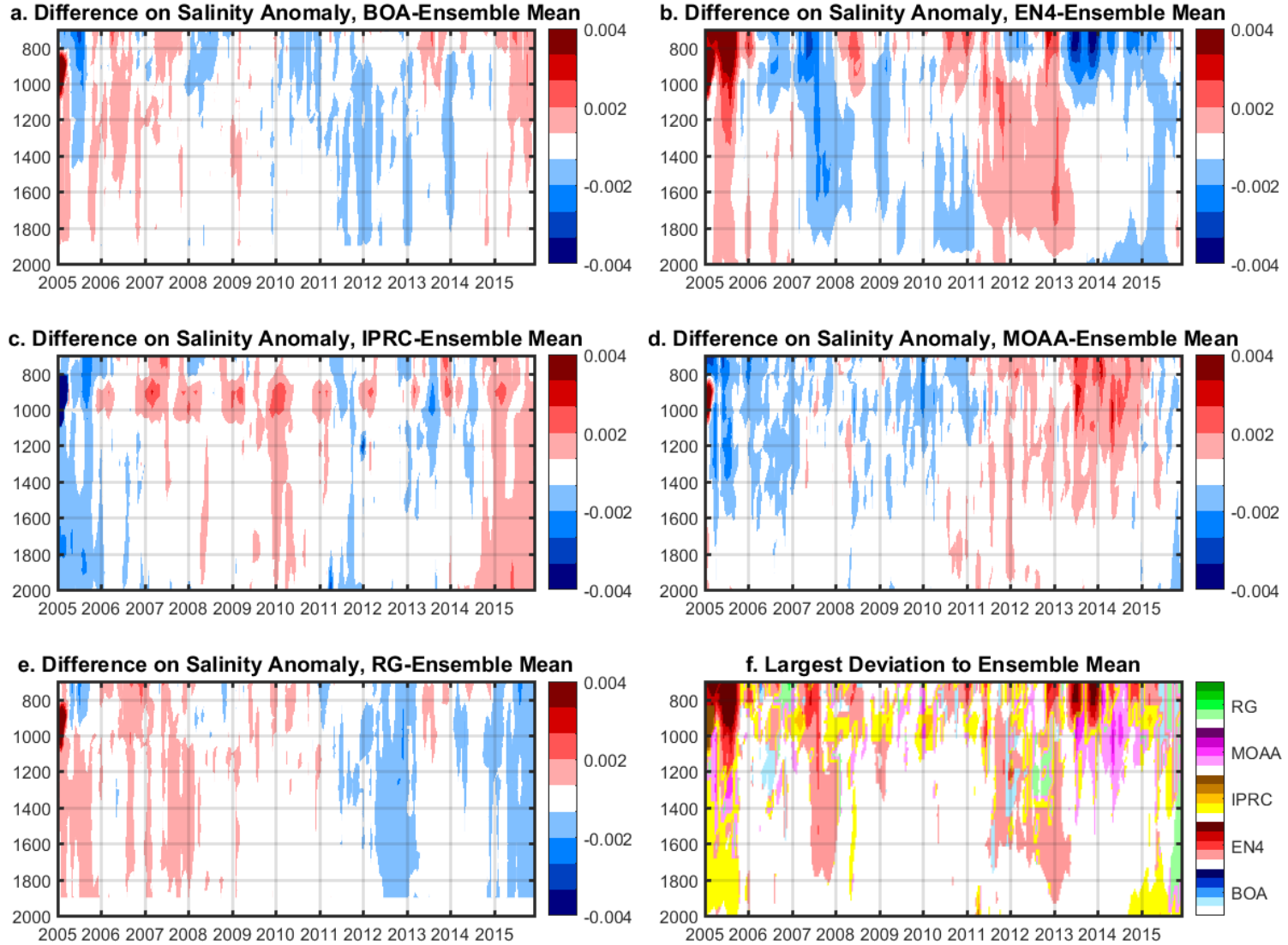


Figure 5.7. The depth distributions of the difference on salinity anomaly over the 700-2000 m layer. (a-e) The difference on salinity anomaly, (f) the largest deviation to the Ensemble Mean. The range for each color is the same as the difference. (unit: psu)

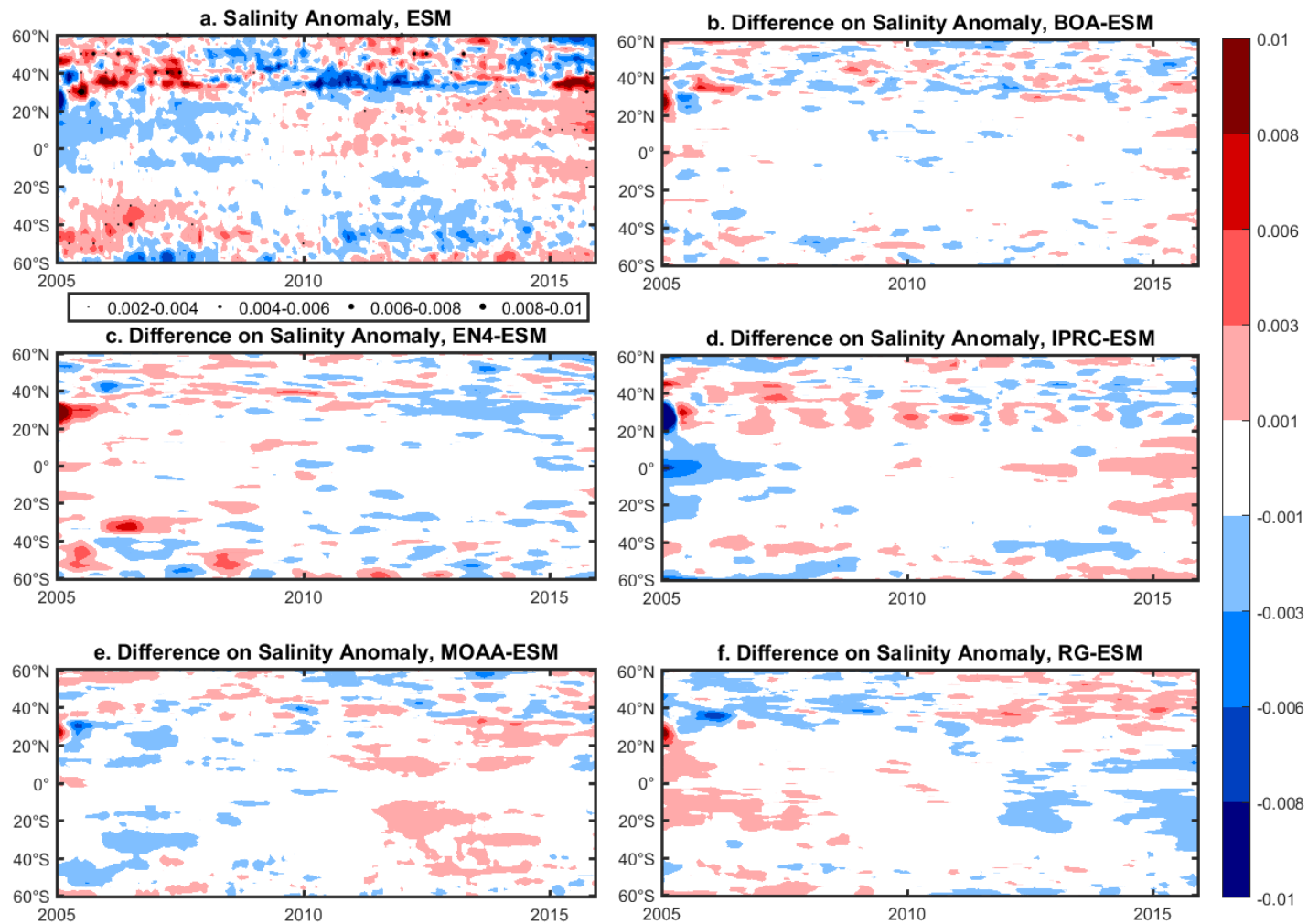


Figure 5.8. The spatial distributions of zonal mean of salinity anomaly of the 700-2000 m layer from 2005 through 2015. (a) The Ensemble Mean, (b-f) the difference between each individual dataset and the Ensemble Mean. The annual signal is removed using an annual sinusoid model. Stippling in (a) indicates the range of the Ensemble Spread. A 7-month running mean is applied to (b-f). (unit: psu)

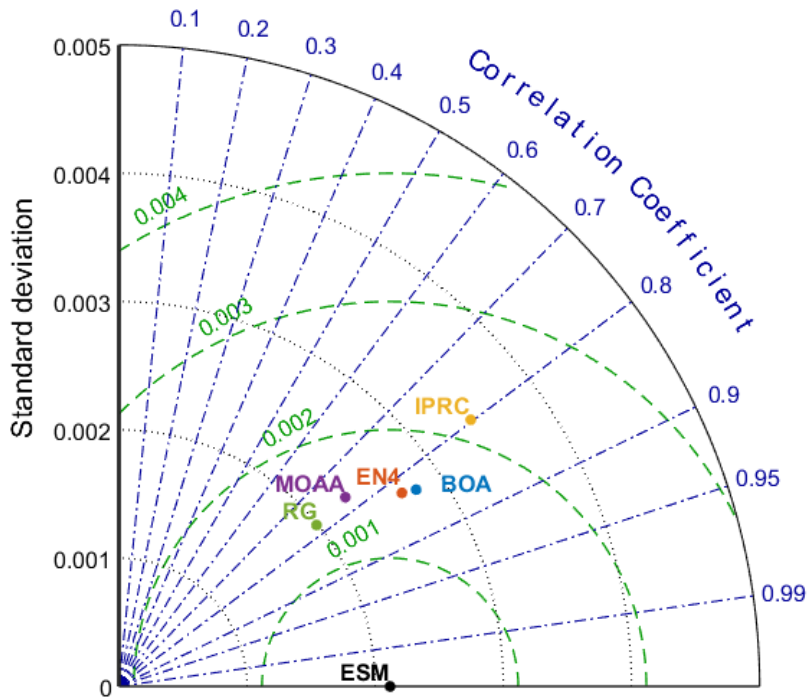


Figure 5.9. Taylor diagram of zonal mean of salinity anomaly of the 700-2000 m layer from 2005 through 2015. The plot summarizes the correlation, root mean square difference, and standard deviation of the observed pattern of each Argo products with respect to ESM.

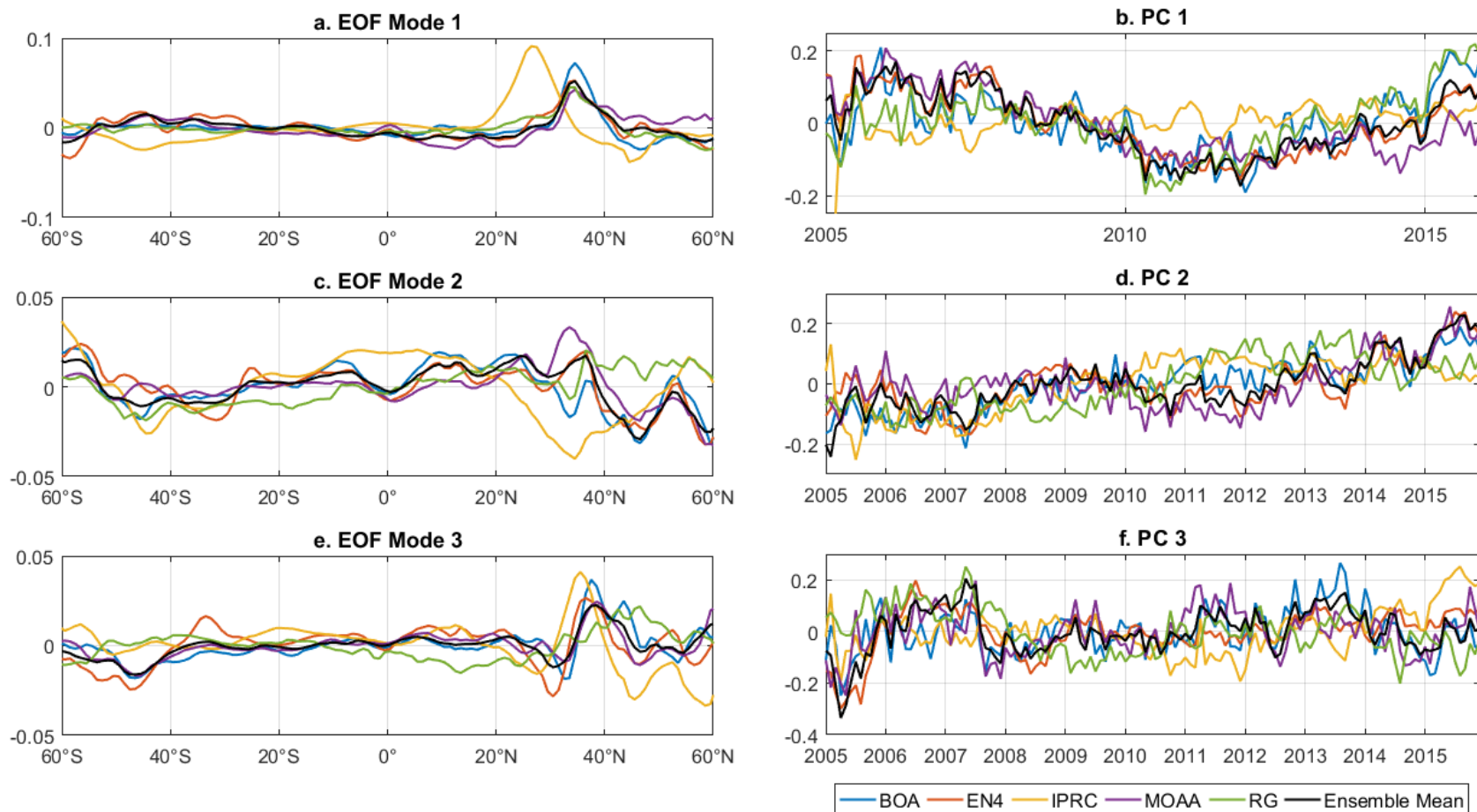


Figure 5.10. First three (a, c, e) EOF modes and (b, d, f) principle components of zonal mean of salinity anomaly of the 700-2000 m layer from 2005 through 2015.

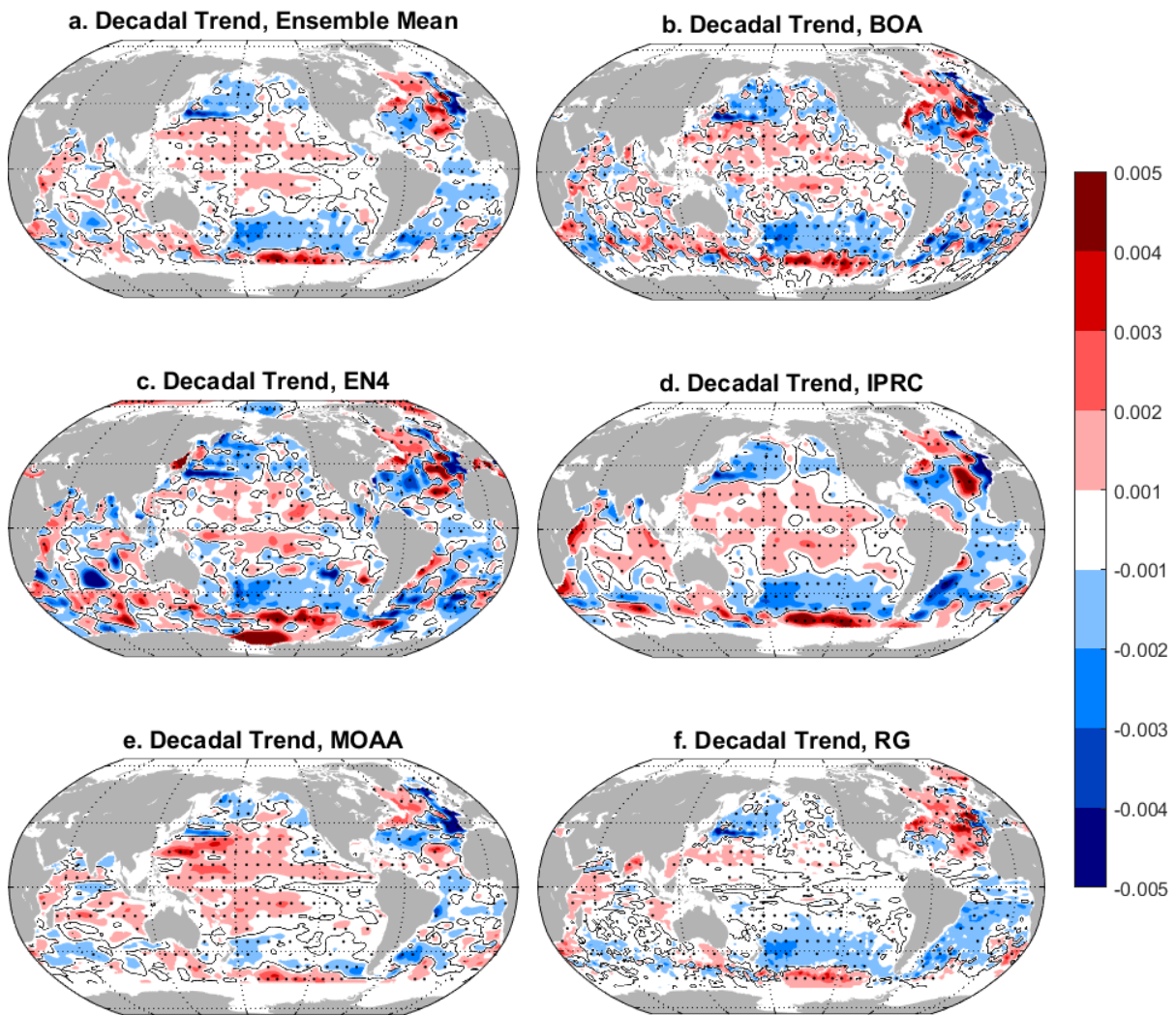


Figure 5.11. The spatial distributions of linear trends of the 700-2000 m layer from 2006 through 2014. (a) The Ensemble Mean, (b-f) each individual dataset. Black contours mark zero. Stippling indicates areas of statistically significant non-zero values at the 95% confidence level. (unit: psu/year)

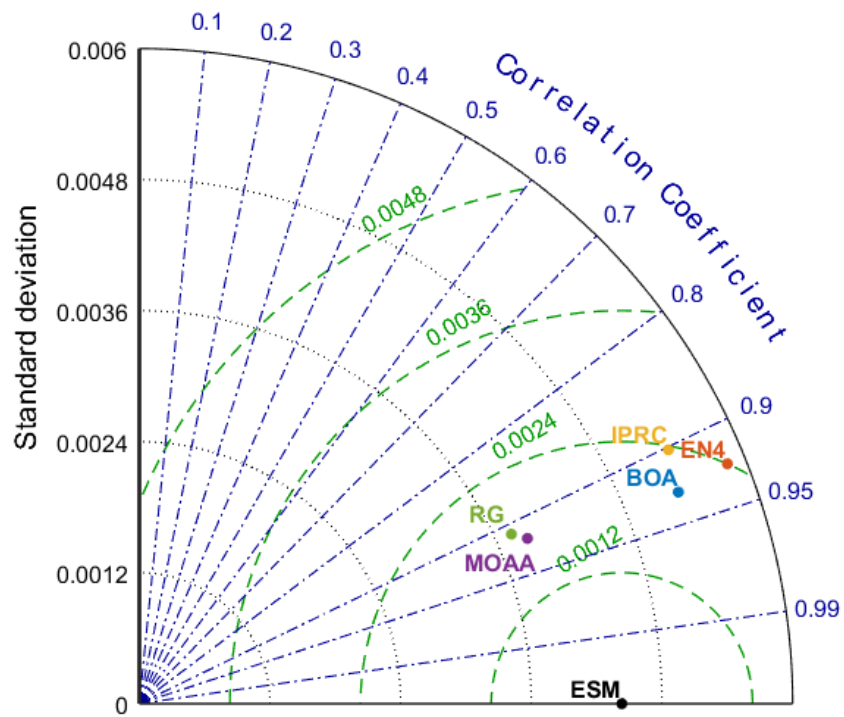


Figure 5.12. Taylor diagram of the spatial distributions of linear trends of the 700-2000 m layer from 2006 through 2014. The plot summarizes the spatial correlation, root mean square difference, and standard deviation of the observed pattern of each Argo products with respect to ESM.

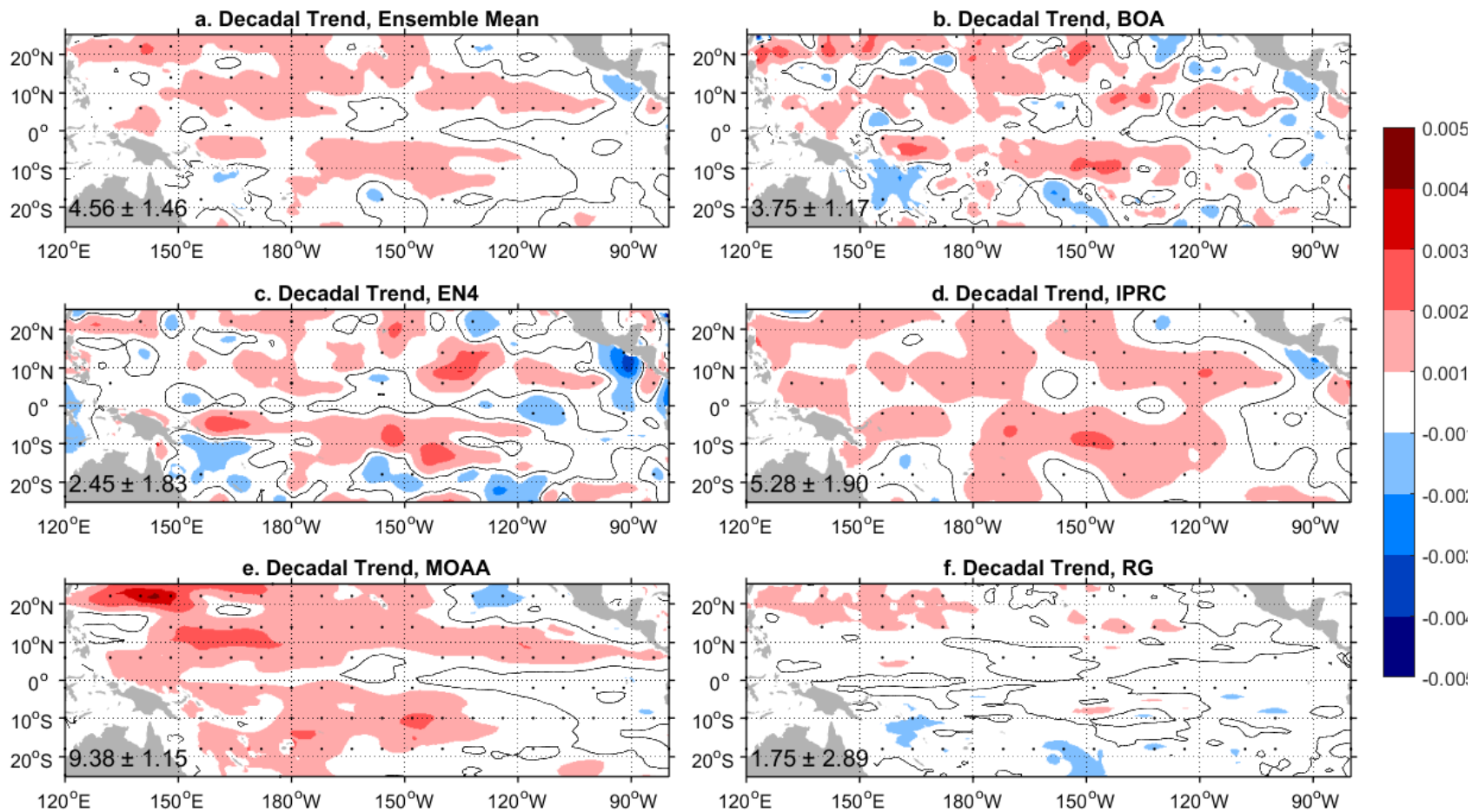


Figure 5.13. The spatial distributions of linear trends of the 700-2000 m layer in the tropical Pacific (120°E-90°W, 20°N-20°S) from 2006 through 2014. (a) The Ensemble Mean, (b-f) each individual dataset. Black contours mark zero. Stippling indicates areas of statistically significant non-zero values at the 95% confidence level. (unit: psu/year)

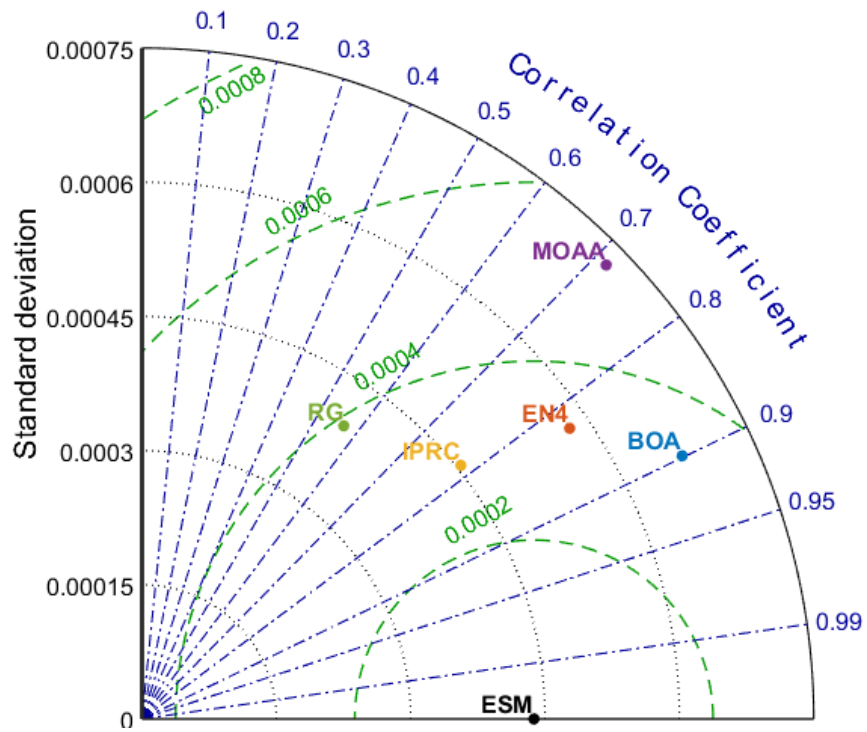


Figure 5.14. Taylor diagram of the spatial distributions of linear trends of the 700-2000 m layer in the tropical Pacific (120°N-80°W, 25°S-25°N) from 2006 through 2014. The plot summarizes the spatial correlation, root mean square difference, and standard deviation of the observed pattern of each Argo products with respect to ESM.

CHAPTER SIX:

A COMPARISON WITH A GLOBAL OCEAN STATE ESTIMATE, ECCOv4r3

Introduction to ECCOv4r3

As previous studies suggest, salinity observations can provide more accurate initial states for models and ocean reanalyses, or state estimate (Hackert et al., 2011; Zhao et al., 2014; Zhu et al., 2014). Many ocean reanalyses show rapid changes on salinity after 2002, which is likely caused by the assimilation of modern global-scale measurements of temperature and salinity from the Argo program (e.g., Shi et al., 2017). While some studies have assessed the salinity products from various ocean reanalyses and have included comparisons to select gridded Argo products (Xue et al., 2011, Chang et al., 2012; Shi et al., 2017), it is worthwhile to consider an objective analysis of a reanalysis product and the Argo products in the framework of this study.

An ocean reanalysis starts with a general ocean circulation model, then assimilates real observations into it using one of a number of statistical methods (e.g., Balmaseda et al., 2015). Various dynamical parameters and/or the ocean initial state (temperature, salinity, velocity, etc) are adjusted so that the ocean states of the model optimally match the observations, accounting for uncertainty in the observations.

The reanalysis we examined is the latest release of the Estimating the Circulation and Climate of the Ocean (ECCO) project (labeled v4r3 for Version 4 Release 3) (Forget et al., 2015; Fukumori et al., 2017). The ECCO estimate is a least squares fitting of the MIT general circulation model (MITgcm) to a large volume of satellite and in situ measurements, including

profiles from Argo floats. The ECCO estimate does not introduce artificial jumps during data assimilation due to the use of the adjoint method, which makes the estimates both dynamically consistent and close to the available observations within the specified levels of data uncertainty (e.g., Wunsch and Heimbach, 2013). Also, ocean properties (i.e., temperature and salinity) and mass (volume) are conserved to machine precision (Forget et al., 2015).

These unique features of the ECCO estimate allow accurate budget analyses for ocean heat and salinity changes (e.g., Liang et al., 2015; Vinogradova and Ponte, 2013; 2017). The ECCO v4r3 solution provides monthly averaged estimates from 1992 through 2015 on a vertical grid with 50 layers of various thickness. The horizontal resolution of the estimates varies between $1/3^\circ$ near the equator and 1° in the mid-latitudes. In this study, we examine the ECCOv4r3 estimates over the same period (2005-2015) as the gridded Argo products that were discussed in the previous chapters.

Mean State

For sea surface and the two depth-averaged layers (0-700 m, and 700-2000 m), the spatial pattern of the climatological mean and temporal standard deviation (Figure 6.1, left column) from ECCOv4r3 is highly similar to that of the Argo products. However, the temporal variation in ECCOv4r3 (dots in Figure 6.1, left column) is comparable to the Argo gridded products only at the sea surface. For the 0-700 m layer and 700-2000 m layer, the magnitudes of the temporal variability are smaller in the ECCOv4r3. There are two possible reasons for the difference: 1) the Argo ESM may be biased due to one or more of the products used to compute the average, or 2) the ECCOv4r3 state below the surface is still adjusting to the input from the new Argo observations and has not reached the true state.

Meanwhile, the differences of the time means (i.e, ECCO-ESM) resemble those of the gridded data to their ESM (Figure 3.2, Figure 4.2 and Figure 5.2), though the actual values are three times larger (Figure 6.1, right column). The largest difference at the sea surface reaches over 0.6 psu, while for the 0-700 m and 700-2000 m layers, it is around 0.3 and 0.15 psu, respectively. For the 700-2000 m layer, in particular, the largest deviation appears in the Mediterranean Outflow region, suggesting the influence of the Mediterranean Sea might be underestimated in ECCOv4r3, or overestimated in the Argo products. The ECCO (climatology of 1992-2015) pattern is similar to EN4 (climatology of 1971-2000) in the 700-2000 m and 700-2000 m layers (correlation at 0.6 and -0.5, respectively), suggesting the ECCO patterns below the surface are more consistent with the longer average climatology. Since the ESM is prone to post 2000, the observed similarity between ECCO and EN4 supports the idea the state of the deeper layers is still adjusting to the current era.

Temporal Variability

The ECCO global mean salinity anomalies vary within the same orders of magnitudes as the ESM of the Argo products at the surface, but there are substantial differences for the 0-700 m and 700-2000 m layers (Figure 6.2). At the sea surface, ECCOv4r3 captures the variability during 2005-2015 with good consistency (correlation at 0.7), though in general ECCO suggests a slight freshening trend with higher salinity in the first four years and lower salinity in the last two years.

Below the sea surface, the differences are more striking, although it should be noted that the range of the variations is smaller than the 0.01 psu. The globally averaged salinity anomalies from ECCOv4r3 have little or no annual/interannual variability, only a slow freshening over the

decade (Figure 6.2). While the Argo variability could be interpreted as artifacts of sampling and mapping error, it could also be interpreted as a deficiency in the ocean model to transmit surface freshwater forcings into the deeper ocean at the correct time-scales.

The non-vertically averaged salinity anomalies (Figure 6.3) from ECCO approximately captured the annual-interannual variations in the upper 50-100 m, and the same 2-year propagation of signal down to 200 m seen in the Argo products. The differences below 700 m are more striking, with ECCO showing a small decrease in salinity from 1000-2000 m. In contrast, ESM exhibits deep convection signals on interannual scales, although it has been noted (Chapter 5) that these are suspicious and may be related to aliasing of localized deep convection signals into the global average.

The subtle differences in the 700-2000 m layer can be further localized. Based on the zonal mean evolution (Figure 6.4), ECCO and the Argo ESM both capture the zonal variations at the sea surface and in the 0-700 m layer, both on interannual fluctuations and trends, with some slight differences for latitudes south of 40°S, especially in the 0-700 m layer. However in the 700-2000 m layer, ECCO and the Argo ESM agree reasonably well outside the tropics (correlation at 0.5 between 20-60°S, 0.4 between 20-50°N), but give completely different trends in the tropics (correlation at -0.4 between 20°S-20°N). While the gridded Argo products suggest an increase in salinity, ECCO indicates a freshening. This difference again supports the adjustment of the state of the deeper layers to the current era.

An EOF analysis provides further information on the agreement and difference on the zonal mean evolution patterns (Figure 6.5-6.7). At the sea surface, the ECCO and Argo ESM agree well with each other for the first three EOF modes, which have similar explained variances (Table 6.1) and high correlations (over 0.85 for EPFs and PCs, Table 6.2).

For the upper 700 m layer, the PCs of ECCO lack high-frequency signals in the Argo data (suggesting noise in the Argo grids), though the general patterns are similar (Figure 6.6). ECCO and Argo ESM agree well with each other for the first two EOF modes with high correlations (Table 6.2). One exception is the spatial pattern of the first EOF mode has a higher peak at 40°N for ECCO compared to Argo. The third EOF mode for ECCO is also significantly different from that of Argo, suggesting it is capturing different modes in each product. It only explains 9% of the total variance.

The EOF modes in the 700-2000 m layer have the largest differences (Figure 6.7) with low correlations (under 0.5 for Mode 2 and Mode 3). The first EOF mode for ECCO explains over 70% of the total variance. These highlight the substantial differences between Argo and ECCO salinity below 700 m.

In general, ECCOv4r3 reasonably captures the same salinity variability near the surface and in the upper 700 m ocean as the Argo gridded data, but there are large differences in the 700-2000 m layer. The primary differences are significantly higher interannual variability in the Argo products. It is hard to physically justify this on a global scale, so it may indicate sampling error. More work is needed to assess this. For example, an experiment taking salinity measurements from a high-resolution ocean model (that simulates eddies) sampled to Argo float locations and gridding in the manner of the various products could be conducted. This would allow the quantification of sampling and mapping error in the Argo products, which may explain some of the differences.

Trend

The estimated salinity trends for different layers from ECCOv4r3 are summarized in Table 6.3. ECCO indicates no significant trends above 700 m, but a freshening in the 700-2000 m layer that is statistically significant ($-1.33 \pm 0.31 \times 10^{-4}$ psu/year for 2005-2015, and $-1.46 \pm 0.43 \times 10^{-4}$ psu/year for 2006-2014, uncertainty at 95% confidence). This drives an overall significant trend for the entire 0-2000 m layer ($-1.92 \pm 1.05 \times 10^{-4}$ psu/year for 2005-2015, and $-1.70 \pm 0.72 \times 10^{-4}$ psu/year for 2006-2014). Although this is in contrast with the Argo gridded data for this layer (Chapter 5) and should be treated with caution, the significant trends from ECCO overlap with the insignificant trends from EN4 and RG.

Regionally, the spatial patterns of the salinity trends at the sea surface and in the upper 0-700 m ocean (Figure 6.8) are almost identical in ECCO and the Argo ESM. There are marked differences for the 700-2000 m layer (Figure 6.8). ECCO suggests an opposite pattern in the Indian Ocean, tropical Pacific and tropical Atlantic. For instance, ECCO shows a freshening Indian Ocean and no change in the tropical Pacific, while Argo ESM indicates salinification in both regions. ECCO shows salinification in the Atlantic, while Argo ESM indicates freshening. However, it should be noted that RG doesn't present any significant salinification in the tropical Pacific as well, suggesting ECCO and RG may share some similar assimilation and mapping techniques on the sparse Argo floats.

In conclusion, the ECCO and the Argo ESM are in good agreement for the upper 700 m layer, with both showing the subtropical Pacific getting saltier, while the North Atlantic and East Indian Ocean are freshening. Major differences occur in the 700-2000 m layer, though. From this comparison, however, it is impossible to say if this is due to sampling error and noise in the Argo

products (since the overall salinity changes are quite small), or issues in the ECCO ocean state estimate.

Table 6.1. Variance explained by the first 5 principal components of the zonal mean salinity anomaly from ECCOv4r3 during 2005-2015. Total number of the first three modes and first five modes and are also given.

Layer	Mode 1	Mode 2	Mode 3	Subtotal	Mode 4	Mode 5	Total
Sea Surface	36.5%	12.4%	7.6%	56.5%	6.3%	5.6%	68.4%
0-700 m	36.8%	22.8%	9.0%	68.6%	5.5%	4.9%	79.0%
700-2000 m	76.4%	7.7%	4.9%	89.0%	2.4%	1.4%	92.8%

Table 6.2. Correlations of the EOF modes and principle components between ECCOv4r3 and Argo ESM.

Layer	EOF Mode	EOF	PC
Sea Surface	Mode 1	0.94	0.91
	Mode 2	0.86	0.89
	Mode 3	0.70	0.70
0-700 m	Mode 1	0.70	0.91
	Mode 2	0.68	0.79
	Mode 3	0.17	0.10
700-2000 m	Mode 1	0.57	0.62
	Mode 2	0.02	0.50
	Mode 3	-0.26	0.13

Table 6.3. Decadal trends of global mean salinity from ECCOv4r3 (unit: 10^{-4} psu/year). Bold number indicates result significantly different from zero at the 95% confidence level.

Layer	Subset 1: 2005-2015	Subset 2: 2006-2014
Sea Surface	$(-3.37 \pm 3.05) \times 10$	$(-2.04 \pm 2.38) \times 10$
0-700 m	-2.52 ± 4.62	-1.58 ± 3.59
700-2000 m	-1.33 ± 0.31	-1.46 ± 0.43
0-2000 m	-1.92 ± 1.05	-1.70 ± 0.72

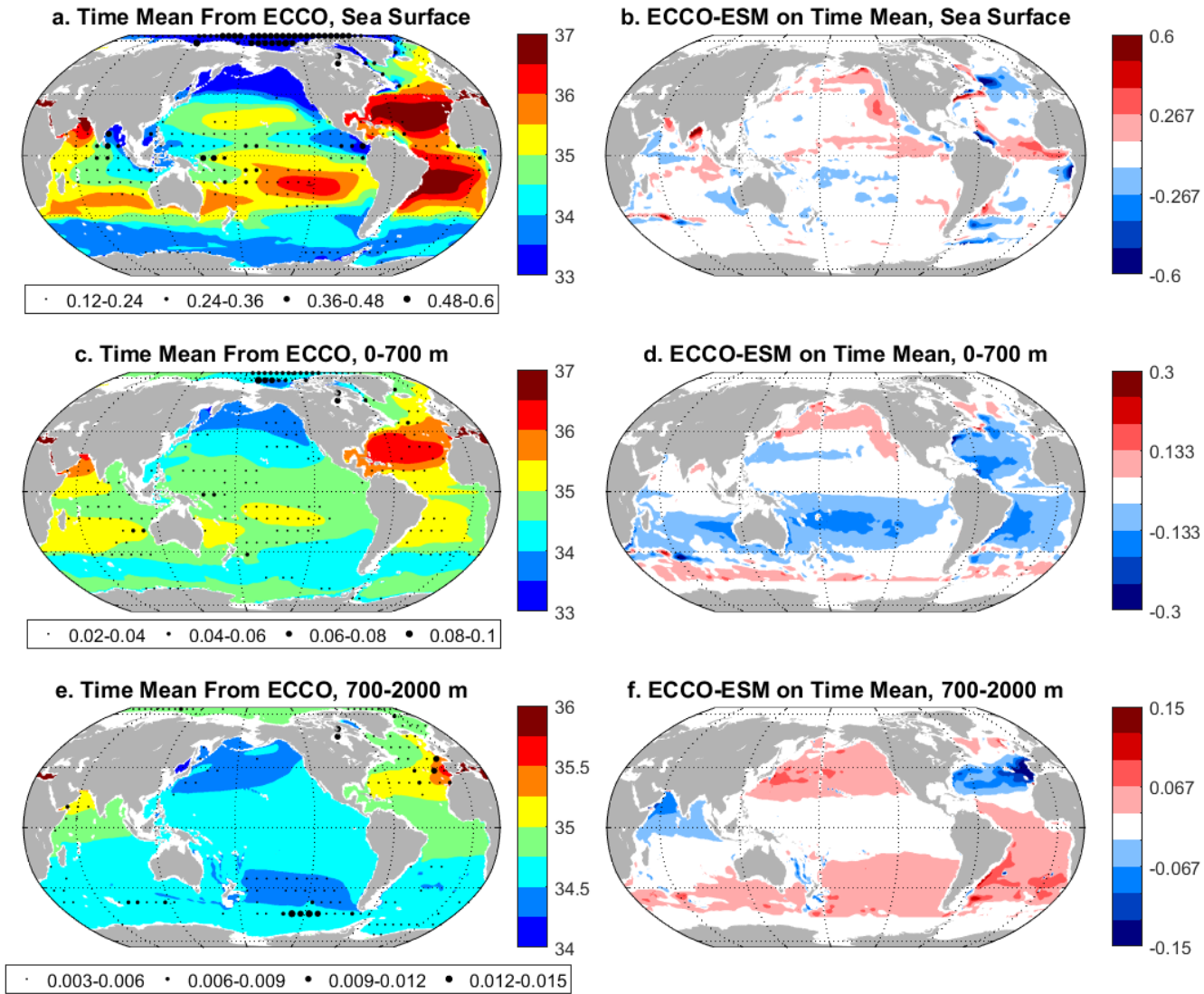


Figure 6.1. The spatial distributions of the time mean and difference from ECCOv4r3 during 2005-2015. (a, c, e) Time Mean, stippling marks the temporal standard deviation; (b, d, f) Difference on Time Mean, ECCOv4r3-Ensemble Mean. (unit: psu)

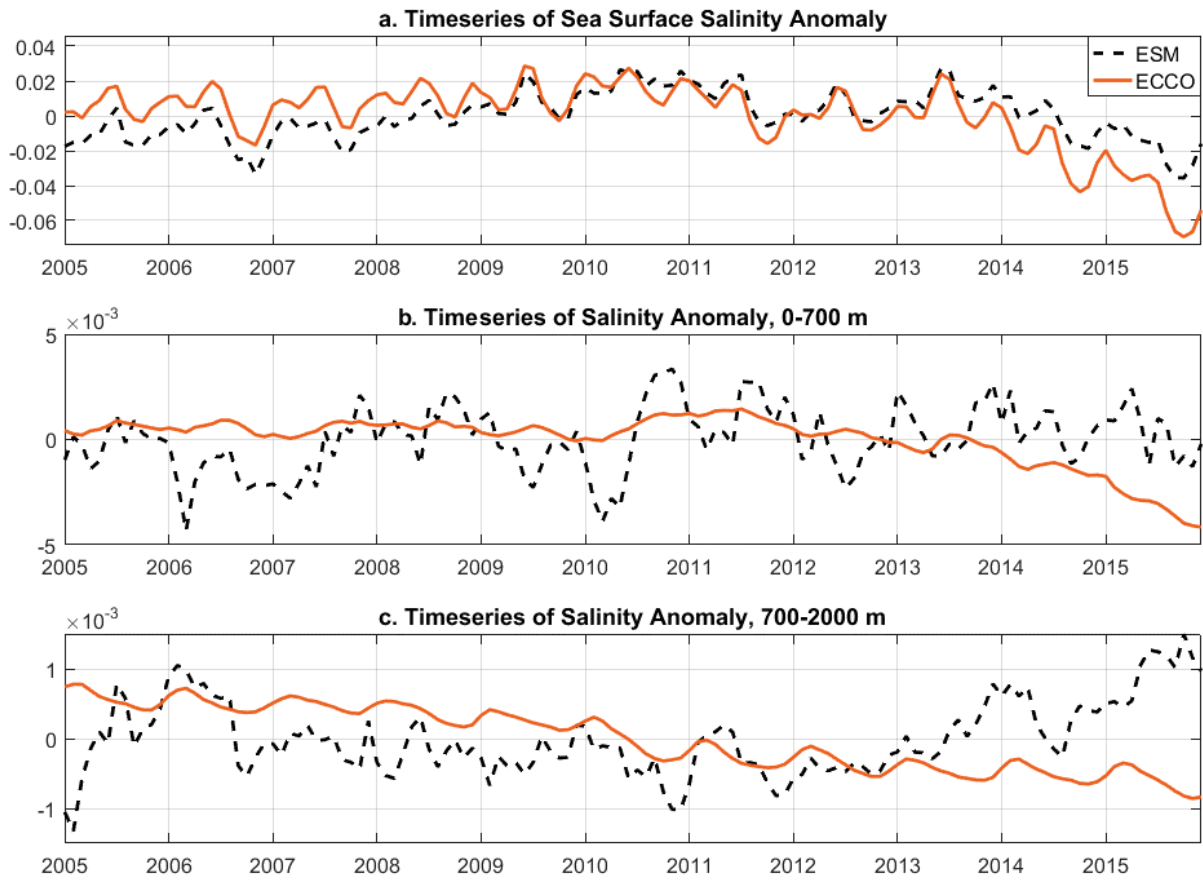


Figure 6.2. Timeseries of global mean salinity anomaly from Ensemble Mean and ECCOv4r3. (unit: psu)

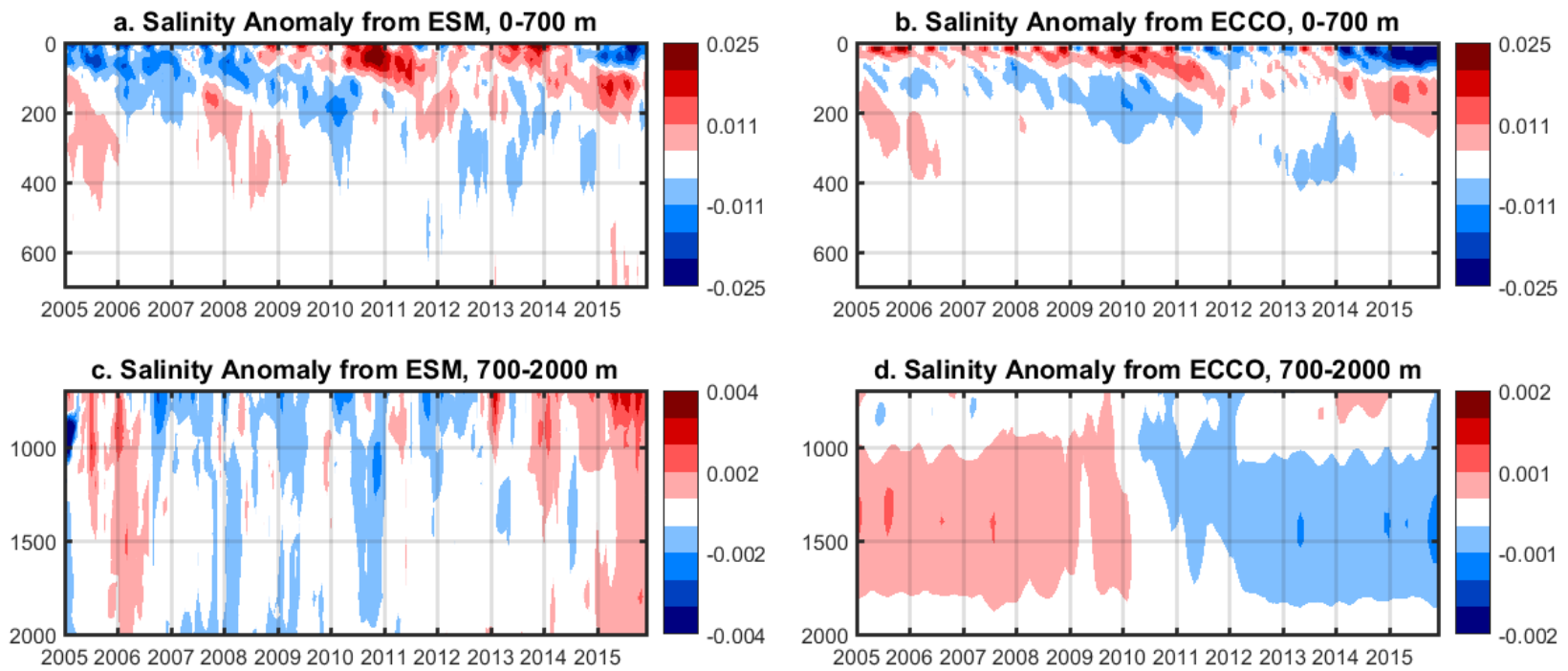


Figure 6.3. The depth distributions of salinity anomaly from 2005 through 2015. (a-b) 0-700 m layer; (c-d) 700-2000 m layer; (a, c) Ensemble Mean; (b, d) ECCOv4r3. (unit: psu)

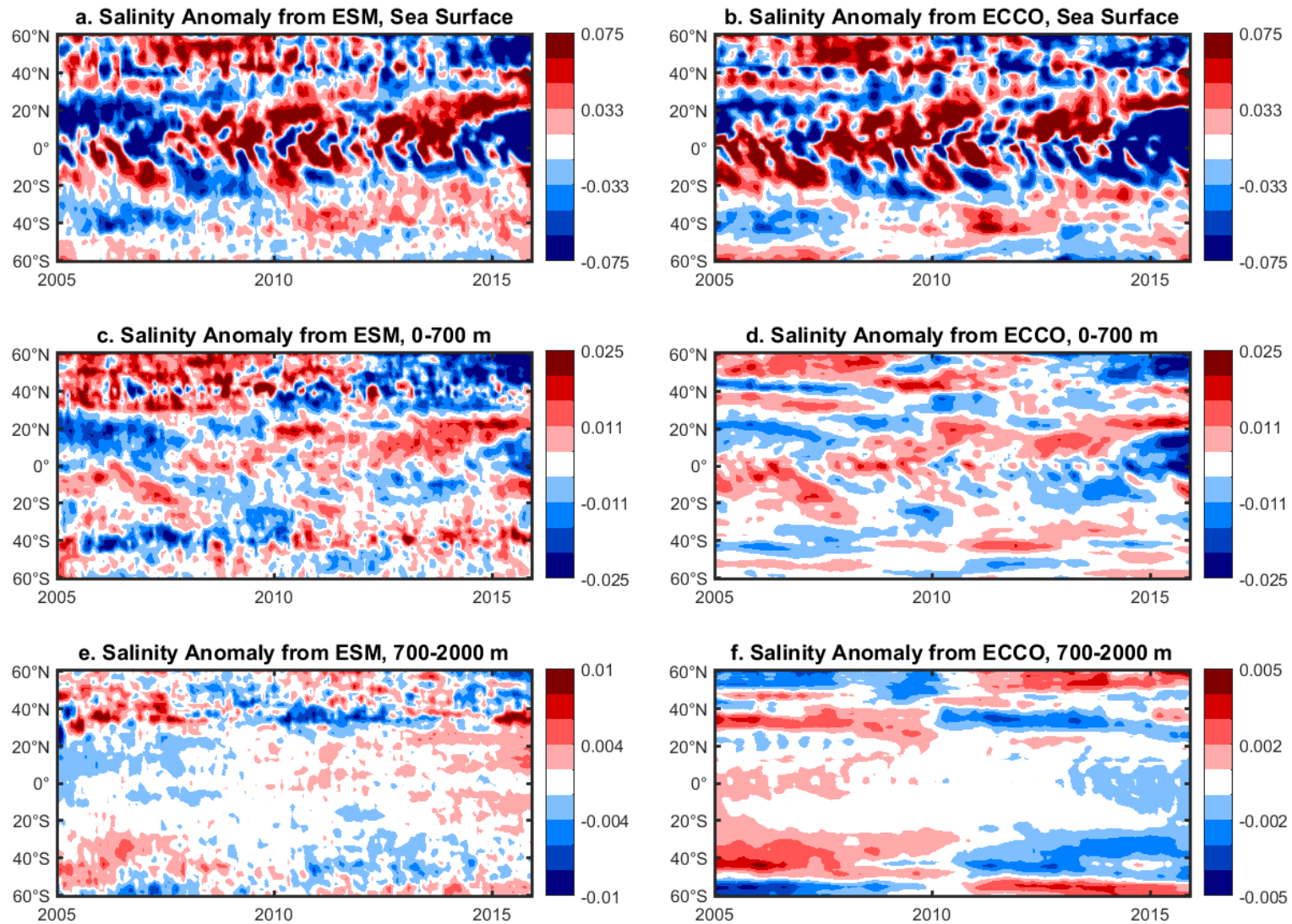


Figure 6.4. The spatial distributions of zonal mean of salinity anomaly from ESM and ECCOv4r3 during 2005-2015. Noting the range of each panel is different. (a, c, e) Ensemble Mean; (b, d, f) ECCOv4r3. (unit: psu)

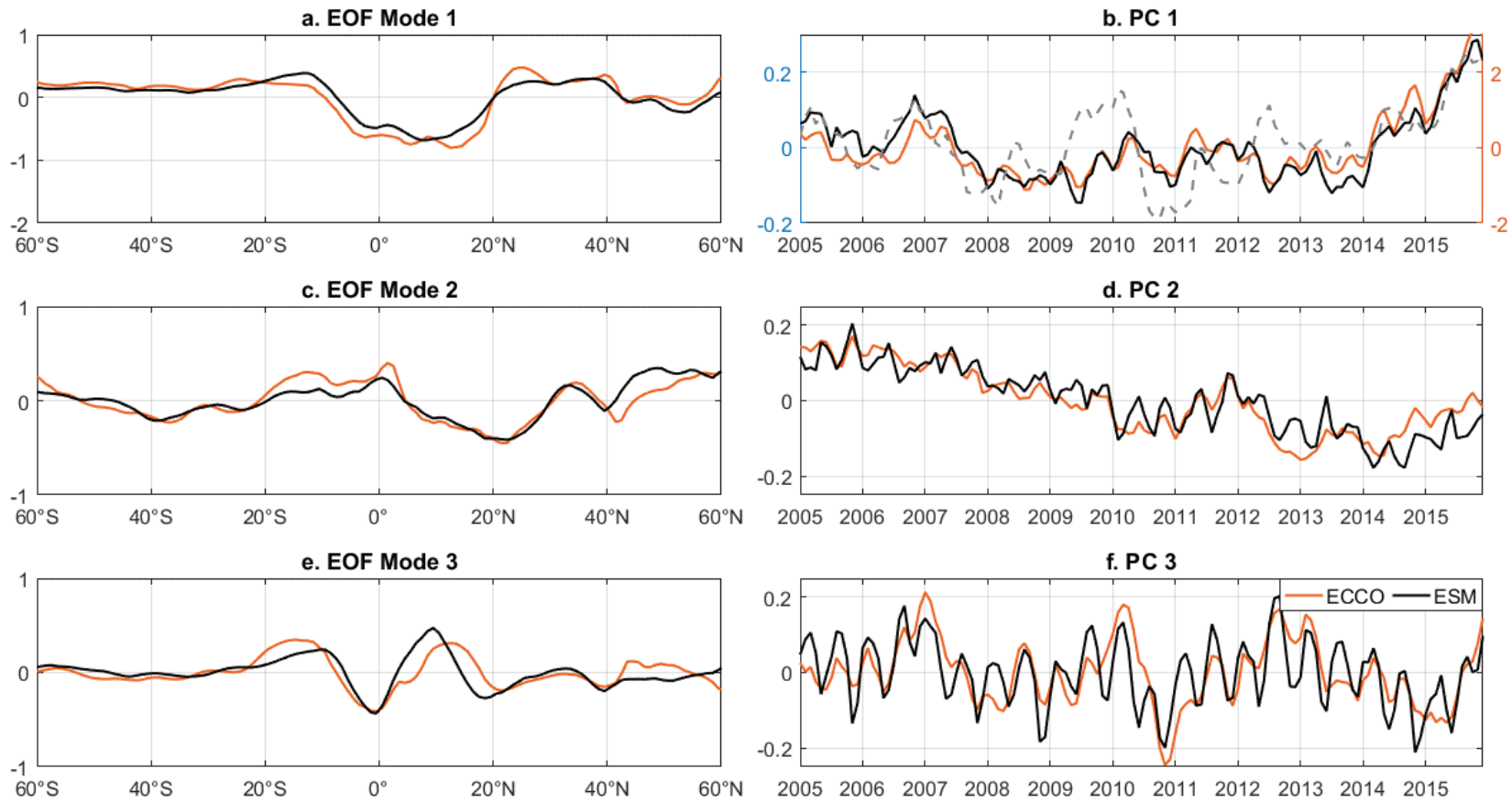


Figure 6.5. First three (a, c, e) EOF modes and (b, d, f) principle components of the zonal mean of sea surface salinity anomaly from Ensemble Mean and ECCOv4r3 during 2005-2015. Dash line in the PC 1 denotes the MEI (right axis).

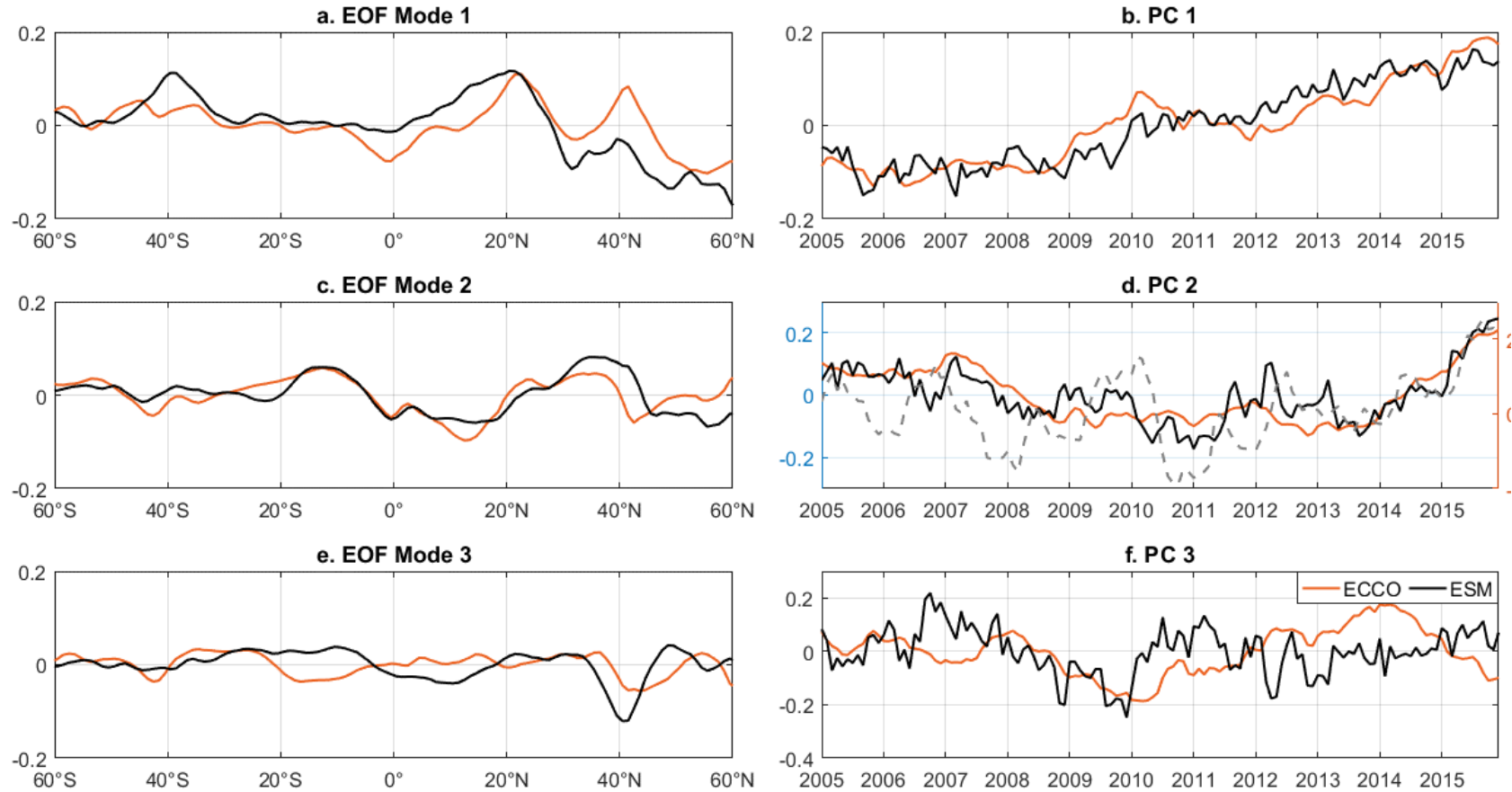


Figure 6.6. First three (a, c, e) EOF modes and (b, d, f) principle components of the zonal mean of salinity anomaly of the 0-700 m layer from Ensemble Mean and ECCOv4r3 during 2005-2015. Dash line in the PC 2 denotes the MEI (right axis).

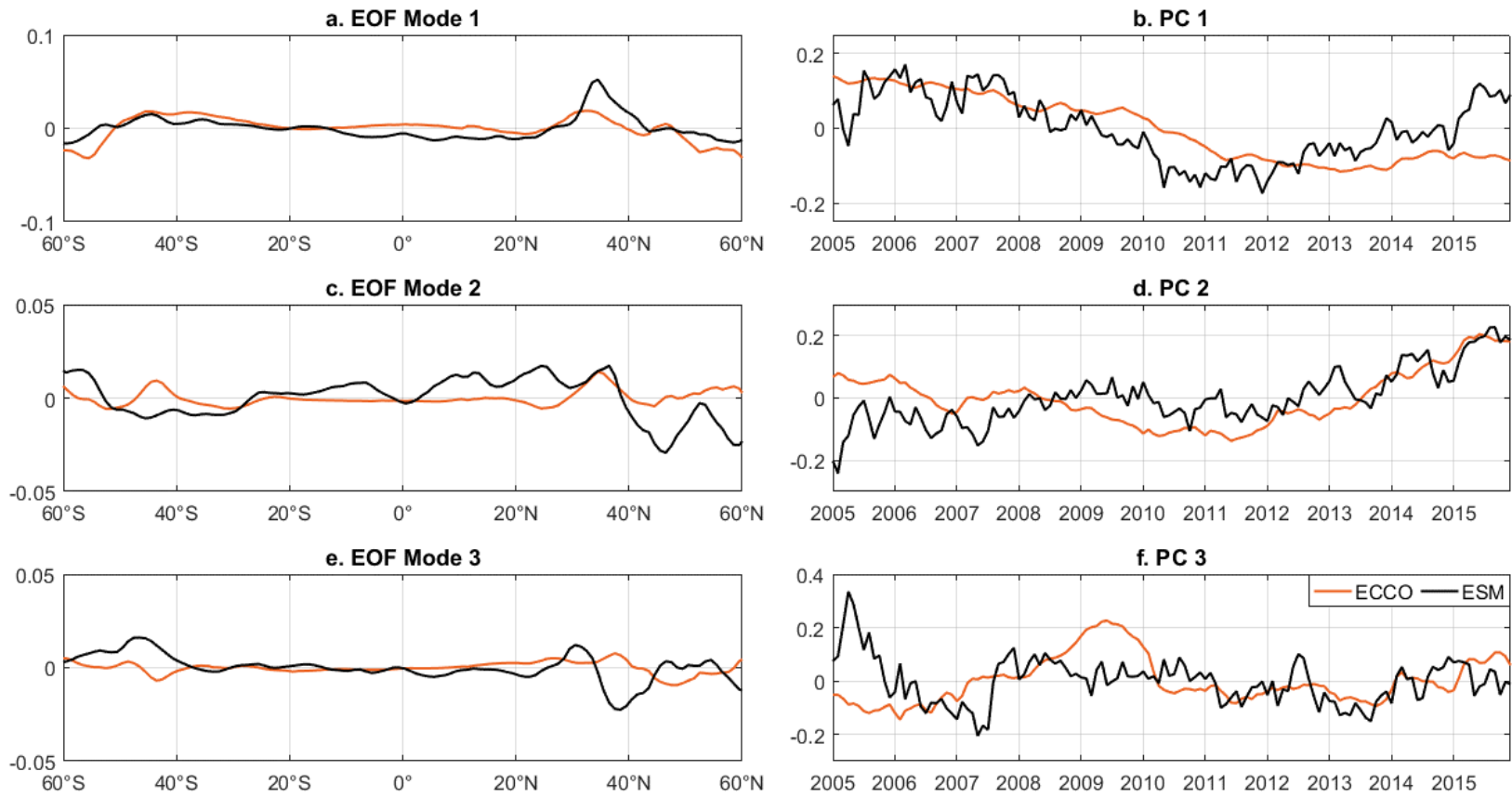


Figure 6.7. First three (a, c, e) EOF modes and (b, d, f) principle components of the zonal mean of salinity anomaly of the 700-2000 m layer from Ensemble Mean and ECCOv4r3 during 2005-2015.

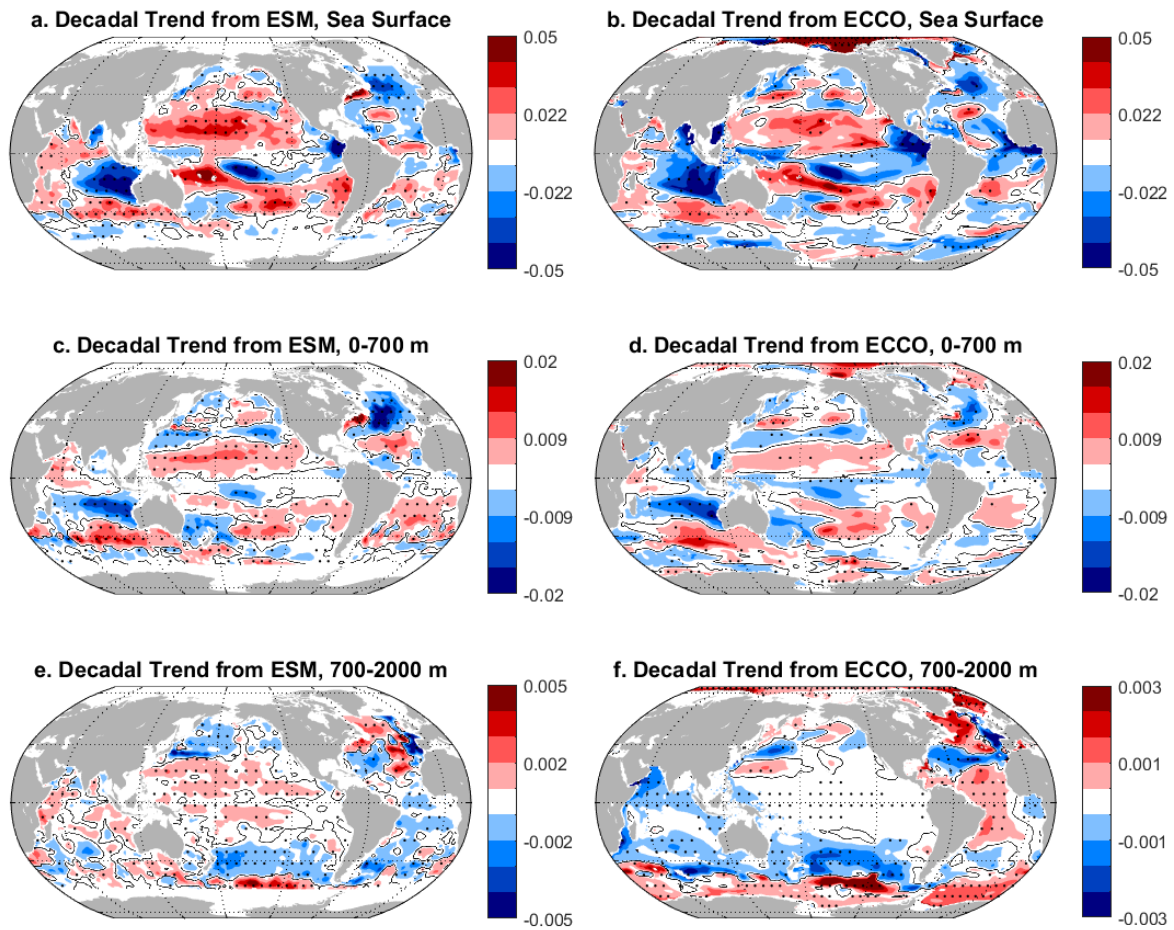


Figure 6.8. The spatial distributions of linear trends from ESM and ECCOv4r3 during 2006-2014. (a, c, e) Ensemble Mean; (b, d, f) ECCOv4r3. Black contours mark zero. Stippling indicates areas of statistically significant non-zero values at the 95% confidence level. Noting the range of each panel is different. (unit: psu/year)

CHAPTER SEVEN:

SUMMARY AND DISCUSSIONS

The climatology mean, temporal variability and decadal trends of the global ocean salinity in the upper 2000 m were examined from various available gridded Argo products and ECCOv4r3. For the period from 2005 through 2015 (and a subset from 2006 through 2014 for linear trends) some key features are robust and reproducible, both globally and regionally. For instance, the spatial pattern of the climatological mean is highly reproducible (the ratio of SPD to ESM is less than 5%) with the saltiest water in the North Atlantic and the Arabic sea, and the freshest water in the subpolar Pacific. Most of the temporal variability occurs in the upper 200 m and corresponds to interannual variations (i.e., ENSO). No significant long-term trend is found for the global mean salinity with existing data measurements. For the sea surface and 0-700 m layer, a statistically significant increase in salinity is found in the tropical Pacific and tropical Atlantic, along with a strong decrease in the North Atlantic that suggests an increase of the freshwater input from the Arctic (e.g., Proshutinsky et al., 2009). Such regional patterns are consistent with other studies based on different measurements (e.g., Tesdal et al., 2018). If the “rain gauge” concept applies for the examined 11 years, these robust results in the surface salinity and upper ocean salinity suggest a continuing intensification of the global water cycle in all major ocean basins except the Atlantic Ocean, where the increasing freshwater input from Arctic also plays an important role (Tesdal et al., 2018). For the 700-2000 m layer, the tropical Pacific shows a broad but subtle increase of salinity, while the subpolar regions are freshening.

However, some discrepancies remain among the global averages of the gridded Argo products in terms of month-to-month changes and long-term trends. An ocean state estimate product (i.e., ECCOv4r3) also show a number of disagreements with the Argo products. For the Argo products, the noise and discrepancies of salinity anomalies are comparable to the seasonal and even interannual variabilities in most circumstances.

For the time mean climatology, IPRC, EN4 and MOAA products show broad-scale deviations from the ensemble mean, which is likely due to the mapping methods and data sources. Most of these discrepancies occur in the Atlantic Ocean and the Southern Ocean where the salinity is historically poorly sampled and fast responses to the changes of surface forcings during the Argo Era. Visible large-scale biases are found in both IPRC and EN4 for the subsurface ocean, which may be related to the choice of background climatology.

Over the examined period, no statistically significant trends of the horizontally averaged salinity are detected at the sea surface and in the subsurface ocean. However, regionally, there is some consistency among the products. All products indicate the upper North Atlantic is getting fresher while the deeper layer is getting saltier, consistent with Robson et al. (2016). The South Atlantic shows freshening at mid-depth, again, consistent with Giglio and Johnson (2017).

Significant differences in products occur in regions of intense mesoscale eddy activity (e.g., western boundary currents, Southern Ocean), and the largest difference occurs in the tropical Pacific below 700 m, where the salinity trend in RG is broadly insignificant, while large and positive trends appear in the other salinity products. It should be noted that the trend in ECCOv4r3 for this layer and region is consistent with RG.

Among the five selected Argo products, BOA is closest to the ensemble mean for the time mean, globally-averaged temporal variations and trends, perhaps attributable to the iterated

background fields and mapping processes. RG shows small deviations on time mean, but has below-average salinity since 2014, which suggests a less saline tropical Pacific than other products. IPRC has zonally anti-correlated residuals to the ESM, which may be due to the mapping technique using mixed layer depth derived from a dynamic topography model. Both MOAA and EN4 contain raw data other than the Argo profiles, and also utilize older pre-Argo background climatologies, so have broad scale disagreements with the other three Argo products and the ESM.

Special attention should be paid to the tropical Pacific, where the gridded Argo product from Scripps (RG) broadly underestimates the linear trends seen in other products. Since the ENSO variation originates in the tropical Pacific region with significant regional impacts (Collins et al., 2010), a large number of studies have focused on the importance of climate variability in salinity changes at interannual time scale (e.g., Hackert et al., 2011; Zhu et al., 2014; Qu and Yu, 2014). Therefore, the science community should at least be aware of the existing regional discrepancies between the gridded Argo products before interpreting the strength of the “observed” interannual variability.

While the analysis presented here should not be considered a complete assessment of the accuracy of the products, it does provide a lower bound of the quality of the salinity products based on mapping methods, sampling, etc. While the Ensemble Mean is widely used over any particular product, extra attention is called to the corresponding Ensemble Spread, which is often not considered. The global mean SPD at sea surface, as well as in the upper 700 m, is above the 0.01 psu Argo target which means the discrepancy is at least detectable. The Atlantic Ocean is the major basin that has a higher SPD than the global mean above 700 m. High SPD values tend to appear where the temporal variability and eddy activity are intense. Below 700 m, the global

mean SPD is below 0.01 psu, but Southern Ocean still has higher values (over 0.01 psu) in all three sectors (i.e., Indian sector, Pacific sector and Atlantic sector). For 700-2000 m layer, relatively high SPDs are found in the Mediterranean Outflow zone.

While many studies (e.g., Shi et al., 2017; Wang et al., 2017) have adopted the Ensemble Mean to represent the optimal scenario with reduced bias, the real question is whether one should use all available datasets, especially since some may be biased due to the choice of background climatology. Including potentially biased products can lead to global and regional under/overestimation of salinity trends. For example, if EN4 or MOAA were not included in this study, better agreements would be achieved on time mean, temporal variabilities, etc. Thus, some further analysis to test the influence of a single product on the ESM is recommended for future work.

Despite improving measurements of salinity since the mid-2000s and its assimilation into ocean state estimates, there is still considerable uncertainty for depths between 700-2000 m. The ongoing deployment of the Deep Argo program will further extend the range of measurements to deep and abyssal ocean (Le Reste et al., 2016; Zilberman, 2017), and will reduce the uncertainties we observed in this study. The agreements/disagreements from this study hence will provide important guidance on how to integrate and improve current oceanic measurements of salinity, as well as the mapping methods and assimilation techniques.

In addition, the comparison between Argo products and ECCOv4r3 shows that our knowledge on the deep ocean physics could capture some of the salinity variability, but that trends are inconsistent, and the Argo gridded products have high- and low-frequency variability that are not present in the ocean state estimate. The discrepancies between the gridded Argo products and the ocean state estimate could be attributed to the different mapping methods and

sparse regional data (Good et al. 2013; Gaillard et al. 2016), or problems with the model assimilating the observations and adjusting the state.

REFERENCES

- Balmaseda, M. A., et al. (2015), The Ocean Reanalyses Intercomparison Project (ORA-IP), *Journal of Operational Oceanography*, 8(sup1), S80-S97, doi:10.1080/1755876x.2015.1022329.
- Boening, C., Willis, J. K., Landerer, F. W., Nerem, R. S., and Fasullo, J. (2012), The 2011 La Niña: So strong, the oceans fell, *Geophys. Res. Lett.*, 39, L19602, doi:10.1029/2012GL053055.
- Boyer, T. P., S. Levitus, J. I. Antonov, R. A. Locarnini, and G. H. E. (2005), Linear trends in salinity for the World Ocean, 1955–1998, *Geophysical Research Letters*, 32(1), doi:10.1029/2004gl021791.
- Boyer, T.P., O.K. Baranova, C. Coleman, H.E. Garcia, A. Grodsky, R.A. Locarnini, A.V. Mishonov, and others (2018), World Ocean Database 2018. A. Mishonov, technical ed., *NOAA Atlas NESDIS 87*, https://data.nodc.noaa.gov/woa/WOD/DOC/wod_intro.pdf.
- Buckley, M. W., and J. Marshall (2016), Observations, inferences, and mechanisms of the Atlantic meridional overturning circulation: A review. *Rev. Geophys.*, 54, 5–63, doi:10.1002/2015RG000493.
- Chang, Y.-S., S. Zhang, A. Rosati, T. L. Delworth, and W. F. Stern (2013), An assessment of oceanic variability for 1960–2010 from the GFDL ensemble coupled data assimilation, *Climate Dynamics*, 40(3), 775-803, doi:10.1007/s00382-012.1412.2.

- Curry, R., B. Dickson, and I. Yashayaev (2003), A change in the freshwater balance of the Atlantic Ocean over the past four decades, *Nature*, 426(6968), 826-829, doi:10.1038/nature02206.
- Dickson, B., I. Yashayaev, J. Meincke, B. Turrell, S. Dye, and J. Holfort (2002), Rapid freshening of the deep North Atlantic Ocean over the past four decades, *Nature*, 416(6883), 832-837, doi:10.1038/416832a.
- Dong, C., J. C. McWilliams, Y. Liu, and D. Chen (2014), Global heat and salt transports by eddy movement, *Nat Commun*, 5, 3294, doi:10.1038/ncomms4294.
- Durack, P. J., and S. E. Wijffels (2010), Fifty-Year Trends in Global Ocean Salinities and Their Relationship to Broad-Scale Warming, *Journal of Climate*, 23(16), 4342-4362, doi:10.1175/2010jcli3377.1.
- Durack, P. J., S. E. Wijffels, and R. J. Matear (2012), Ocean salinities reveal strong global water cycle intensification during 1950 to 2000, *Science*, 336(6080), 455-458, doi:10.1126/science.1212222.
- Durack, P. J., S. E. Wijffels, and P. J. Gleckler (2014), Long-term sea-level change revisited: the role of salinity, *Environmental Research Letters*, 9(11), doi:10.1088/1748-9326/9/11/114017.
- Foltz, G. R., S. A. Grodsky, J. A. Carton, and M. J. McPhaden (2004), Seasonal salt budget of the northwestern tropical Atlantic Ocean along 38 degrees W, *J Geophys Res-Oceans*, 109(C3), doi:10.1029/2003jc002111.
- Forget, G., J. M. Campin, P. Heimbach, C. N. Hill, R. M. Ponte, and C. Wunsch (2015a), ECCO version 4: an integrated framework for non-linear inverse modeling and global ocean

- state estimation, *Geoscientific Model Development*, 8(10), 3071-3104, doi:10.5194/gmd-8-3071-2015.
- Fukumori, I., O. Wang, I. Fenty, G. Forget, P. Heimbach, and R. M. Ponte, (2017), ECCO Version 4 Release 3, <http://hdl.handle.net/1721.1/110380>, doi:1721.1/110380. Available at ftp://ecco.jpl.nasa.gov/Version4/Release3/doc/v4r3_summary.pdf.
- Gaillard, F., T. Reynaud, V. Thierry, N. Kolodziejczyk, and K. von Schuckmann (2016), In situ-based reanalysis of the global ocean temperature and salinity with ISAS: Variability of the heat content and steric height. *J. Climate*, 29, 1305–1323, doi:10.1175/JCLI-D-15-0028.1.
- Giglio, D., and G. C. Johnson (2016). Subantarctic and polar fronts of the Antarctic Circumpolar Current and Southern Ocean heat and freshwater content variability: A view from Argo. *Journal of Physical Oceanography*, 46(3), 749-768, doi: 10.1175/JPO-D-15-0131.1.
- Giglio, D., and G. C. Johnson (2017), Middepth decadal warming and freshening in the South Atlantic, *J Geophys Res-Oceans*, 122(2), 973-979, doi:10.1002/2016jc012246.
- Good, S. A., M. J. Martin, and N. A. Rayner (2013), EN4: Quality controlled ocean temperature and salinity profiles and monthly objective analyses with uncertainty estimates, *J Geophys Res-Oceans*, 118(12), 6704-6716, doi:10.1002/2013jc009067.
- Jayne, S. R., D. Roemmich, N. Zilberman, S. C. Riser, K. S. Johnson, G. C. Johnson, and S. R. Piotrowicz (2017), The Argo Program Present and Future, *Oceanography*, 30(2), 18-28, doi:10.5670/oceanog.2017.213.

- Hackert, E., J. Ballabrera-Poy, A. J. Busalacchi, R. H. Zhang, and R. Murtugudde (2011), Impact of sea surface salinity assimilation on coupled forecasts in the tropical Pacific, *J Geophys Res-Oceans*, *116*(C5), doi:10.1029/2010jc006708.
- Haumann, F. A., Gruber, N., Münnich, M., Frenger, I., and Kern, S. (2016). Sea-ice transport driving Southern Ocean salinity and its recent trends. *Nature*, *537*(7618), 89, doi:10.1038/nature19101.
- Hosoda, S., Ohira, T., and Nakamura, T. (2008). A monthly mean dataset of global oceanic temperature and salinity derived from Argo float observations. *JAMSTEC Report of Research and Development*, *8*, 47-59.
- Hosoda, S., Suga, T., Shikama, N., and Mizuno, K. (2009). Global surface layer salinity change detected by Argo and its implication for hydrological cycle intensification. *Journal of Oceanography*, *65*(4), 579, doi:10.1007/s10872-009-0049-1.
- Kosempa, M., and Chambers, D. P. (2016). Mapping error in Southern Ocean transport computed from satellite altimetry and argo. *J Geophys Res-Oceans*, *121*(11), 8063-8076.
- Lee, T. (2016), Consistency of Aquarius sea surface salinity with Argo products on various spatial and temporal scales, *Geophys. Res. Lett.*, *43*(8), 3857-3864, doi:10.1002/2016gl068822.
- Levitus, S., Antonov, J. I., Boyer, T. P., Garcia, H. E., and Locarnini, R. A. (2005), Linear trends of zonally averaged thermosteric, halosteric, and total steric sea level for individual ocean basins and the world ocean, (1955–1959)–(1994–1998), *Geophys. Res. Lett.*, *32*, L16601, doi:10.1029/2005GL023761.

- Li, H., F. H. Xu, W. Zhou, D. X. Wang, J. S. Wright, Z. H. Liu, and Y. L. Lin (2017),
Development of a global gridded Argo data set with Barnes successive corrections, *J
Geophys Res-Oceans*, 122(2), 866-889, doi:10.1002/2016jc012285.
- Liang, X. F., C. Wunsch, P. Heimbach, and G. Forget (2015), Vertical Redistribution of Oceanic
Heat Content, *Journal of Climate*, 28(9), 3821-3833, doi:10.1175/Jcli-D-14-00550.1.
- Llovel, W., B. Meyssignac, and A. Cazenave (2011), Steric sea level variations over 2004.2010
as a function of region and depth: Inference on the mass component variability in the
North Atlantic Ocean, *Geophysical Research Letters*, 38, L15608,
doi:10.1029/2011gl047411.
- Llovel, W., and T. Lee (2015), Importance and origin of halosteric contribution to sea level
change in the southeast Indian Ocean during 2005-2013, *Geophysical Research Letters*,
42(4), 1148-1157, doi:10.1002/2014gl062611.
- Maes, C., K. Ando, T. Delcroix, W. S. Kessler, M. J. McPhaden, and D. Roemmich (2006),
Observed correlation of surface salinity, temperature and barrier layer at the eastern edge
of the western Pacific warm pool, *Geophysical Research Letters*, 33(6),
doi:10.1029/2005gl024772.
- Mauritzen, C., A. Melsom, and R. T. Sutton (2012), Importance of density-compensated
temperature change for deep North Atlantic Ocean heat uptake. *Nat. Geosci.*, 5, 905–910,
doi:10.1038/ngeo1639.
- Proshutinsky, A., and Coauthors (2009), Beaufort Gyre freshwater reservoir: State and
variability from observations. *J. Geophys. Res.*, 114, C00A10,
doi:10.1029/2008JC005104.

- Purkey, S. G., and G. C. Johnson (2013), Antarctic Bottom Water Warming and Freshening: Contributions to Sea Level Rise, Ocean Freshwater Budgets, and Global Heat Gain, *Journal of Climate*, 26(16), 6105-6122, doi:10.1175/Jcli-D-12-00834.1.
- Rao, R. R., and R. Sivakumar (2003), Seasonal variability of sea surface salinity and salt budget of the mixed layer of the north Indian Ocean, *J Geophys Res-Oceans*, 108(C1), 9-1-9-14, doi:10.1029/2001jc000907.
- Le Reste, S., Dutreuil, V., André, X., Thierry, V., Renaut, C., Le Traon, P. Y., and Maze, G. (2016), “Deep-Arvor”: A New Profiling Float to Extend the Argo Observations Down to 4000-m Depth, *Journal of Atmospheric and Oceanic Technology*, 33(5), 1039-1055. doi:10.1175/JTECH-D-15-0214.1.
- Robson, J., P. Ortega, and R. Sutton (2016), A reversal of climatic trends in the North Atlantic since 2005, *Nature Geoscience*, 9(7), 513, doi:10.1038/Ngeo2727.
- Roemmich, D., and J. Gilson (2009), The 2004.2008 mean and annual cycle of temperature, salinity, and steric height in the global ocean from the Argo Program, *Progress in Oceanography*, 82(2), 81-100, doi:10.1016/j.pocean.2009.03.004.
- Roemmich, D., G. C. Johnson, S. Riser, R. Davis, J. Gilson, W. B. Owens, S. L. Garzoli, C. Schmid, and M. Ignaszewski (2009), The Argo Program Observing the Global Ocean with Profiling Floats, *Oceanography*, 22(2), 34-43, doi:10.5670/oceanog.2009.36.
- Saji, N. H., Goswami, B. N., Vinayachandran, P. N., and Yamagata, T. (1999). A dipole mode in the tropical Indian Ocean. *Nature*, 401(6751), 360, doi:10.1038/4385.
- Schroeder, K., Chiggiato, J., Bryden, H. L., Borghini, M., and Ismail, S. B. (2016). Abrupt climate shift in the Western Mediterranean Sea. *Scientific reports*, 6, 23009, doi:10.1038/srep23009.

- von Schuckmann, K., and P. Y. Le Traon (2011), How well can we derive Global Ocean Indicators from Argo data?, *Ocean Science*, 7(6), 783-791, doi:10.5194/os-7-783.2011.
- Shi, L., et al. (2017), An assessment of upper ocean salinity content from the Ocean Reanalyses Inter-comparison Project (ORA-IP), *Climate Dynamics*, 49(3), 1009-1029, doi:10.1007/s00382-015-2868-7.
- Singh, A., T. Delcroix, and S. Cravatte (2011), Contrasting the flavors of El Niño-Southern Oscillation using sea surface salinity observations, *J Geophys Res-Oceans*, 116(C6), doi:10.1029/2010jc006862.
- Storto, A., S. Masina, M. Balmaseda, S. Guinehut, Y. Xue, T. Szekely, I. Fukumori, G. Forget, Y.-S. Chang, and S. A. Good (2017), Steric sea level variability (1993–2010) in an ensemble of ocean reanalyses and objective analyses, *Climate Dynamics*, 49(3), 709-729, doi: 10.1007/s00382-015-2554.9.
- Tesdal, J. E., Abernathy, R. P., Goes, J. I., Gordon, A. L., and Haine, T. W. (2018), Salinity trends within the upper layers of the subpolar North Atlantic. *Journal of Climate*, 31(7), 2675-2698. Doi:10.1175/JCLI-D-17-0532.1.
- Thompson, P. R., Piecuch, C. G., Merrifield, M. A., McCreary, J. P., and Firing, E. (2016). Forcing of recent decadal variability in the Equatorial and North Indian Ocean. *J Geophys Res-Oceans*, 121(9), 6762-6778. doi:10.1002/2016JC012132.
- Trenberth, K.E., J.T. Fasullo, K. von Schuckmann, and L. Cheng (2016), Insights into Earth's Energy Imbalance from Multiple Sources. *J. Climate*, 29, 7495–7505, doi:10.1175/JCLI-D-16-0339.1.

- Vinogradova, N. T., and Ponte, R. M. (2013). Clarifying the link between surface salinity and freshwater fluxes on monthly to interannual time scales. *Journal of Geophysical Research: Oceans*, 118(6), 3190-3201, doi:10.1002/jgrc.20200.
- Vinogradova, N. T., and Ponte, R. M. (2017). In search of fingerprints of the recent intensification of the ocean water cycle. *Journal of Climate*, 30(14), 5513-5528, doi:10.1175/JCLI-D-16-0626.1.
- Wang, G. J., L. J. Cheng, T. Boyer, and C. Y. Li (2017), Halosteric Sea Level Changes during the Argo Era, *Water*, 9(7), 484, doi:10.3390/w9070484.
- Wunsch, C., and P. Heimbach (2013a), Dynamically and Kinematically Consistent Global Ocean Circulation and Ice State Estimates, *International Geophysics*, 103, 553-579, doi:10.1016/b978-0-12-391851-2.00021-0.
- Xue, Y., M. A. Balmaseda, T. Boyer, N. Ferry, S. Good, I. Ishikawa, A. Kumar, M. Rienecker, A. J. Rosati, and Y. H. Yin (2012), A Comparative Analysis of Upper-Ocean Heat Content Variability from an Ensemble of Operational Ocean Reanalyses, *Journal of Climate*, 25(20), 6905-6929, doi:10.1175/Jcli-D-11-00542.1.
- Yu, L. S. (2011), A global relationship between the ocean water cycle and near-surface salinity, *J Geophys Res-Oceans*, 116(C10), doi:10.1029/2010jc006937.
- Yu, L. S., X. Z. Jin, S. A. Josey, T. Lee, A. Kumar, C. H. Wen, and Y. Xue (2017), The Global Ocean Water Cycle in Atmospheric Reanalysis, Satellite, and Ocean Salinity, *Journal of Climate*, 30(10), 3829-3852, doi:10.1175/Jcli-D-16-0479.1.

Zhao, M., H. H. Hendon, Y. H. Yin, and O. Alves (2016), Variations of Upper-Ocean Salinity Associated with ENSO from PEODAS Reanalyses, *Journal of Climate*, 29(6), 2077-2094, doi:10.1175/Jcli-D-15-0650.1.

Zheng, F., and R. H. Zhang (2015), Interannually varying salinity effects on ENSO in the tropical pacific: a diagnostic analysis from Argo, *Ocean Dynamics*, 65(5), 691-705, doi:10.1007/s10236-015-0829-7.

Zhu, J. S., B. H. Huang, R. H. Zhang, Z. Z. Hu, A. Kumar, M. A. Balmaseda, L. Marx, and J. L. Kinter (2014), Salinity anomaly as a trigger for ENSO events, *Scientific Reports*, 4, 6821, doi:10.1038/srep06821.

Zilberman, N. V., 2017: Deep Argo: Sampling the Total Ocean Volume in State of the Climate in 2016. *Bull. Am. Meteorol. Soc.*, 98, S73-S74, doi:10.1175/2017BAMSStateoftheClimate.1

APPENDIX A:
ZONAL ANALYSES OF MAJOR OCEAN BASINS

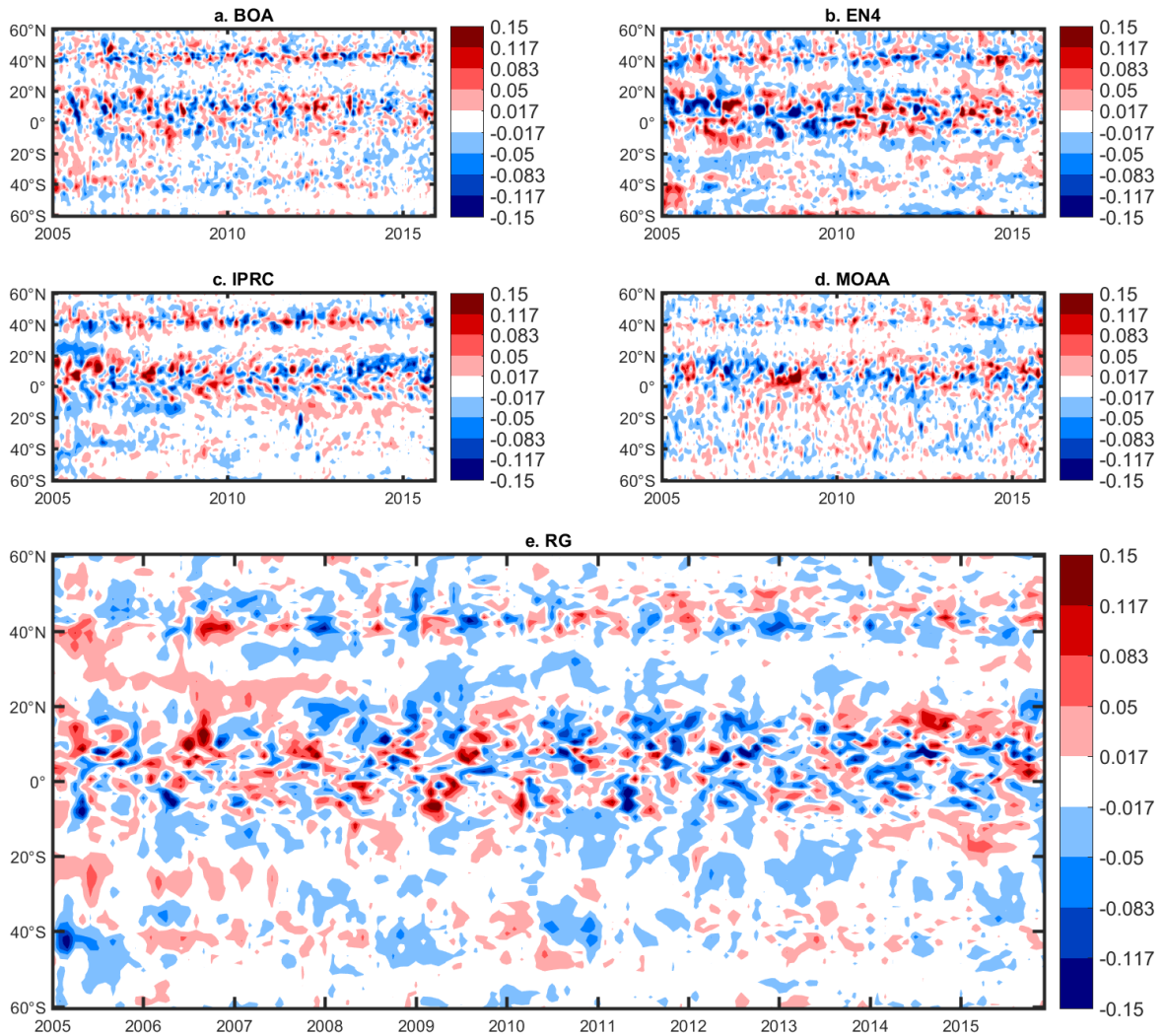


Figure A1: At the sea surface of the Atlantic Ocean, the spatial distributions of the difference on zonal mean salinity anomaly from 2005 through 2015 between each individual and the Ensemble Mean. (unit: psu)

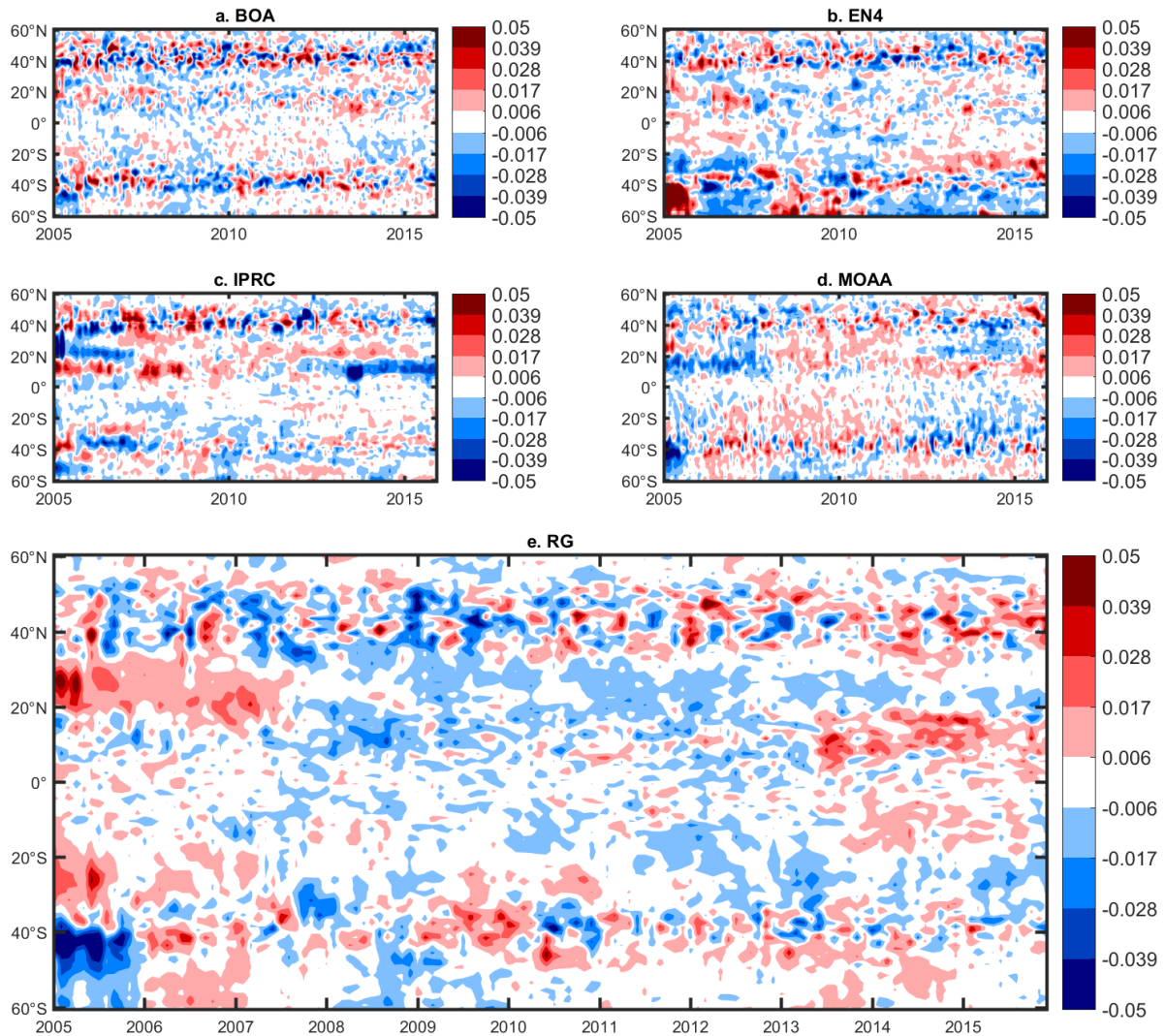


Figure A2: For the 0-700 m layer of the Atlantic Ocean, the spatial distributions of the difference on zonal mean salinity anomaly from 2005 through 2015 between each individual and the Ensemble Mean. (unit: psu)

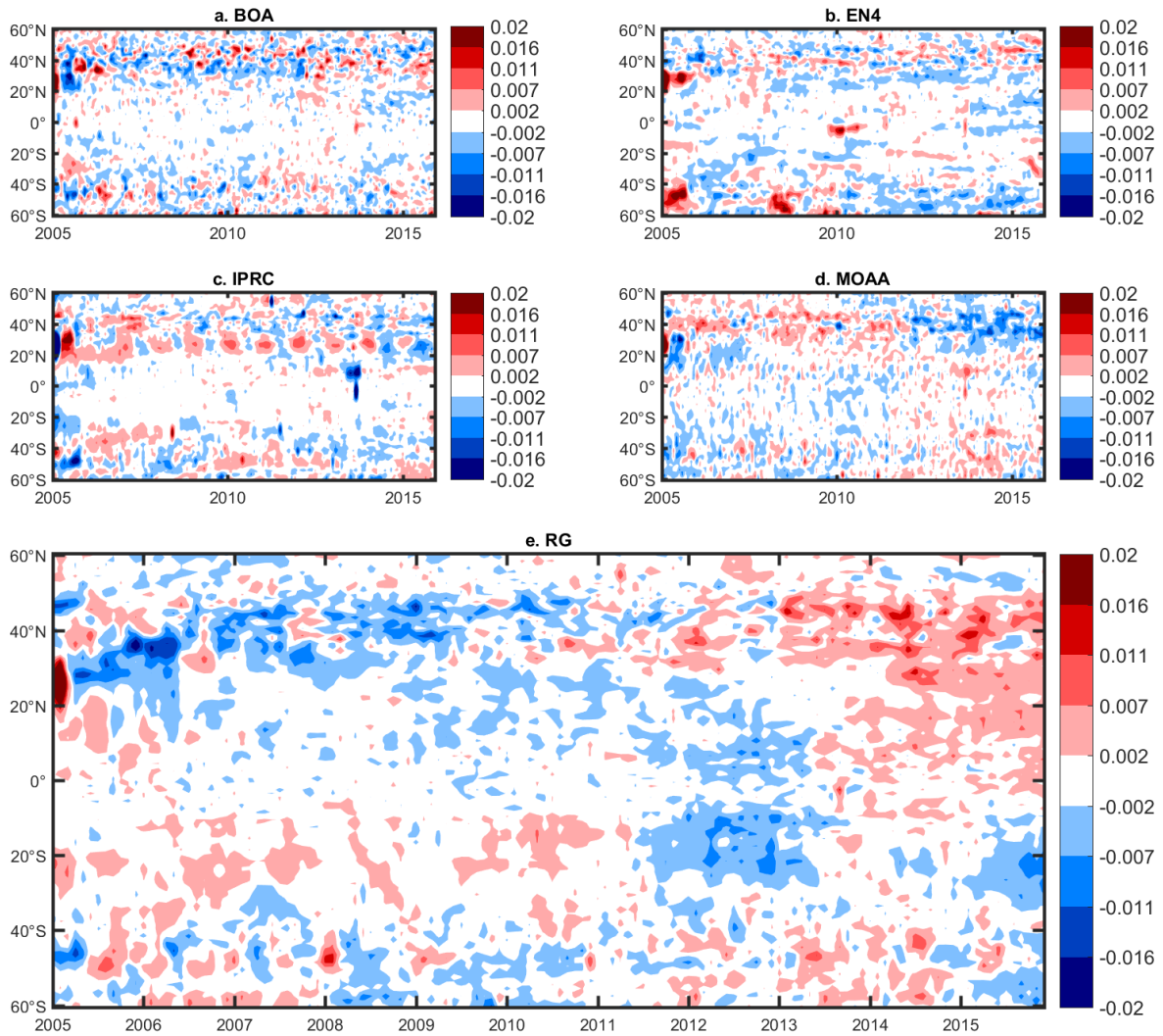


Figure A3: For the 700-2000 m layer of the Atlantic Ocean, the spatial distributions of the difference on zonal mean salinity anomaly from 2005 through 2015 between each individual and the Ensemble Mean. (unit: psu)

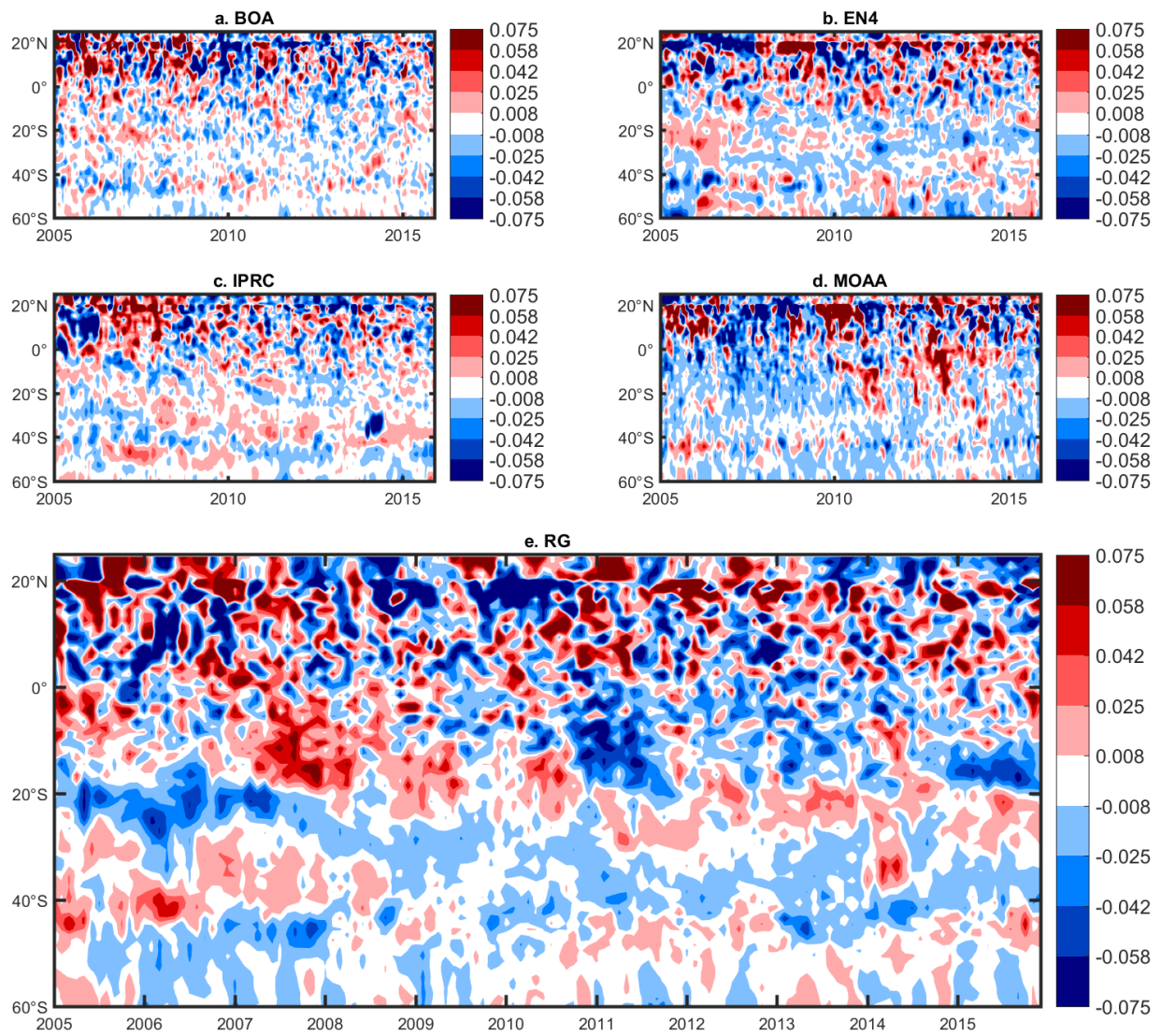


Figure A4: At the sea surface of the Indian Ocean, the spatial distributions of the difference on zonal mean salinity anomaly from 2005 through 2015 between each individual and the Ensemble Mean. (unit: psu)

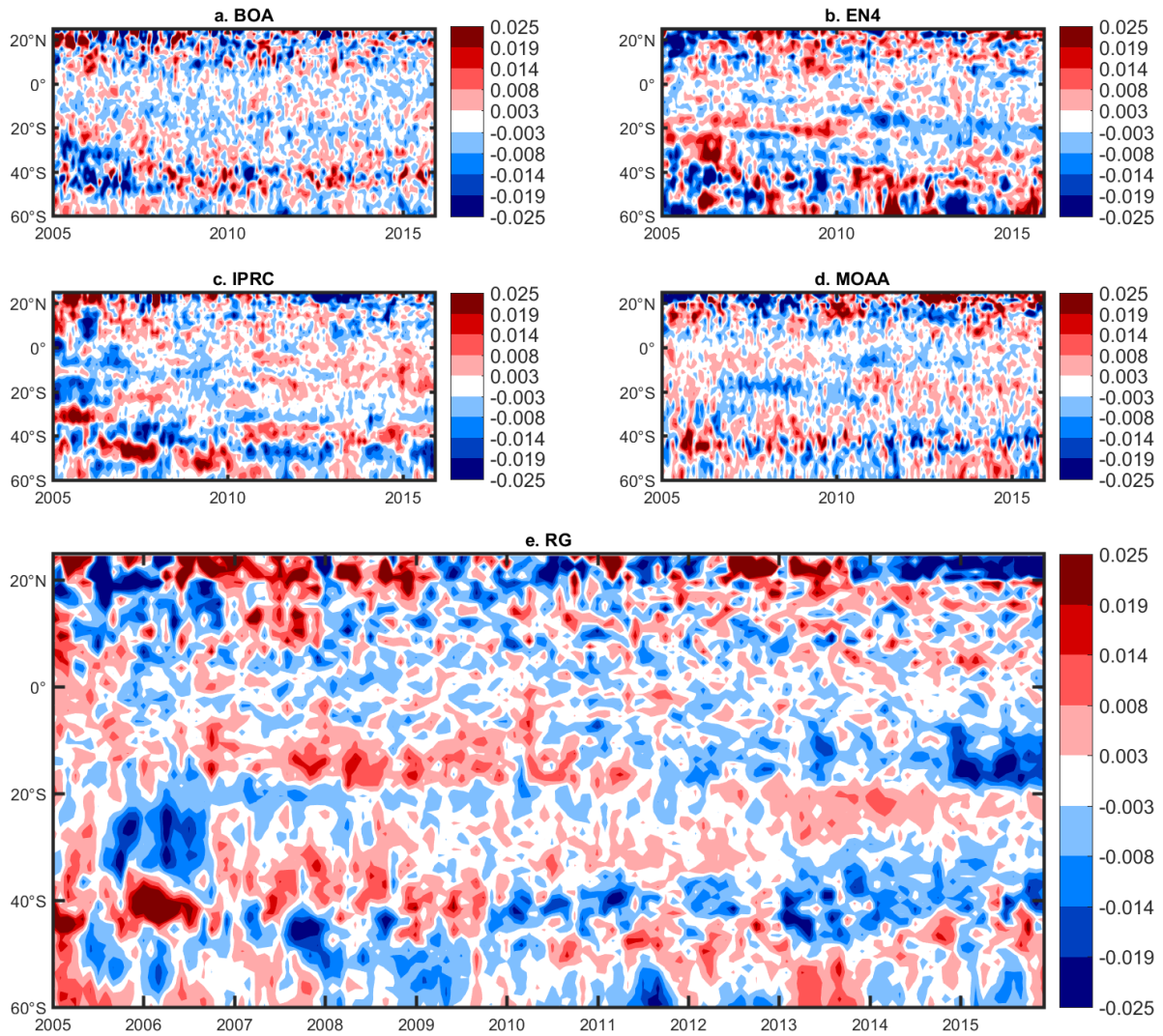


Figure A5: For the 0-700 m layer of the Indian Ocean, the spatial distributions of the difference on zonal mean salinity anomaly from 2005 through 2015 between each individual and the Ensemble Mean. (unit: psu)

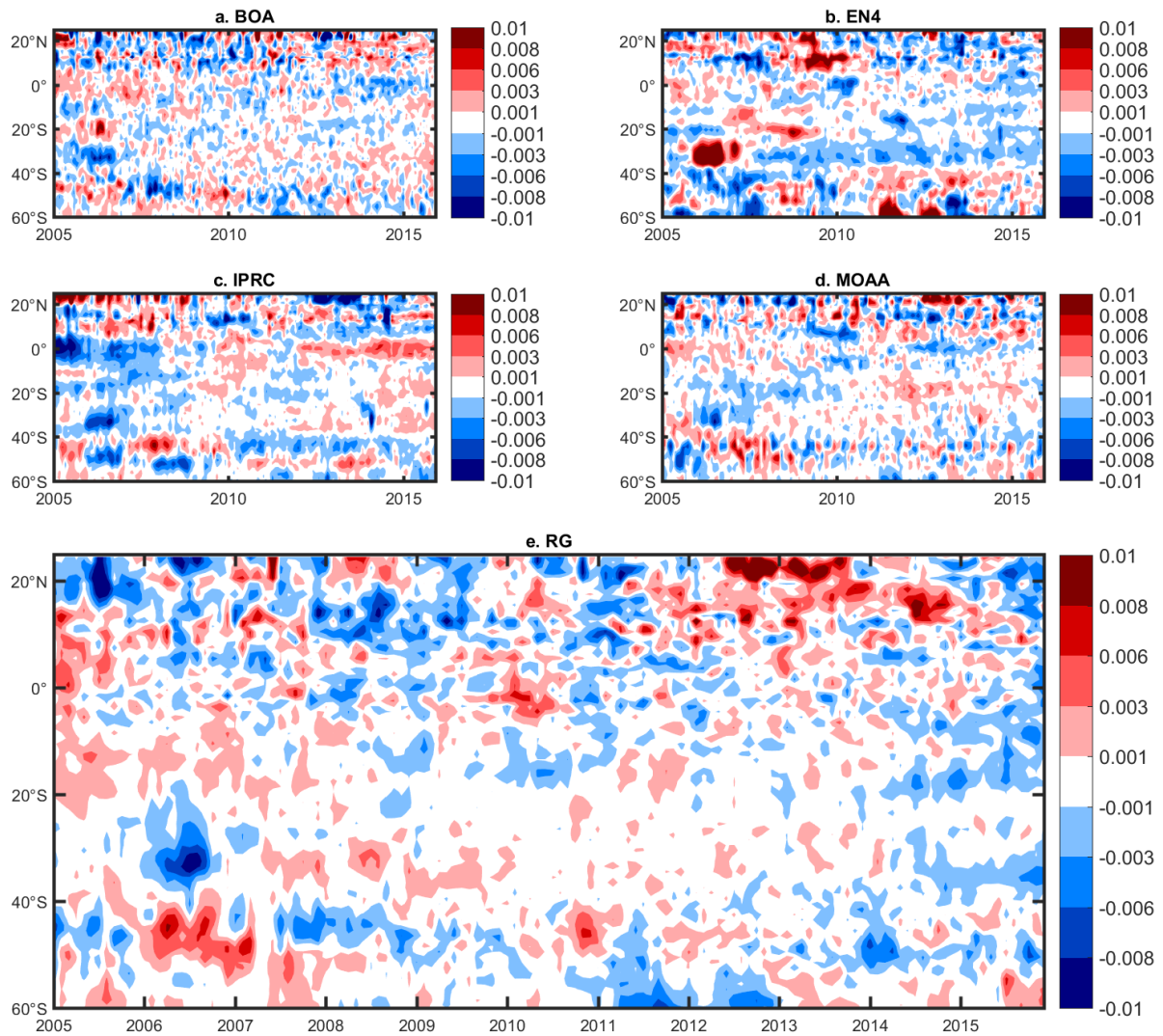


Figure A6: For the 700-2000 m layer of the Indian Ocean, the spatial distributions of the difference on zonal mean salinity anomaly from 2005 through 2015 between each individual and the Ensemble Mean. (unit: psu)

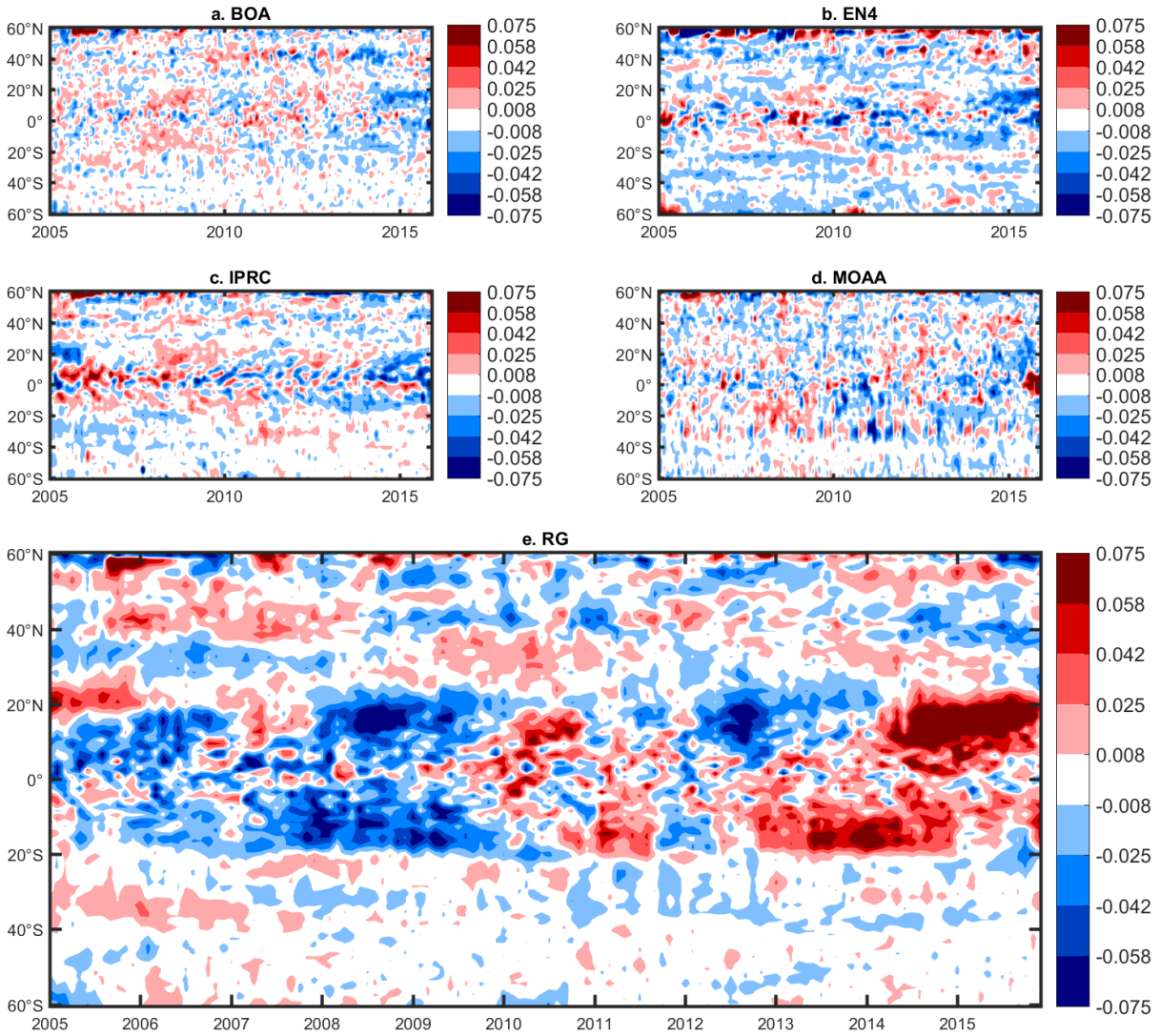


Figure A7: At the sea surface of the Pacific Ocean, the spatial distributions of the difference on zonal mean salinity anomaly from 2005 through 2015 between each individual and the Ensemble Mean. (unit: psu)

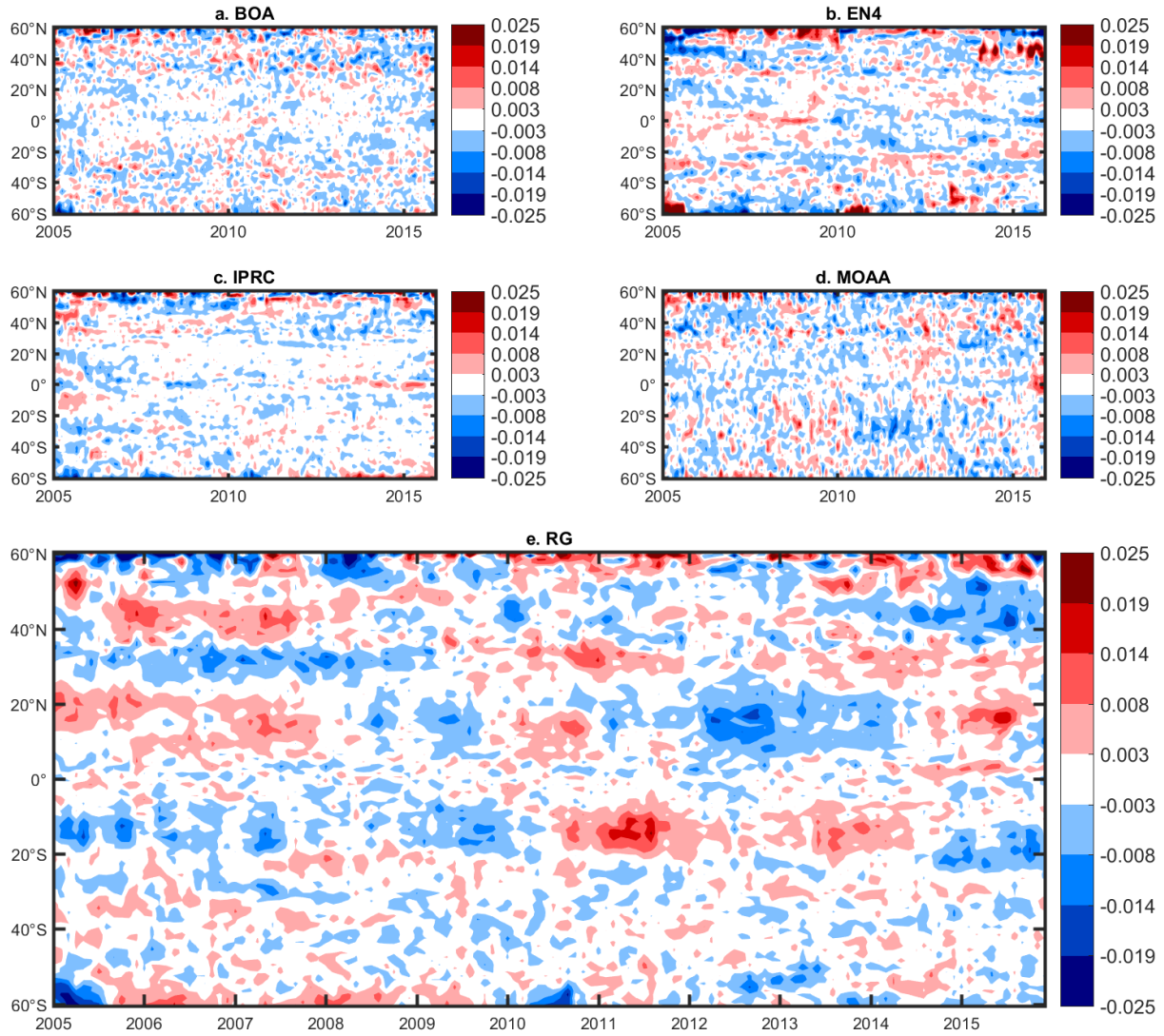


Figure A8: For the 0-700 m layer of the Pacific Ocean, the spatial distributions of the difference on zonal mean salinity anomaly from 2005 through 2015 between each individual and the Ensemble Mean. (unit: psu)

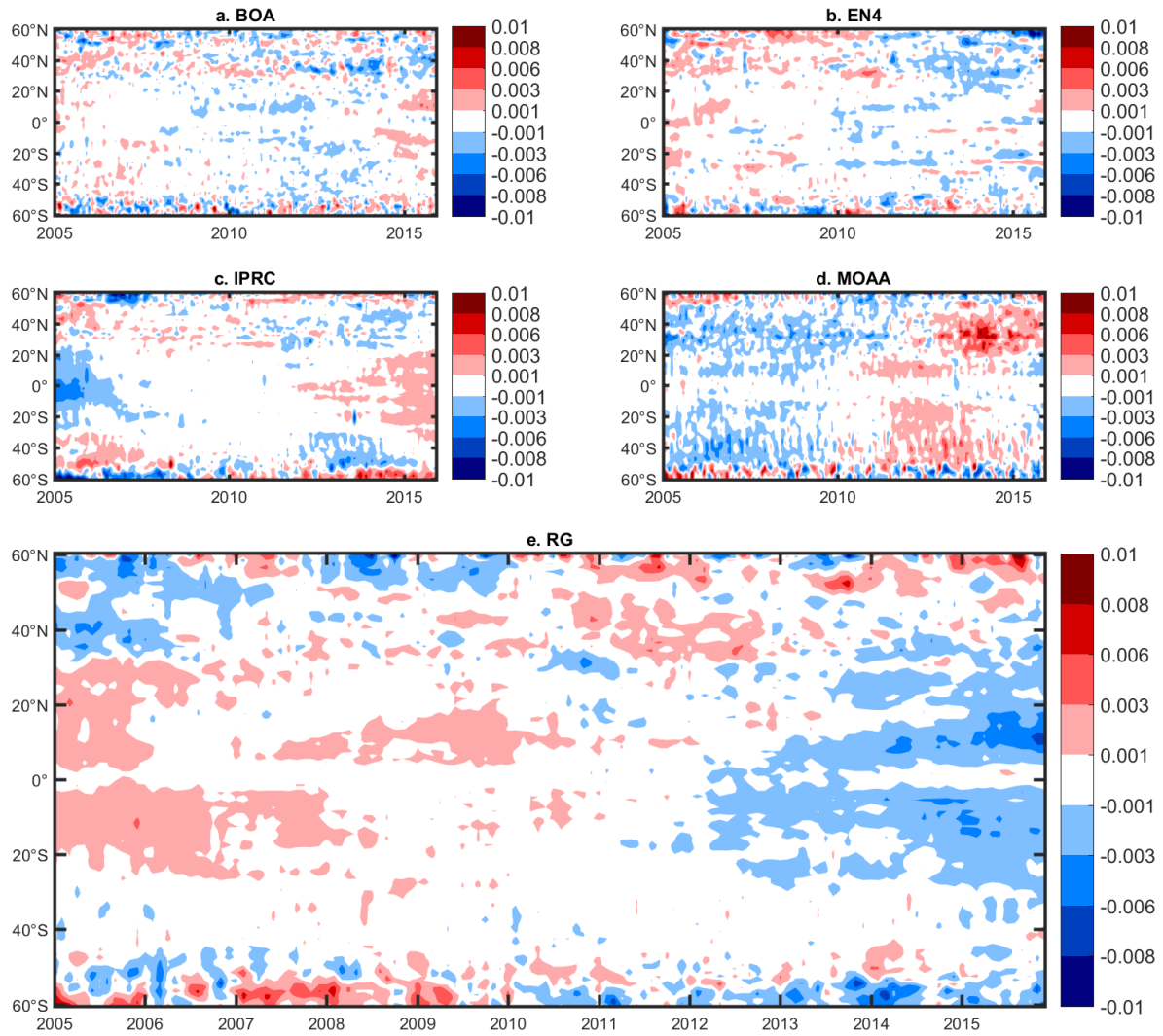


Figure A9: For the 700-2000 m layer of the Pacific Ocean, the spatial distributions of the difference on zonal mean salinity anomaly from 2005 through 2015 between each individual and the Ensemble Mean. (unit: psu)

APPENDIX B:
MERIDIONAL ANALYSES OF SUBPOLAR REGIONS

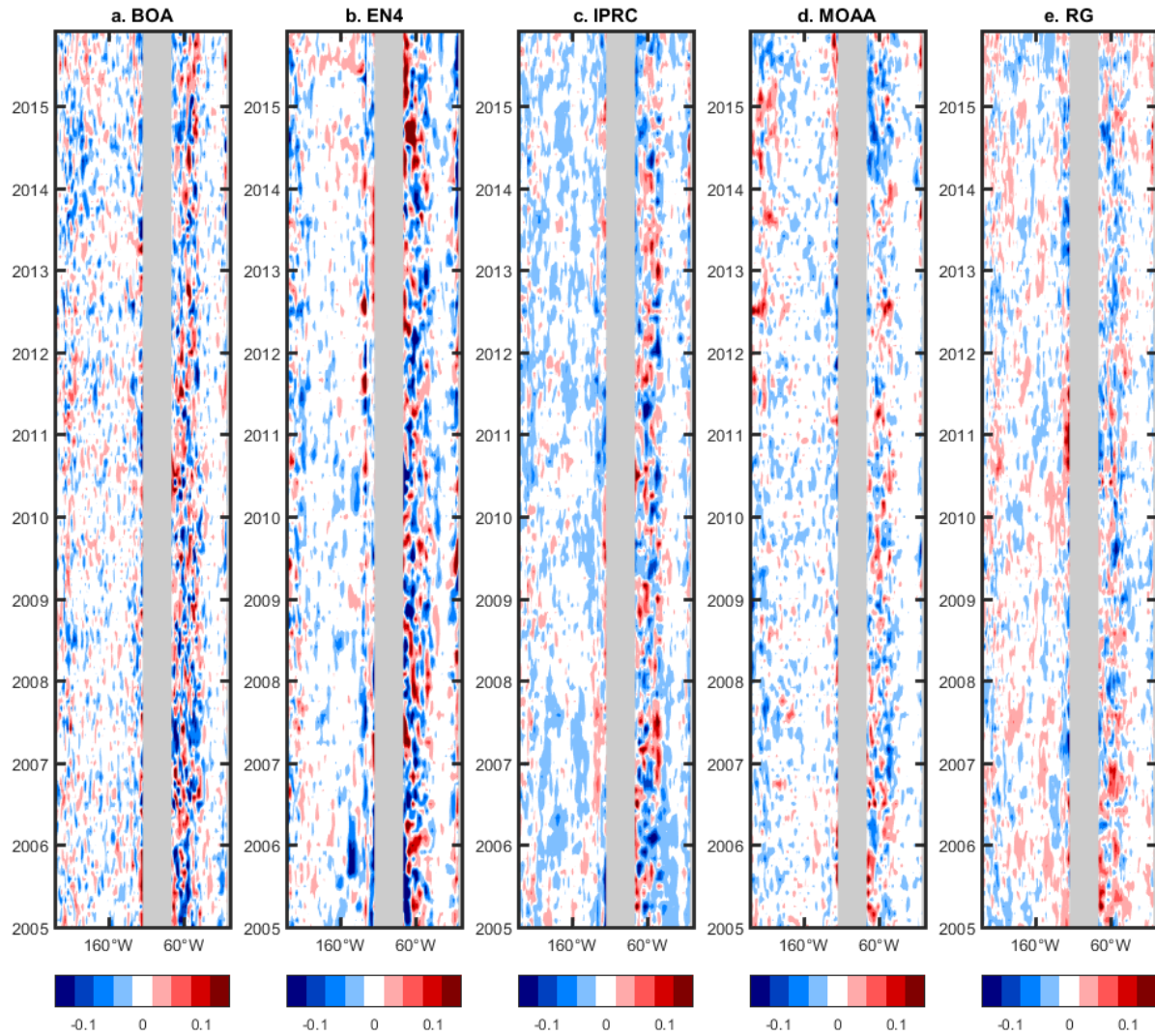


Figure B1: At the sea surface of 30-60°N, the spatial distributions of the difference meridional mean salinity anomaly from 2005 through 2015 between each individual and the Ensemble Mean. (unit: psu)

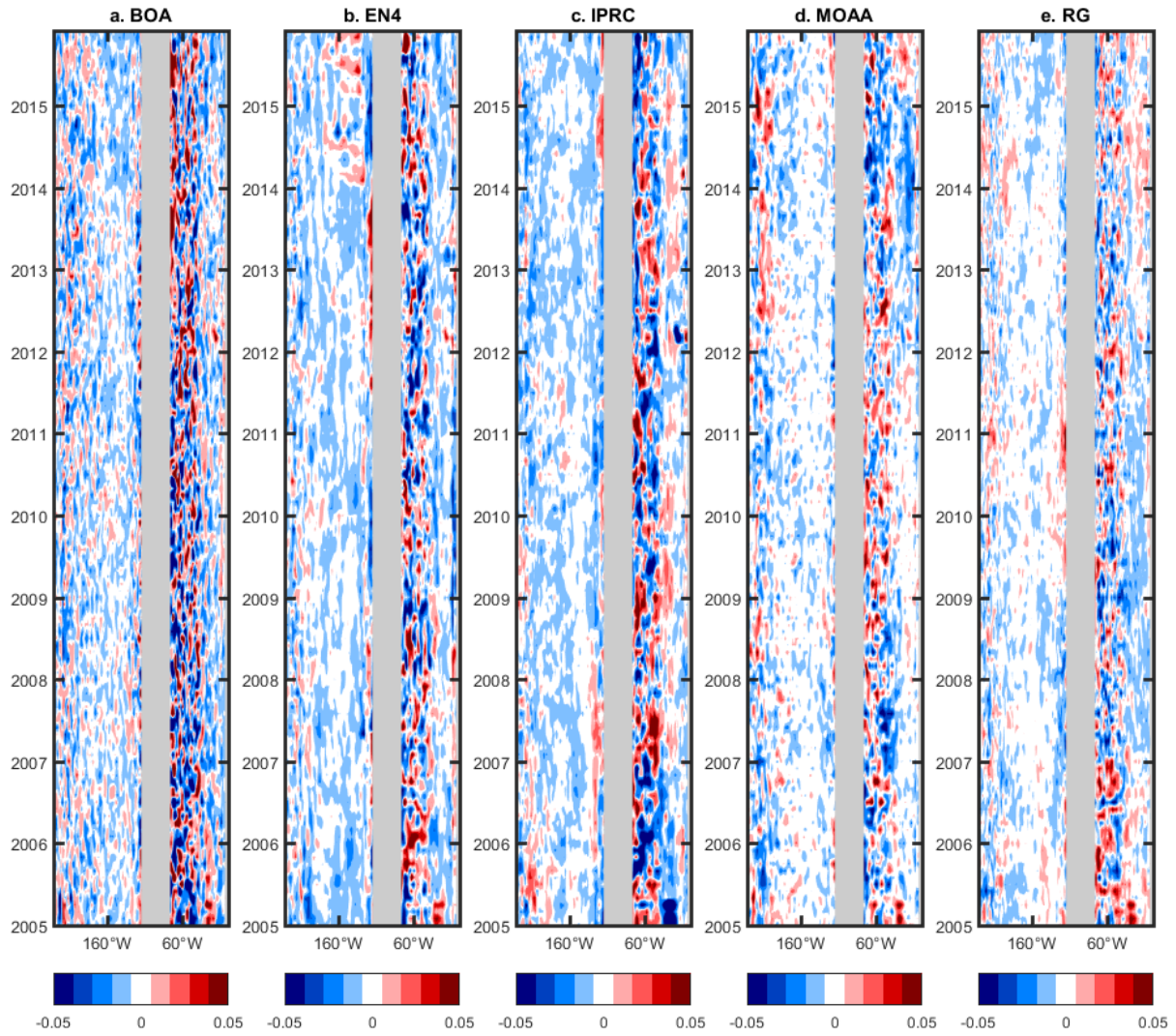


Figure B2: For the 0-700 m layer of 30-60°N, the spatial distributions of the difference meridional mean salinity anomaly from 2005 through 2015 between each individual and the Ensemble Mean. (unit: psu)

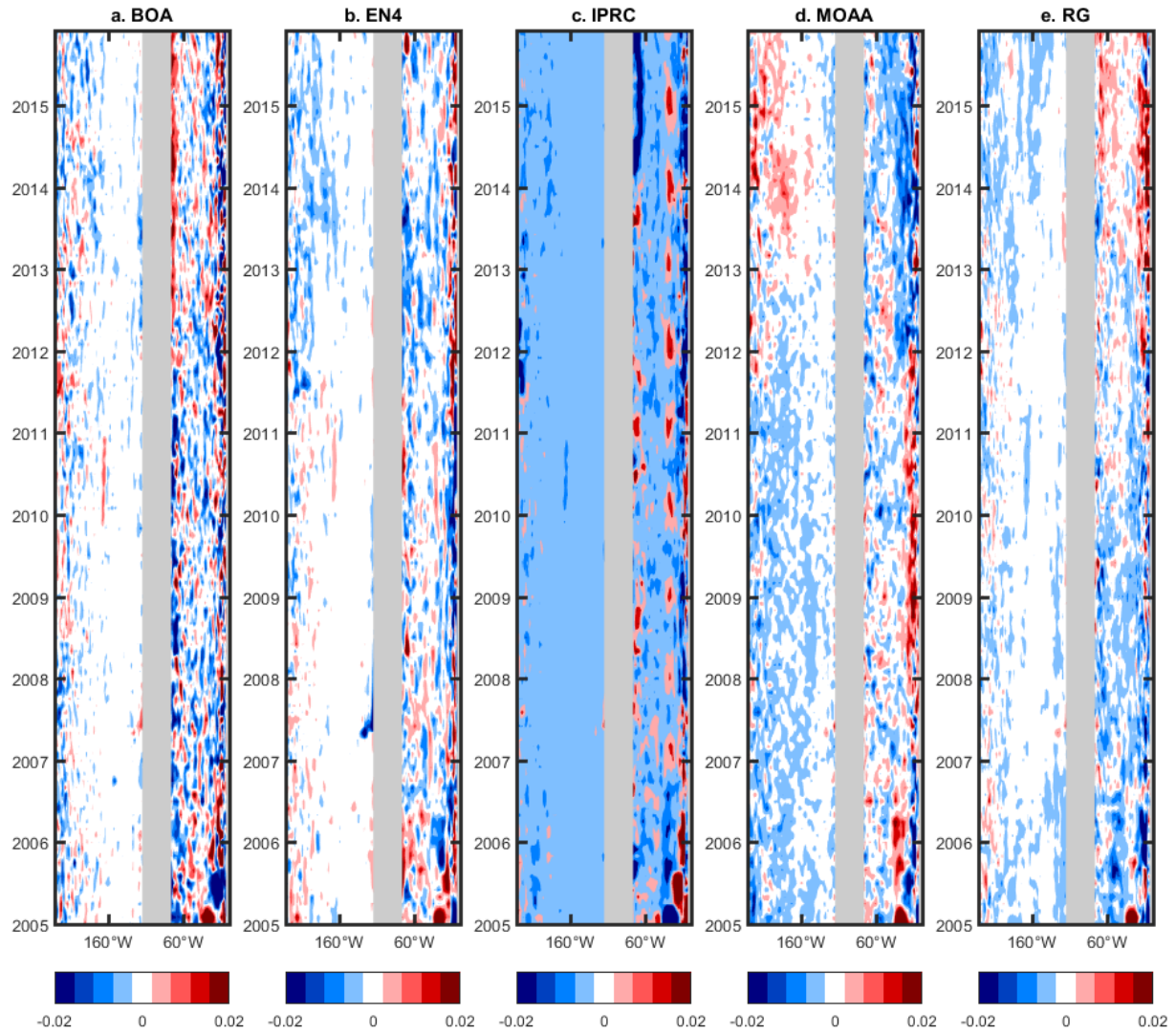


Figure B3: For the 700-2000 m layer of 30-60°N, the spatial distributions of the difference meridional mean salinity anomaly from 2005 through 2015 between each individual and the Ensemble Mean. (unit: psu)

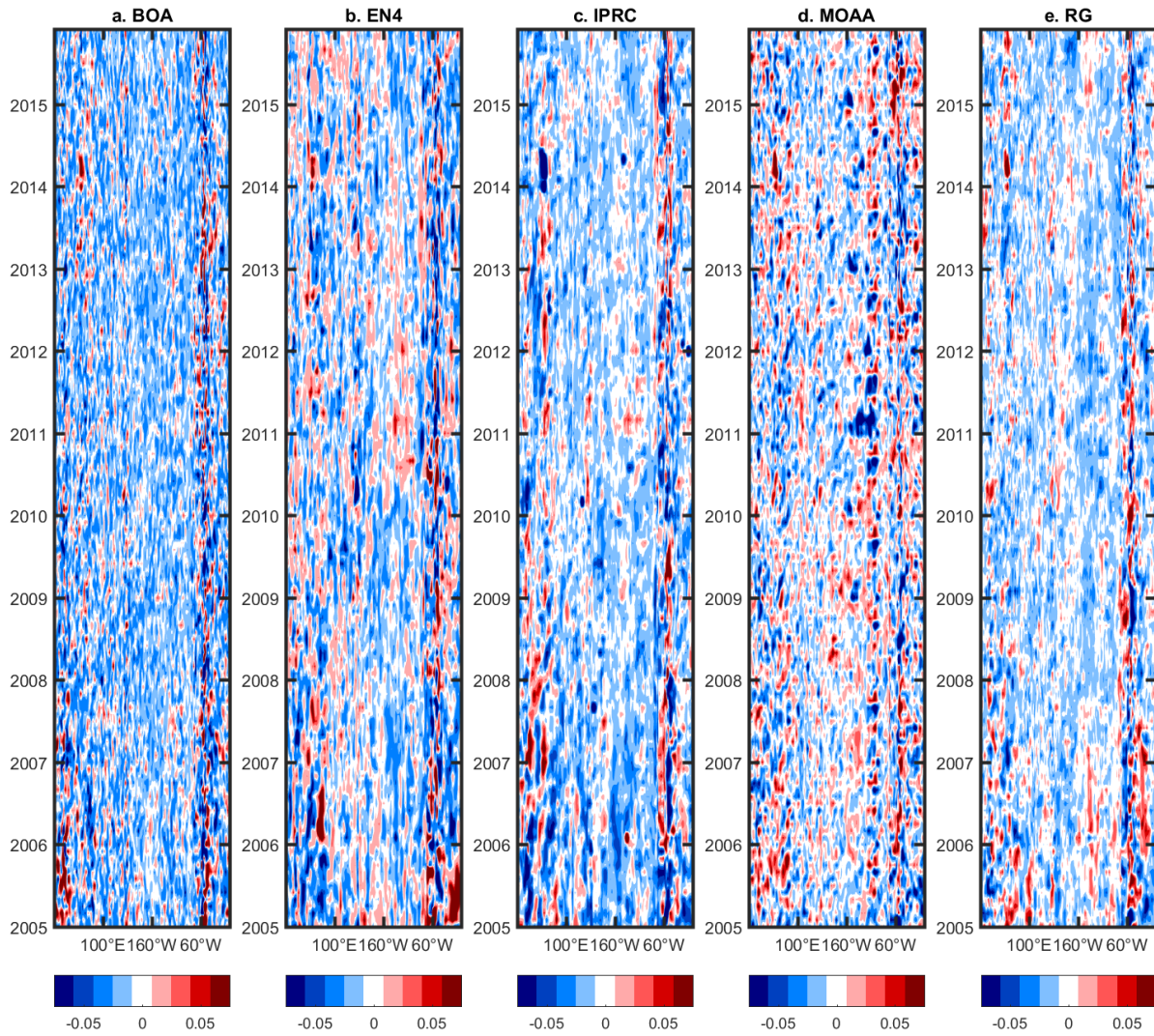


Figure B4: At the sea surface of 30-60°S, the spatial distributions of the difference meridional mean salinity anomaly from 2005 through 2015 between each individual and the Ensemble Mean. (unit: psu)

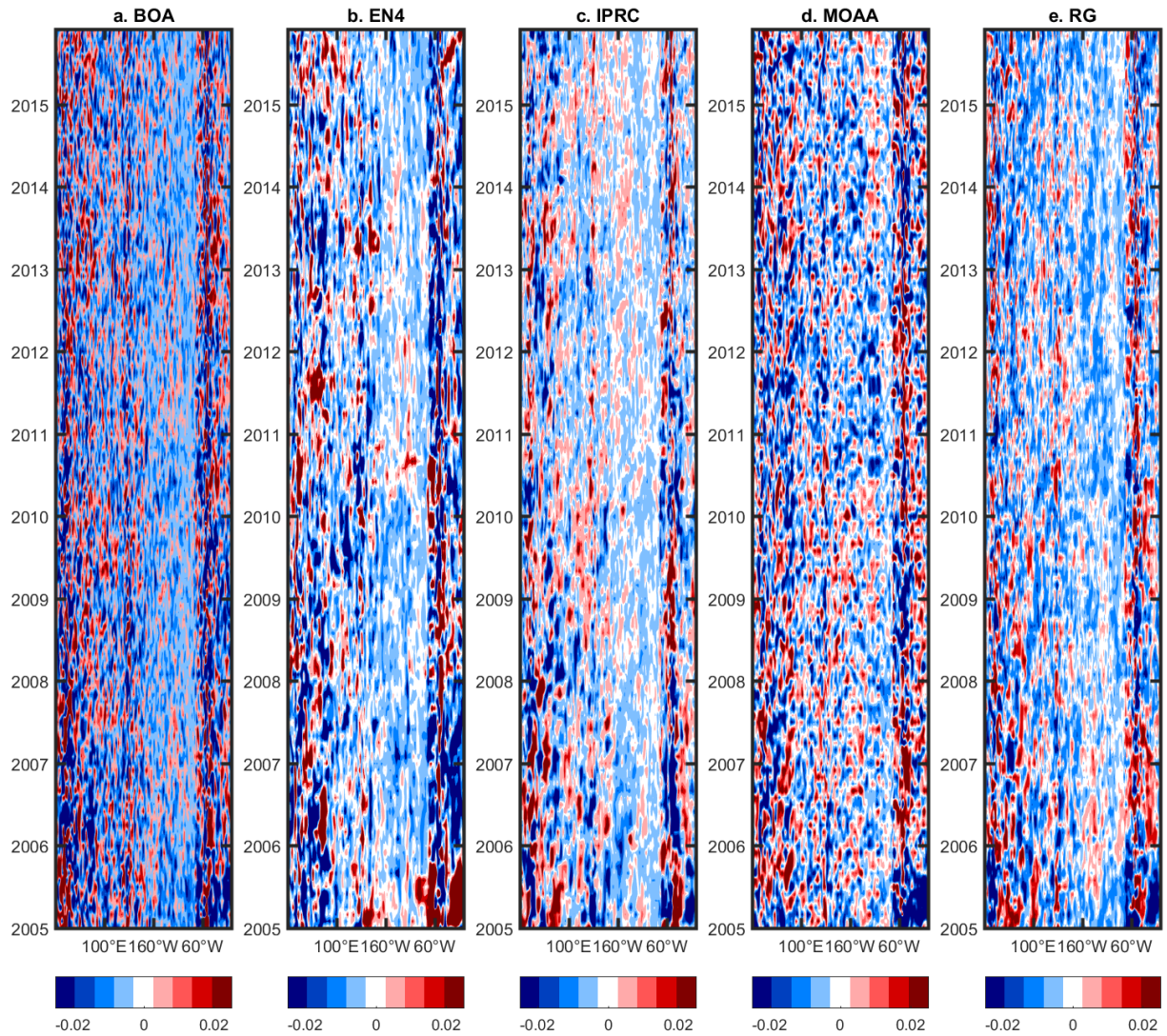


Figure B5: For the 0-700 m layer of 30-60°S, the spatial distributions of the difference meridional mean salinity anomaly from 2005 through 2015 between each individual and the Ensemble Mean. (unit: psu)

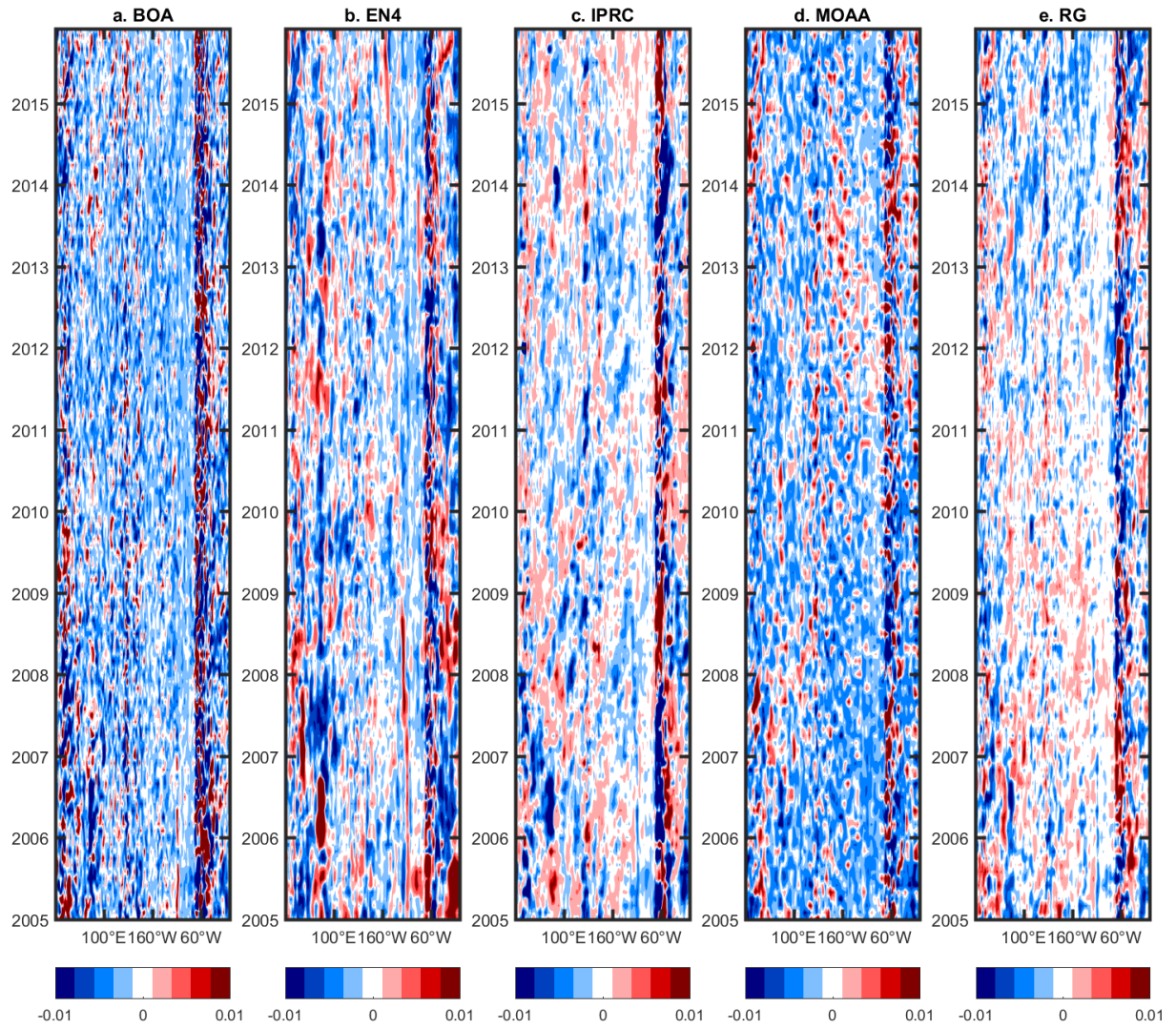


Figure B6: For the 700-2000 m layer of 30-60°S, the spatial distributions of the difference meridional mean salinity anomaly from 2005 through 2015 between each individual and the Ensemble Mean. (unit: psu)

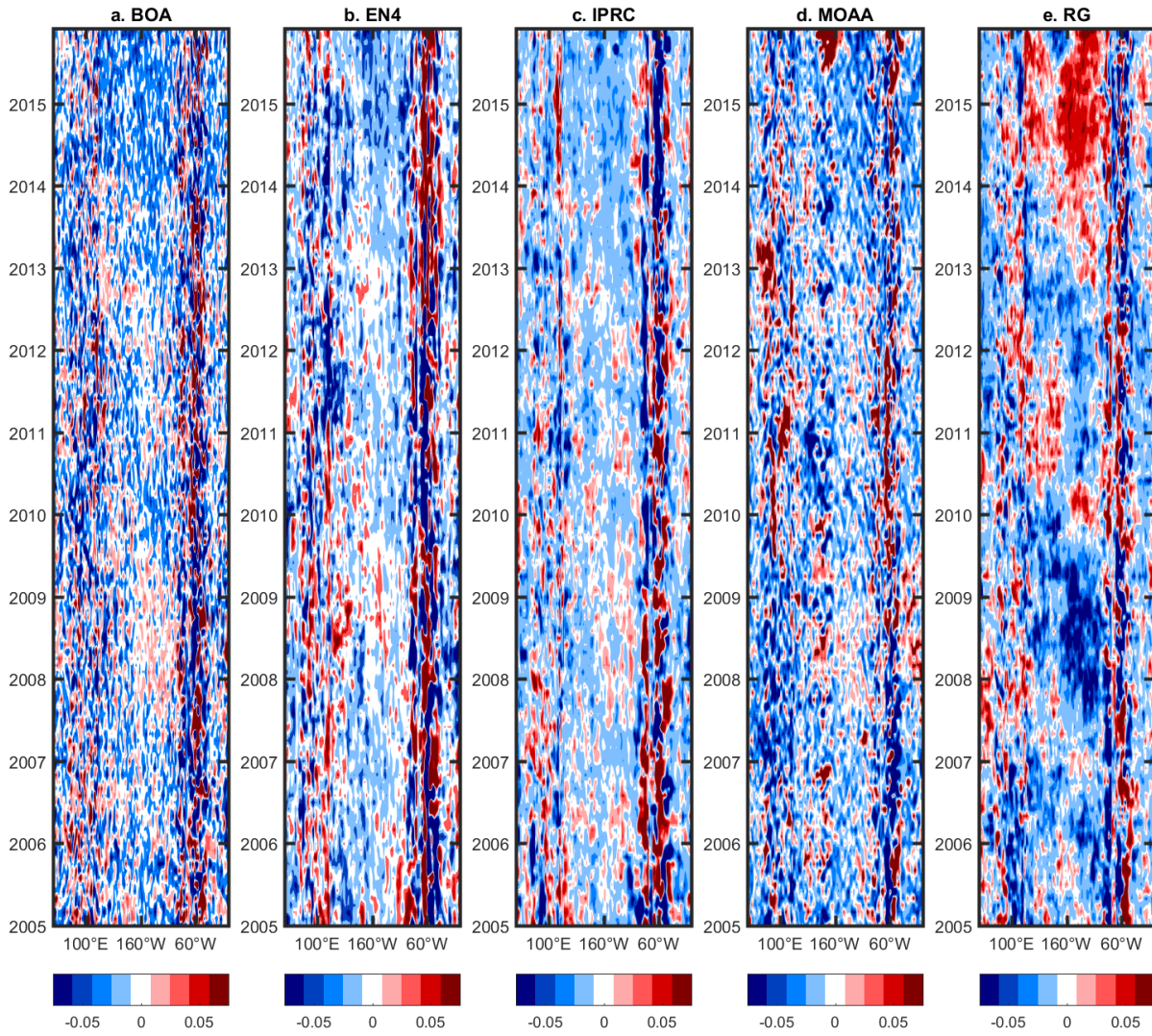


Figure B7: At the sea surface of 30°S-30°N, the spatial distributions of the difference meridional mean salinity anomaly from 2005 through 2015 between each individual and the Ensemble Mean. (unit: psu)

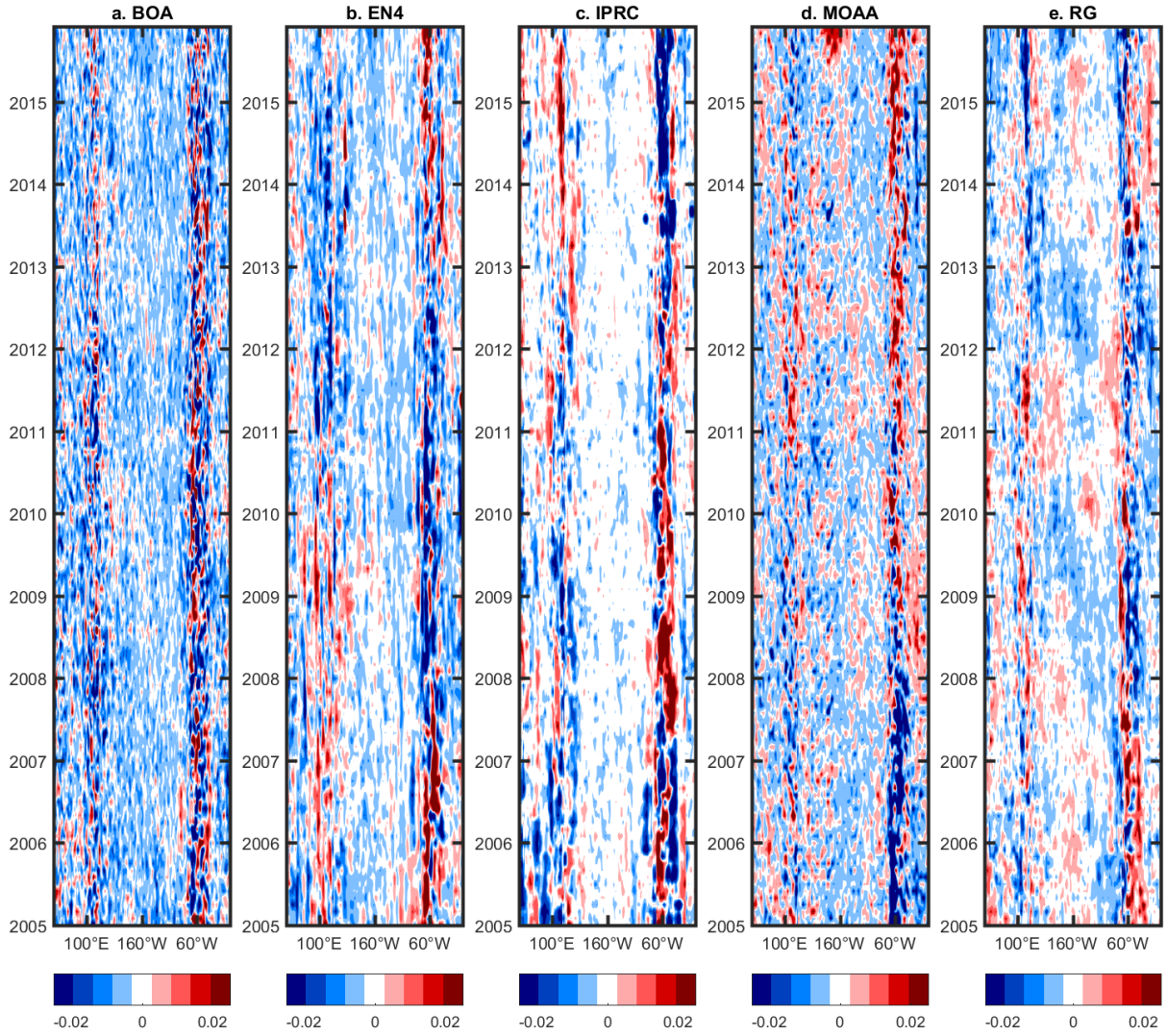


Figure B8: For the 0-700 m layer of 30-60°S, the spatial distributions of the difference meridional mean salinity anomaly from 2005 through 2015 between each individual and the Ensemble Mean. (unit: psu)

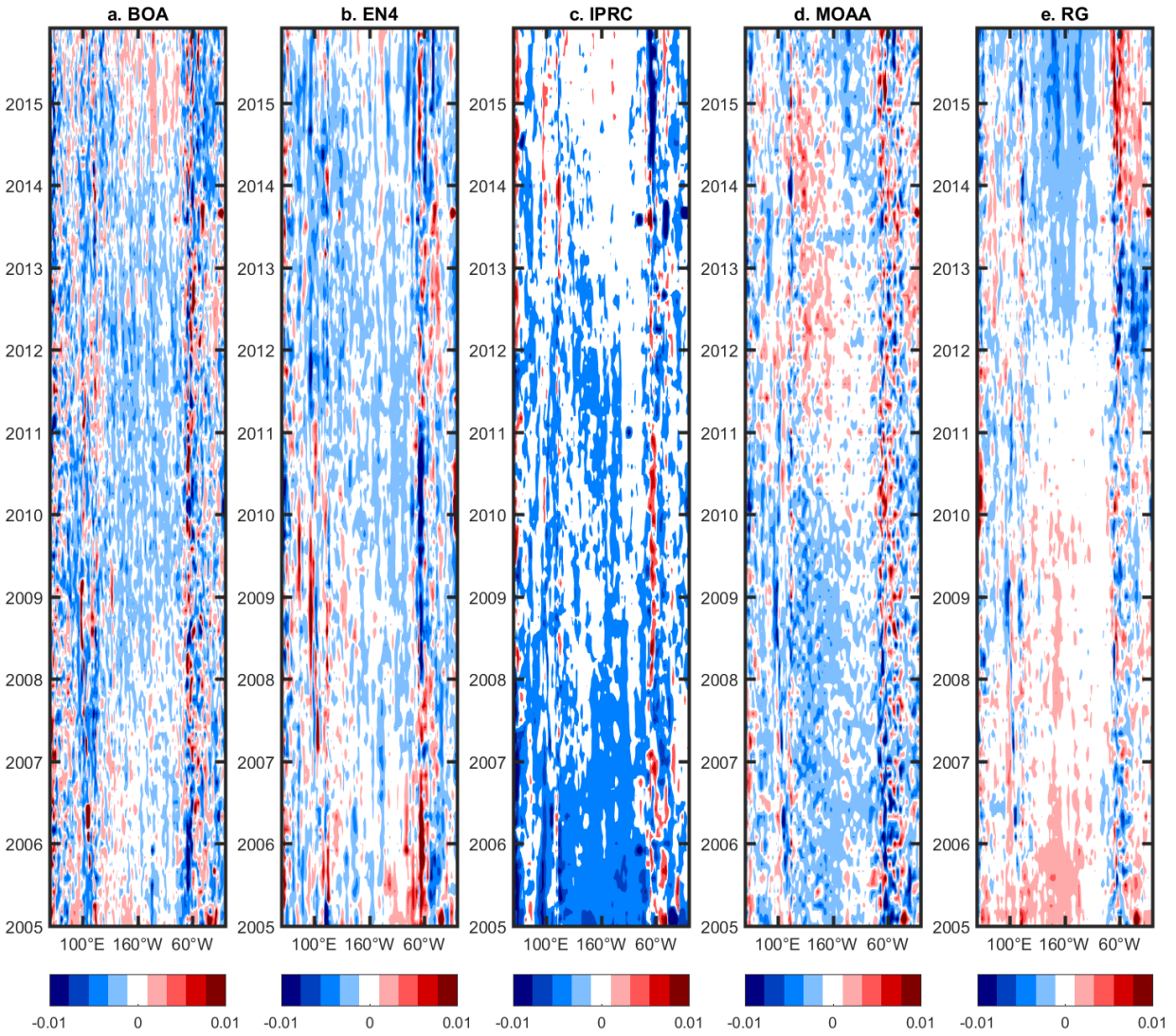


Figure B9: For the 700-2000 m layer of 30-60°S, the spatial distributions of the difference meridional mean salinity anomaly from 2005 through 2015 between each individual and the Ensemble Mean. (unit: psu)